SIMULATION OF SUPERSONIC INJECTION OF UNDEREXPANDED AERATED LIQUID JET

By

ABHIJIT S. CHOUDHARI

Bachelors of Engineering in Mechanical Engineering

Shivaji University

Kolhapur, India

2010

Submitted to the Faculty of the
Graduate College of the
Oklahoma State University
in partial fulfillment of
the requirements for
the Degree of
MASTER OF SCIENCE
December, 2016

SIMULATION OF SUPERSONIC INJECTION OF

UNDEREXPANDED AERATED LIQUID JET

Thesis Approved:

Dr. Khaled Sallam

Thesis Advisor

Dr. Rick Gaeta

Dr. Arvind Santhanakrishnan

ACKNOWLEDGEMENTS

First, I would like to thank my advisor, Dr.Khaled Sallam, for his support and encouragement. I am also thankful to my committee members, Dr. Rick Gaeta and Dr. Arvind Santhanakrishnan for their time in reviewing my thesis.

I would like to special thank CEAT IT team for their help in software installation and granting access to computer labs and to MAE staff including Dr. Charlotte Fore, Beth Powers, and Diane Compton for the guidance and service throughout my graduate study.

Finally, I would like to express my sincere gratitude to my parents for supporting and motivating me. Sincere thanks to my father for being a spirit of wisdom of my life, and heartfelt thanks to my mother for the love she has always shown me, and to my brother for always trust on me.

Name: ABHIJIT SUBHASH CHOUDHARI

Date of Degree: DECEMBER, 2016

Title of Study: SIMULATION OF SUPERSONIC INJECTION OF UNDEREXPANDED AERATED LIQUID JET

Major Field: MECHANICAL & AEROSPACE ENGINEERING

Abstract:
The present computational study for underexpanded 2D and axisymmetric nozzle configuration is carried out for both gas-only and aerated liquid jet. The study is motivated by the application of fuel injection in air-breathing propulsion systems, e.g. scramjet engines, ramjet engines and afterburners. The simulation of gas-only jet carried out using Ansys-Fluent student version. The results show that air reaches sonic condition at the injector exit due to the Fanno flow effect in the injector passage. The aerated liquid jet flow from the injector is alternately expanded by Prandtl-Meyer expansion fan and compressed by oblique shock waves due to the difference between the back (chamber) pressure and the flow pressure. The process then repeats itself and shock (Mach) diamonds are formed downstream of the injector exit similar to those typical of exhaust plumes of propulsion system. The numerical results of gas-only jet for 2D and axisymmetric configuration are validated with theory of gas dynamics and experimental results. The numerical results of gas-only jet are in good agreement with theory and experiment. Similar to gas-only jet, simulation of aerated liquid jet is carried out for both 2D and axisymmetric nozzle configuration. The simulation of aerated liquid jet is conducted using VOF model and SST k-ω turbulence model. The test conditions included: jet exit diameter of 1 mm and Gas to Liquid Ratio as 4%. The simulated result of 2D aerated liquid jet is compared with 2D gas-only jet using the contours of Mach number and static pressure. The flow field of axisymmetric aerated liquid jet differs from the 2D aerated liquid jet field; this can be explained based on the nozzle configuration. The present results also compare the cone angle expansion of aerated liquid jet. The cone angle expansion of aerated liquid jet is agreed with Prandtl-Meyer expansion analysis for 2D configuration and method of characteristics for axisymmetric configuration. The computed cone angle is always smaller than the theory, and this is probably due to inertia of the liquid jet. Present investigation shows that, the experimental results for aerated liquid jet expansion angle can be explained with the method of characteristics rather than the 2D Prandtl-Meyer expansion analysis.

TABLE OF CONTENTS

Acknowledgements……..ii
Abstract……iii
List of Tables……vi
List of Figures……vii
Nomenclature……x

Chapter Page

I. INTRODUCTION 1

Background 1
Problem Statement 1
Literature Review 2
Specific Objective 4
Organization of Thesis 5

II. THEORETICAL ANALYSIS AND NUMERICAL METHODS 9

Introduction 9
Numerical Methods 9
Theoretical Validation 15
Experimental Validation 18
Test Conditions 19

III. RESUTLS AND DISCUSSION 39

Introduction 39
Flow Visualization 39
Jet Expansion Angle 41
Liquid Volume Fraction 42
Oblique Shock Waves 43
Mach Disk 44
Mach Diamond Dissipation 44

Chapter Page

IV. SUMMARY AND CONCLUSION 59

Summary 59
Conclusions 60
Future Recommendations 61

REFERENCES 62

APPENDIX A 65

LIST OF TABLES

Table		Page
2.1	Theoretical and Simulated Values	20
2.2	Fluid properties and test conditions for 2D gas-only injector	21
2.3	Fluid properties and test conditions for axisymmetric gas-only injector	22
2.4	Fluid properties and test conditions for 2D aerated liquid injector	23
2.5	Fluid properties and test conditions for axisymmetric aerated liquid injector	24

LIST OF FIGURES

Figure Page

1.1 (a) Scramjet engine 6
(b) Geometry of inlet section and nozzle

1.2 Typical aerated fuel injector 7

1.3 Shadowgraph of aerated liquid jet injected in supersonic crossflow (M =1.97).....7

1.4 Jet expansion angle near the injector region as a function of injector pressure ratio 8

1.5 Injector configuration.....8
(a) Planar
(b) Axisymmetric

2.1 Schematic of geometry and mesh structure 25

2.2 Mesh structure for axisymmetric geometry 26

2.3 Mesh structure for planar aerated liquid injector 27

2.4 Mesh structure for axisymmetric aerated liquid injector 28

2.5 Contours of static gauge pressure inside the injector 29

2.6 Schematic of external flow field for underexpanded nozzle 30
(a) Simulation results of Mach number contours
(b) Schematic of flow structure

2.7 Contours of static gauge pressure inside the chamber 31

2.8 Contours of gauge pressure.....32
(a) Static pressure
(b) Stagnation pressure

2.9 Contours of static gauge pressure (Experimental validation) 33
(a) Inside the injector
(b) At the exit of the injector

2.10 Contours of Mach number at the exit of injector 34

2.11 Contours of Velocity vectors 35

2.12 Velocity vectors colored by Mach number 36

2.13 Experimental results for the location and the diameter of the Mach disk for dry and humid air.....37

2.14 Contours of static gauge pressure inside the injector (Test conditions) 38
(a) Air injector (2D geometry)
(b) Aerated liquid injector (2D geometry)
(c) Aerated liquid injector (Axisymmetric geometry)

3.1 Velocity vectors colored by Mach number (air) for 2D geometry 46
(a) Air injector (2D geometry)
(b) Aerated liquid injector (2D geometry)

3.2 Velocity vectors colored by the Mach number (air) for axisymmetric geometry for aerated liquid injector 47

3.3 The cone angle measured 48
(a) Numerically for 2D geometry
(b) Numerically for axisymmetric jet
(b) Experimentally

3.4 Best fit curve of MOC for axisymmetric jet expansion 49

3.5 Spread cone angle as a function of nozzle pressure ratio 49

3.6 Contours of volume fraction (air) for 2D geometry 50
(a) Outside the injector
(b) Film thickness resolved using current mesh
(c) Contours of Mach number (air)

3.7 Contours of volume fraction (air) outside the injector for axisymmetric geometry 51

3.8 Liquid volume fraction inside the injector 52
(a) 2D configuration
(b) Axisymmetric configuration

3.9 Contours of volume fraction (water) on Log scale 53
(a) Planar geometry
(b) Axisymmetric geometry

3.10 Contours of static gauge pressure inside the chamber for 2D geometry 54
(a) Air injector
(b) Aerated liquid injector

3.11 Contours of static gauge pressure inside the chamber for axisymmetric geometry 55

3.12 (a) Mach diamonds Swiss propulsion laboratory……..56
(b) Contours of Mach number for air injector (2D geometry)
(c) Aerated liquid injector (2D geometry)

3.13 Contours of Mach number for axisymmetric aerated liquid injector……....57

3.14 Contours of velocity magnitude (mixture) of aerated liquid jet ……...58
(a) Axisymmetric geometry
(b) Planar geometry

NOMENCLATURE

b	film thickness
d	injector diameter
D	nozzle diameter
D_e	exit nozzle diameter
D_m	diameter of the Mach disk
f	fanning friction factor
F	surface tension force
g	acceleration due to gravity
L	nozzle passage length
L_{max}	maximum nozzle passage length
M	Mach number
$\dot{m}$	mass flow rate
P	stagnation pressure
P_b	back pressure
$\dot{Q}$	volumetric flow rate
S	source term constant
v	jet streamwise velocity
$\vec{V}$	velocity vector
x_m	from the exit of the nozzle to the Mach disk
X	axis co-ordinate
Y	axis co-ordinate

Greek

α	fluid fraction
γ	ratio of specific heat
δ	deflection angle
δ_j	half expansion angle
θ	expansion angle
ν	Prandtl-Meyer expansion function
ρ_g	gas density
ρ_l	liquid density

Subscript

b	back
e	exit
j	jet
L	liquid phase property
m	Mach disk
o	initial or stagnation value
q	type of fluid
surf	property at the liquid surface

Superscript

T	Transpose function

CHAPTER I

INTRODUCTION

1.1 Background

Understanding liquid fuel injection processes is important for designing diesel engines and air-breathing propulsion systems including afterburners, ramjets and scramjet engines similar to Fig. 1.1. The motivation for this thesis is to investigate the effects of geometry and operating test conditions on the exit flow of aerated liquid jet from fuel injectors typical of those used in air breathing propulsion systems. A typical aerated fuel injector is shown in Fig. 1.2. Successful operation of the combustor requires the fuel and air to mix efficiently and burn completely before exiting the combustor. The fuel injector design should incorporate turbulence, jet-to-crossflow-momentum flux ratio (q), and gas-liquid-mass-flowrate-ratio (GLR) to improve spray penetration and reduce droplets sizes in order to improve fuel/air mixing. At large GLR the gas/liquid flow inside the injector passage forms an annular two-phase flow forcing the liquid into a thin film near the wall. Upon exiting form the injector the thin film breaks into smaller droplets similar to those shown in Fig. 1.3. Sizes and velocities of the droplets depend on the properties of the annular liquid sheet.

1.2 Problem Statement

The goal of the present study is to understand the flow physics of aerated liquid jet injection from underexpanded nozzle injector configurations. The present result will explore the geometry effects on pressure, velocity, and waves structures with direct impact of penetration height and droplets size of practical injectors. The present results are validated using previous experimental results for round aerated

liquid jets in supersonic crossflow [Sallam et al., 11] as well as theoretical results for underexpanded supersonic nozzles.

1.3 Literature Review

Liquid atomization is the process of breakup of liquid jet into droplets. This process was studied extensively due to numerous applications in nature and industries. Atomization process is not only useful in combustion but also in printing, medical and agriculture industry. Atomizers and injectors are the devices, which are useful in the formation of droplets from liquid jet. The liquid jet converts into small droplets lead to increase in surface area and effectively increases the rate of mixing and evaporation process. The goal for this study is to understand the physics of the exit flow of aerated liquid jet typical of fuel injectors of air breathing propulsion systems [1]. The fuel injector design should incorporate turbulence, jet-to-crossflow-momentum flux ratio (q), and gas-liquid-mass-flow rate-ratio (GLR) to improve spray penetration and reduce droplet sizes in order to improve fuel/air mixing. Aerated-liquid jet become popular due to formation of fine droplets with high velocity at lower injection pressure than conventional jets, and deep penetration inside the combustion chamber due to a higher effective momentum flux than conventional jets [2]. Air is injected into the liquid immediately upstream of the injector exit passage. Injection of small amount of air inside the liquid jet injector will facilitate rapid vaporization, mixing, and combustion. Two phase flow inside the aerated liquid injector was numerically investigated by Tian [3, 4] at different GLR. At large GLR the gas/liquid flow inside the injector passage forms an annular two-phase flow forcing the liquid into a thin film near the wall. Effective area occupied by the liquid decreases due to the expansion of gas phase along the injector passage. This results into squeezing of liquid jet into thin liquid sheet along the injector walls forming annular flow regime inside the injector.

Core length and velocity profile for subsonic and supersonic jets were studied previously [5, 6, 7] motivated by applications in propulsion systems and particle coating applications [8]. The interaction of supersonic jet with the ambient pressure results in the formation of alternate expansion and compression

waves [9] and associated jet noise. The structure of the waves was studied by Lagumbay et al [10] and by Pianthong [11]. Under-expanded and over-expanded nozzles produce shockwaves and shockwaves affect the density, stream wise velocity, pressure and temperature of the gas around them. Shock waves play a crucial role in air/liquid mixing and temperature distribution at the exit of injector [12]. The strength of bow shock and the size of the barrel shock and Mach disk increases with increasing jet to crossflow momentum ratio as well as the nozzle pressure ratio. The effect of jet to crossflow momentum ratio on sonic jet is of practical interest and studied by Wang [13] using LES. Vuorinen et al [14], Fu et al [15] and Thanigaiarasu et al [16] simulated the under-expanded jet and validated the results with theory of gas dynamics and experimental data. Injection of supersonic aerated liquid jet affects combustion efficiency of the engine. Penetrating length and injecting cone angle are the parameters which play significant role in the process of formation of spray structure. Experimental and numerical study of diesel injection was done by Bensler et al. [17] regarding penetration length and cone angle. Liu [18] simulated the transient jet flow in supersonic crossflow and concluded that air momentum flux ratio affects penetration height. Injector internal flow and spray characteristics of the aerated liquid jet is affected by the geometry of the nozzles [19] [20]. Thickness of the liquid film in the annular flow structure becomes thinner as Gas to Liquid Ratio (GLR) and liquid to gas momentum flux increases at the nozzle exit. This was studied experimentally by Lin et al [21] by observing the internal flow structures of aerated liquid injectors. The injection of aerated liquid jet in supersonic crossflow was studied experimentally by Sallam et al. [22] using holographic imaging. They plotted the spread cone angle as a function of injection pressure ratio and compared their results with theoretical spray cone angle. Prandtl-Meyer expansion angle is the function of injection pressure ratio. Prandtl-Meyer expansion angle in 2D geometry is depending on the Mach number at the exit flow. Mach number at the exit of the nozzle is calculated using the following equation.

$$M = \left\{ \frac{2}{\gamma - 1} \left[\left(\frac{P_{inj}}{P_b} \right)^{\gamma - 1 / \gamma} - 1 \right] \right\}^{1/2} \tag{1.1}$$

P_{inj} is the nozzle exit stagnation pressure and P_j is chamber back pressure. To calculate the Prandtl-Meyer function (ν) following equation is used.

$$\nu = \sqrt{\frac{\gamma+1}{\gamma-1}} * \tan^{-1}\sqrt{\frac{\gamma-1}{\gamma+1} * (M^2-1)} - \tan^{-1}\sqrt{(M^2-1)} \quad (1.2)$$

This Prandtl-Meyer function (ν) is the half jet expansion angle. The jet expansion cone angle is the double of the Prandtl-Meyer function (ν). Jet expansion cone angle is represented as θ.

$$\theta = 2 * \nu \quad (1.3)$$

However, measurements of cone angle of Sallam et al. (2006) were not resolved using their theoretical analysis. This could have been due to the fact that the geometries of the two-dimensional and axisymmetric configurations are different as shown in Fig. 1.5. In case of axi-symmetric flow (i.e. conical flows) the increase in the cross-sectional area imposes large penalty on the mass flux thus limiting the cone angle. Another concern is that Sallam et al. related the spread cone angle to the injection pressure ratio but the effects of the interaction of shock waves/expansion fans with the liquid sheet is still missing.

The present study is investigating the flow physics of the injection of underexpanded aerated liquid jet into the combustion chamber and use computational and experimental analyses to explain the properties of the injected conical liquid sheet. The exit flow of aerated liquid jet is studied computationally using ANSYS-Fluent and theoretically using the theory of gas dynamics. The properties of interest of the conical liquid sheet include spray cone angle, liquid film thickness, velocities of the liquid sheet, contours of pressure and Mach number, waves/liquid sheet interaction, and location of Mach discs.

1.4 Specific Objective

The goal of this study is to investigate the flow physics of the injection of aerated liquid jet into the combustion chamber and observe the properties of the conical liquid sheet emitted from the injector exit. Properties of conical liquid sheet includes spray cone angle, , liquid film thickness, velocities of the liquid sheet. The specific objectives are as follows:

1. Investigate the effect of liquid sheet on the dynamics of underexpanded (a) aerated liquid jet and (b) gas-only jet injected from a typical aerated fuel injector.
2. Investigate the effect of the injector geometry by simulating (a) axi-symmetric aerated liquid jet and (b) axi-symmetric gas-only jet and comparing the results with the 2D cases.
3. Validate the present computational results for both gas-only jet and for aerated liquid jet using previous experimental results (Sallam et al [22] and Baek [27]) and Theory of Gas Dynamics (Love et al [33] and Keith [26]).
4. Use a theoretical analysis to correlate the measurements of jet expansion angle for underexpanded aerated liquid jet injected in supersonic crossflow (Sallam et al [22]).

1.5 Organization of Thesis

This thesis report is organized into four chapters. Background, problem statement, literature review, and specific objectives of the study are presented in the first chapter. Second chapter explains the theoretical analysis, validation of numerical results by matching with experimental results. Simulation of aerated water jet is presented in the third chapter. Finally, summary, conclusions, and recommendations for future work are included in the last chapter.

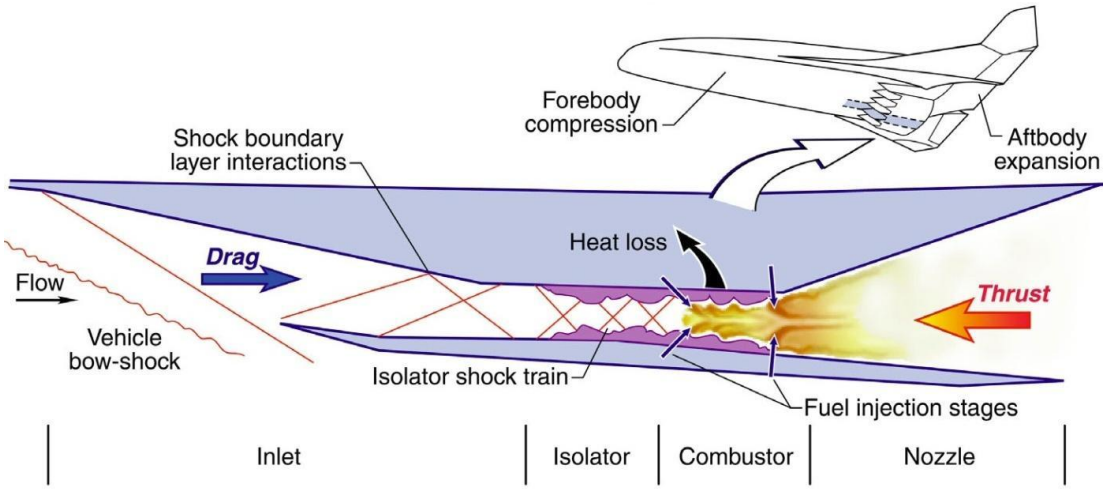

(a)

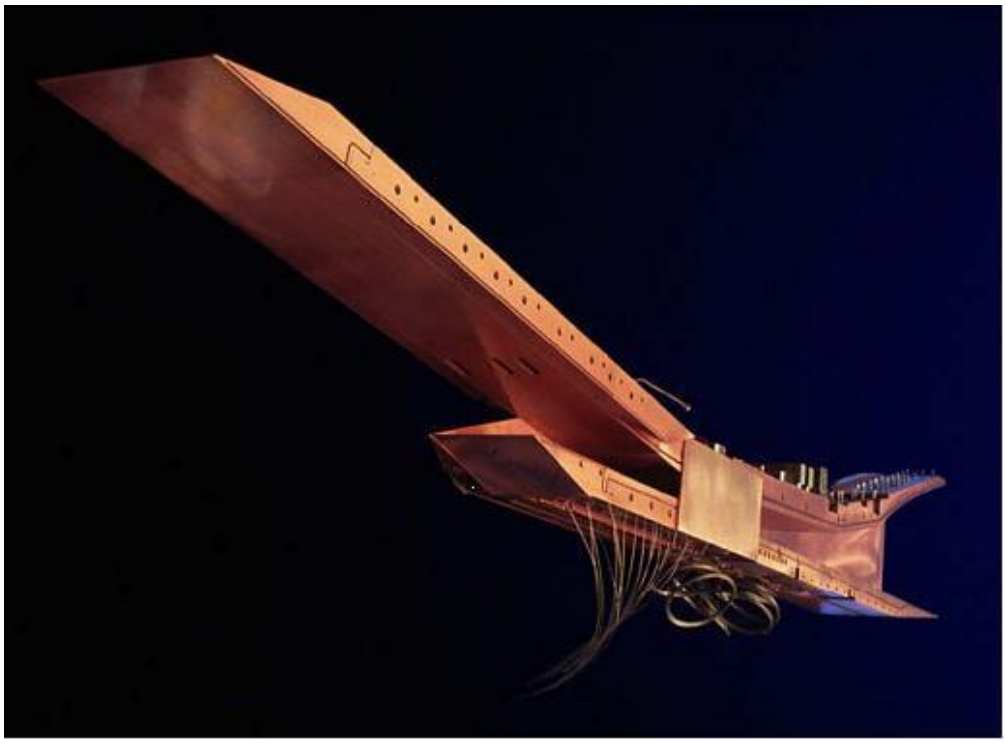

(b)

Figure 1.1 (a) A sketch of scramjet engine [30].

(b) Geometry of inlet section and the nozzle [31].

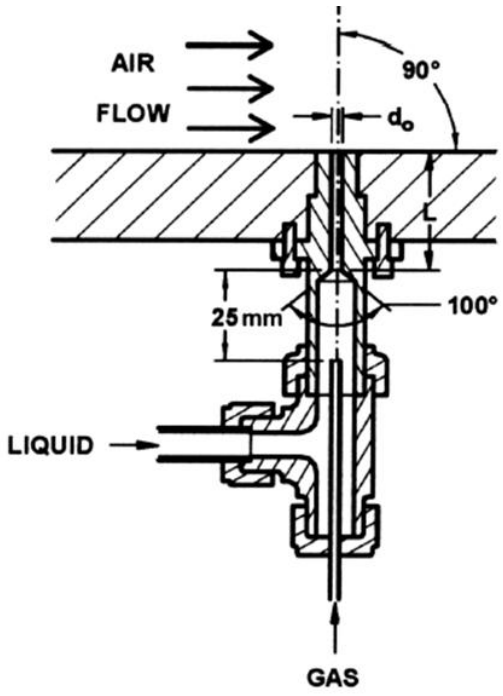

Figure 1.2 Typical aerated fuel injector (Sallam et.al, [22]).

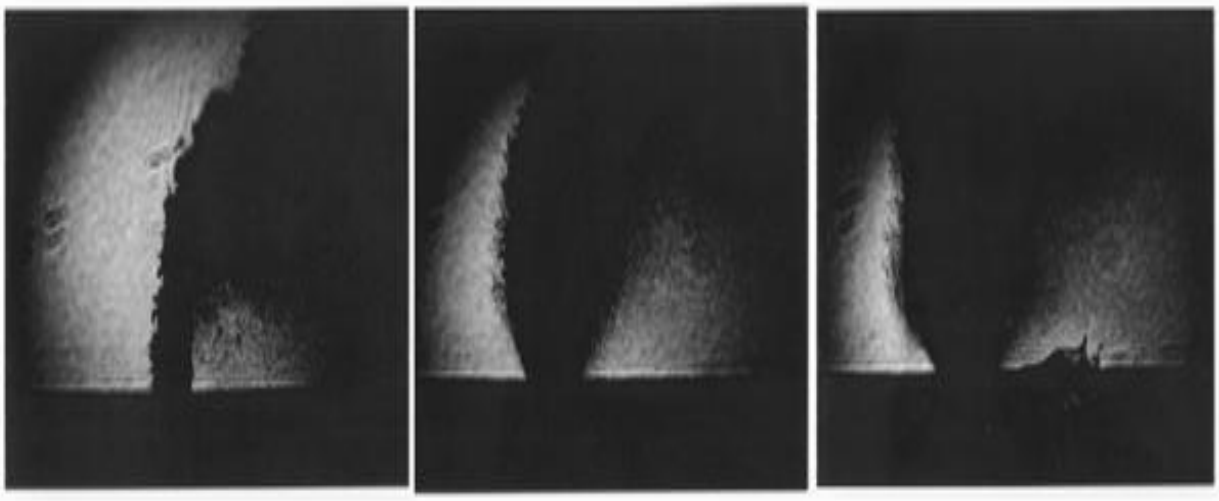

(a) (b) (c)

Figure 1.3 Shadowgraph of aerated liquid jet injected in supersonic crossflow (M =1.97) at various aeration levels (a) GLR = 0 (b) GLR = 2% (c) GLR = 4% (Sallam et.al, [22]).

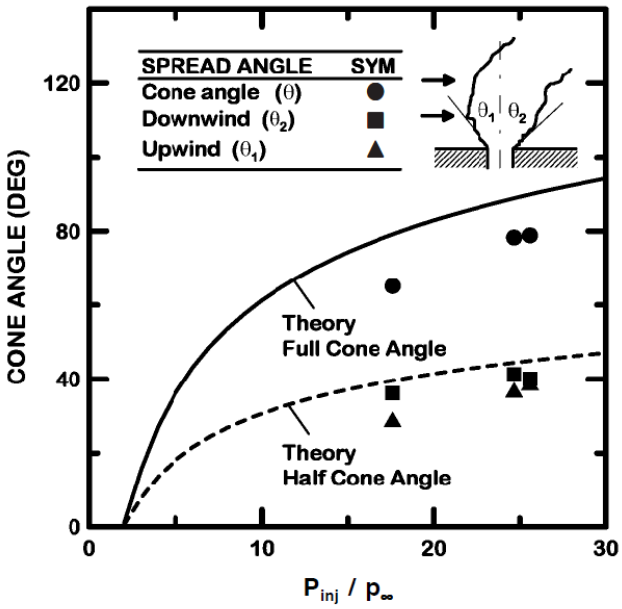

Figure 1.4 Jet expansion angle near the injector region as a function of injector pressure ratio (Sallam et al [22]).

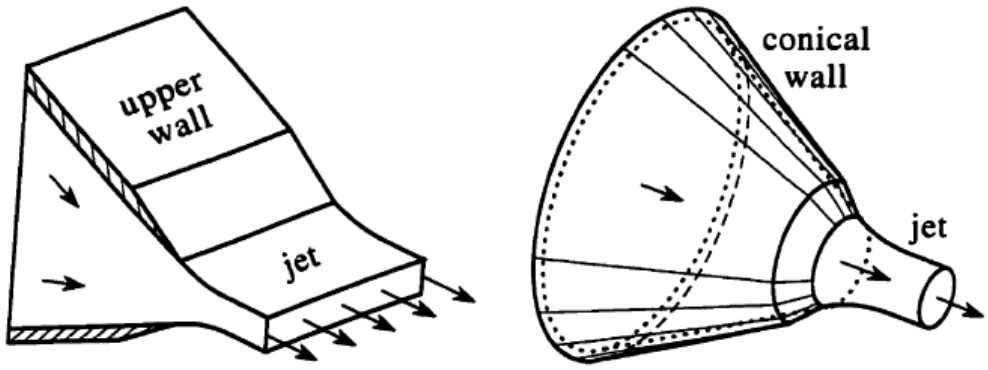

(a) **(b)**

Figure 1.5 Injector configurations for (a) planar (two-dimensional) (b) axisymmetric (Linfield [29]).

CHAPTER II

NUMERICAL AND THEORETICAL METHODS

2.1 Introduction

This chapter includes numerical methods used for the simulation, theoretical validation for air jet in planar geometry, and experimental validation of the results for air jet in axisymmetric geometry. The mesh generation for planar and axisymmetric jet, numerical scheme used for simulation and the boundary conditions used for simulation are discussed in numerical method section.

2.2 Numerical Methods

This section describes the mesh generation, and the numerical schemes used for simulating air jet as well as aerated liquid jet through supersonic nozzle. This numerical model is used to analyze the flow field of air jet and aerated liquid jet coming out from under expanded supersonic nozzle.

2.2.a Mesh Structure

Mesh structure and geometry of the injector is discussed in this section. There are two different types of structures; one is for planar geometry and other one for axisymmetric one.

2.2.a.I Mesh generation for theoretical validation

Schematic of a full-configuration of 2D geometry without assuming a plane of symmetry within the flow field is as shown in Fig. 2.1. It is used with initial grid of 8,000 cells. The mesh is refined within the chamber at the exit of nozzle with final grid size of 55,000 cells. The grid was uniform and quadrilateral face cells were used to mesh the computational domain in order to maintain a good computational

accuracy. The mesh region at the exit of the nozzle inside the chamber was refined. Fine mesh was made by adapting the region. For that refinement, adaptive feature of the fluent was employed.

2.2.a.II Mesh generation for experimental validation

Experimental validation of the numerical methods is done using axisymmetric injector configuration. Axisymmetric geometry is generated as explained in Appendix. I. The mesh structure for axisymmetric geometry is as shown in Fig.2.2. Axisymmetric geometry is used with initial grid of 1800 cells. Refinement of the mesh is done at the exit of nozzle inside the chamber. Initial grid size is 1800 cells and after refinement grid size becomes fine with 200,000 cells. Refinement of the mesh is done using adapting the defined region.

2.2.a.III Mesh generation for aerated liquid jet

Mesh generation for both 2D and axisymmetric aerated liquid jet is similar to 2D gas-only jet mesh generation. However, mesh is more refined than gas-only injector mesh. Mesh structure for planar as well as axisymmetric geometry is shown in Fig.2.3 and 2.4 respectively. For 2D configuration refined grid is with 370,000 cells, and for axisymmetric configuration refined grid is with 480,000 cells. The same method of adaption is used for both cases, i.e. adapting the defined region.

2.2.b Numerical Scheme

Different numerical formulations are used for gas-only jet and aerated liquid jet. These numerical formulations are briefly discussed in this section. Pressure based solver was used to simulate the compressible gas and aerated liquid jet. Originally pressure based solver was designed only for low speed incompressible flows, however recently this method is improved and extended for using wide range of flow conditions.

2.2.b.I Computational method for air jet

Numerical schemes used for air jet and aerated liquid jet is similar. The boundary conditions for the gas-only jet was made similar to the aerated liquid jet by using an inlet boundary condition with air mass flow rate and a liquid flow with almost-zero mass flow rate. Implicit formulation was used as required by FLUENT to simulate the compressible gas. For simulating the compressible gas, coupled pressure velocity coupling scheme was used. Least square cell based gradient type was used with second order discretization method. second order upwind scheme was introduced for getting accurate results The convergence was judged based on continuity, x-, y-, velocity, energy, k-, ω- residuals to drop at least by 3 orders of magnitude.

2.2.b.II Computational method for aerated liquid jet

To simulate the aerated liquid jet multiphase model is used. In this multiphase system, air is considered as compressible phase and liquid water as incompressible fluid. For solving multiphase system, Euler-Euler approach is used. In this approach, different phases are treated mathematically and conservation equations for each phase should be derived to obtain the set of governing equations for all phases in the system. There are three different multiphase models are available and out of that VOF model is used in this case.

A. VOF Model

To analyze the behavior of liquid gas interface in aerated liquid jet, VOF formulation was used in Ansys Fluent. This formulation is used for solving single set of momentum equations and tracking the volume fraction of each phase inside the computational domain. In VOF model, the volume fraction of all phases sum to unity. The volume fraction of each of the phases is known at each and every location and thus the variables and properties in any given cell will represent one of the phases or mixture of the phases.

Suppose q^{th} fluid's fraction in the mesh cell is denoted as α_q and there are three different conditions are possible inside the domain.

$\alpha_q = 0$: cell is empty for fluid q

$\alpha_q = 1$: cell is full of the fluid q

$0 < \alpha_q < 1$: cell contains the interface between q^{th} fluid and one or more other fluids.

Continuity equation for volume fraction is used to track the interface between one or more phases. For the q^{th} phase the volume fraction is given by:

$$\frac{1}{\rho_q}\left[\frac{\partial}{\partial t}(\alpha_q \rho_q) + \nabla.\left(\alpha_q \rho_q \overrightarrow{v_q}\right) = S_{\alpha_q} + \sum_{p=1}^{n}(\dot{m}_{pq} - \dot{m}_{qp})\right] \quad (2.1)$$

where $\dot{m}_{pq}$ is the mass transfer from phase p to phase q and $\dot{m}_{qp}$ is the mass transfer from phase q to phase p. S_{α_q} is source term which is constant or user defined mass source for each phase. The primary phase volume fraction should be calculated based on the following constraints:

$$\sum_{q=1}^{n} \alpha_q = 1 \quad (2.2)$$

The phases in each control volume can be determined by the properties of the transport equations and in two phase system with subscripts 1 and 2, density can be calculated as below:

$$\rho = \alpha_2 \rho_2 + (1 - \alpha_1)\rho_1 \quad (2.3)$$

To get the resulting velocity field among the phases by solving the single momentum equation and this depends on the density and dynamic viscosity of phases:

$$\frac{\partial}{\partial t}(\rho v) + \nabla.(\rho \overrightarrow{v}\overrightarrow{v}) = -\nabla p + \nabla.[\mu(\nabla \vec{v} + \nabla \vec{v}^T)] + \rho\vec{g} + \vec{F} \quad (2.4)$$

where p is the pressure and μ is the dynamic viscosity, $\rho\vec{g}$ and $\vec{F}$ represents gravitational body force and surface tension force respectively. Velocity field will get affected adversely if there is large velocity difference existing between two phases and this is the only limitation for this approximation. Evaporation-condensation model is enabled in this simulation; as there is mass transfer occurs across the air and water. Evaporation and condensation frequency is specified as 0.1 by default for VOF formulation.

B. Solver

The Volume of Fluid (VOF) model in FLUENT was computed using the segregated implicit solver employing the first-order implicit time-stepping. A segregated solver solves the continuity, momentum, energy, species, and additional scalar equations (i.e., turbulence equations) sequentially. The manner in which the governing equations are linearized to facilitate their solution may take an "implicit" or "explicit" form with respect to the dependent variable (or set of variables) of interest. In short, the segregated implicit approach solves for a single variable field (i.e., pressure) by considering all cells simultaneously, before computing other dependent variables (i.e., velocity, etc.) in the same manner. The segregated implicit solver uses under-relaxation to control the update of computed variables at each iteration.

C. Discretization

The flow surrounding the liquid-gas interface involved a curved domain. As such, the PRESTO! discretization for pressure interpolation in FLUENT software applicable for solving flows within strongly curved domains was employed in this study. Coupled discretization with Coupled with Volume Fractions for pressure-velocity coupling which solves all equations for couples velocity corrections, shared pressure corrections and the correction for volume fraction simultaneously. Second order discretization scheme was applied for reasonable stability for pressure-correction equation and gives good results for calculating compressible flows with shocks and applied to volume fraction equations to minimize the diffusivity and accuracy of the converged solution.

2.2.c Boundary Conditions

Numerical Simulation of aerated liquid jet through supersonic nozzle was conducted for nozzle diameter of 1 mm. The liquid and gas properties as well as test conditions considered during the present investigation are summarized below:

1. Velocity inlet boundary condition used for liquid jet inlet, and velocity of liquid was maintained such that Gas to Liquid Ratio (GLR) should be 4 %.
2. Mass flow inlet condition was used for air and it was constant.
3. Pressure outlet boundary condition was used for the chamber.
4. No slip wall boundary condition was used for wet and non-wet surfaces.

The test conditions for different flow configuration are detailed at the end of the chapter.

2.2.f Solution Convergence:

The convergence criteria are based on continuity and x-, y- and z-velocity, energy, omega and volume fraction of water residuals. A popular approach for judging the convergence is to require the unscaled residuals to drop by three orders of magnitude in each time step. However, this particular approach is not appropriate in the following cases: (1) If a good initial guess is provided, (2) if the governing equation contains non-linear source terms, and (3) if the variable of interest is nearly zero everywhere. In the present study, integrated quantities were monitored in addition to examining residual levels in order to determine convergence. At the beginning of the simulation when the jet was placed in still air, the jet diameter was monitored at a fixed stream wise distance from the nozzle exit and the solution was judged to be convergent when the jet diameter agrees with the experimental data of jet diameter. Additionally the effect of the presence of surface tension at the liquid-gas interface was evaluated on a two-dimensional cylindrical element, as shown in Fig. 3.4(a). The pressure enclosed within a two-dimensional liquid column is balanced by the surface tension: When under expanded supersonic jet is coming out of the convergent nozzle, it expands because the outside pressure is less than nozzle exit pressure. Then, the flow at the edge turns out by sending the Prandtl-Meyer expansion waves. When, these P-M expansion

waves go outward as the flow expands further and these expansion waves reach the outer boundary. This makes the inside pressure lower than outside and forces the flow to turn back in and pressure rise occurs across an oblique shock. These alternate expansion and compression waves are repeated until the kinetic energy of the flow is dissipated by shock waves and viscous dissipation.

2.3 Theoretical Validation

Theoretical analysis of compressible flow through supersonic nozzles will be discussed in this section. A one dimensional compressible flow with wall friction is passing through a constant area duct where the effect of friction is considered. The flow is to be considered as steady, isentropic and without body forces. This type of compressible flow through the duct with friction, but without heat transfer is termed as "Fanno flow". Properties of the flow changed due to wall friction along the duct. For this, the compressible flow is passing through the injector as shown in Fig.2.5. Inlet pressure at location 1 is 13.50 atm. To calculate the pressure at location 2, use fanno flow friction equation. This gives the exit flow condition through a constant diameter duct with friction

$$\left(\frac{f\,L_{max}}{D}\right)_2 = \left(\frac{f\,L_{max}}{D}\right)_3 + \left(\frac{f\,L}{D}\right) \tag{2.5}$$

Exit velocity from the supersonic nozzle is at sonic condition i.e. Mach number of 1. Location 3 is at sonic condition and $M_3 = 1$. $M_3 = 1$ results into $(f\ L_{max}/D)_3 = 0$ and $(f\ L_{max}/D)_2 = 1.05$, $M_2 = 0.50$ and $P_2 = 11$ atm [26]. Pressure inside the chamber is 2.1 atm and it is represented as "P_b" and $P_b = P_4 = P_6 = 2.1$ atm. Compressible isentropic gas is injected through a 1.0 mm diameter injector into a closed chamber. Prandtl-Meyer expansion phenomena take place at the exit of the injector nozzle. Mach number inside the chamber is calculated using the following equation:

$$\frac{P_2}{P_b} = \left(1 + \frac{\gamma-1}{2}\,M^2\right)^{\gamma/\gamma-1} \tag{2.6}$$

Compressible flow exits from location 3 isentropically and the direction of the flow is away from the center. This turning of the flow is called "Prandtl-Meyer function". Prandtl-Meyer function is denoted as 'υ'. The expansion of the under expanded jet takes place at the exit of supersonic nozzle. The stream of

jet which is at Mach 1 expanded to reach the Mach number inside the chamber. Here, flow turns isentropically through initial and final Mach number. It is the maximum angle through which sonic flow (M=1) turned around to reach M = 1.73.

Flow is turned from M_3=1 to M_4= 1.73. Therefore, turning angle from location 3 to 4 is given as below

$$turning = \upsilon_4 - \upsilon_3 \tag{2.7}$$

υ_3= 0 and υ_4 = 18.5^0 [26] Expansion of flow takes place till it matches with the pressure inside the chamber. The flow is turned out to reduce the higher exit pressure to the lower back pressure. This forms the constant pressure boundary inside the chamber which is called as 'free surface'. Pressure is constant across the free surface. When expanded Mach waves intersect with free surface then they were reflected back as compression waves and forms oblique shock wave. These compression waves turn through the same angle as expansion waves turn outwards from the center.

Turning of the Mach waves from location 4 to 5 is given as,

$$turning = \upsilon_5 - \upsilon_4 \tag{2.8}$$

Inward turning of compression waves from free surface is same as outward turning of expansion waves. From this, Prandtl- Meyer function at location 5 is calculated and the values are υ_5= 37^0 and M_5 = 2.40 [26]. Mach number at location 5 is the highest one as shown in Fig.2.6 and pressure at location 5 is the lowest one as shown in Fig.2.7. The pressure at location 5 and 6 calculates the shock wave angle.

P_5 = 0.74 atm and $P_6 = P_b$ = 2.1 atm. Normal Mach number at location 5 is M_{5n}, and M_{5n} = 1.60 @ (P_b / P_5 = 2.82) [26]

$$M_{5n} = M_5 \times sin\theta \tag{2.9}$$

Shock wave angle (θ_5) = 41.6^0 and deflection angle (δ) = 18^0 Normal Mach number at location 6 is M_{6n} and M_{6n} = 0.6684 @ (P_6 / P_5 = 2.82).

$$M_{6n} = M_6 \times \sin(\theta - \delta) \tag{2.10}$$

Mach number at location 6 is M_6 = 1.67, and shock wave angle at location 6 (θ_6) = 66^0 [14].

Normal Mach number at location 6, M_{6n} = 1.50 is calculated accurately using M_6 and θ_6.and the pressure at location at 7 (P_7) = 5.14 bar

$$M_{6n} = M_6 \times sin\,(\theta_6) \tag{2.11}$$

Location 5 is the highest Mach number region with lowest pressure inside the chamber and location 7 is the highest pressure region with lowest Mach number. As a combination of low Mach number and highest pressure, it forms Mach disc at location 7. There are three types of shock waves: normal shock, oblique shock and Prandtl-Meyer expansion wave. Shock wave is very thin section of the flow, across which sudden changes in fluid properties take place. Pressure, temperature, density and Mach number of the fluid flow take place across the shock wave. Shock wave is characteristic of supersonic compressible flow only. When the shock waves occur normal to the direction of the flow is called as Normal shock. Enthalpy remains constant across this shock. Supersonic flow across the normal shock becomes subsonic. In the normal shock there is no heat or work exchange and because of this there is no change in pressure, temperature and enthalpy across this shock. But, Mach number changes substantially across the normal shock. In certain situations shock is not normal to the flow and in such cases shock waves are inclined at a certain angle to the flow. These shock waves are known as oblique shocks. The angle though which turning of the flow occurs is known as deflection angle and the inclination of the shock is known as shock angle. In oblique shocks downstream Mach number may be supersonic, sonic or subsonic depends on the upstream Mach number and deflection angles. Normal component of velocity does not change across the oblique shock however, tangential component of velocity changes across the oblique shock. The properties of the flow across the oblique shock depend on deflection angle, shock angle and Mach number of the upstream flow. They are interlinked with each other and properties across the oblique shock will get from them. In some flow situations, supersonic flow is expanding which is known as expansion fan or expansion waves. In some oblique shock case flow is expanding across the one of the corner and which originates infinite number of Mach waves from the particular point. These Mach waves referred as

Prandtl-Meyer expansion waves. Difference between upstream and downstream Prandtl-Meyer function gives the turning angle value across the expansion fan.

2.4 Experimental Validation

The supersonic gas-only jet injected through under-expanded axisymmetric nozzle configuration forms alternate expansion and compression waves at the exit of the nozzle. In under-expanded jet, nozzle exit pressure is much higher than the back pressure, result into the jet expansion. Once the pressure of the expanded jet matches with surrounding pressure the expansion waves start reflecting from the jet boundary as compression waves. In case of axisymmetric flow, the jet is highly underexpanded and due to high NPR, compression waves coalesce to form the mach disk at the center of the jet.

The experimental results of Baek [27] for axi-symmetric gas-only jet are used in this section to validate the present computational methods. The location of the Mach disk and its diameter were computed using an axisymmetric mesh outlined in Fig. 2.10 and compared it with the experimental results. The empirical equation was developed for highly underexpanded sonic jets by Baek [27] for supersonic dry air jet injection is as follows:

$$\frac{x_m}{D_e} = 0.65 \left({P_0}/{P_b} \right)^{\frac{1}{2}} \tag{2.12}$$

$$\frac{D_m}{D_e} = 0.36 \left({P_0}/{P_b} - 3.9 \right)^{\frac{1}{2}} \tag{2.13}$$

This equation predicts the location of Mach disk in supersonic dry air jet injection. Location of Mach disk depends on Nozzle Pressure Ratio (NPR). Theoretical calculation for location and diameter of the Mach disk from the exit of the nozzle at P_b = 1.17 atm, P_0 = 22.50 atm and D_e = 1 mm is x_m = 2.85 mm, D_m = 1.30 mm. Present computational results show the Mach disk location and diameter are, x_m= 2.75 mm and D_m= 1.2 mm. The computational and experimental results show that the location and diameter of the Mach disk is influenced by NPR.

Contours of static gauge pressure and stagnation gauge pressure are shown in Figs. 2.8 and 2.9, respectively. Compressible air flow through injector follows the fanno flow principle. Due to coalesce of compression waves Mach disk region is highly compressed and heated one. Therefore, Mach disk region has the highest pressure and highest temperature region inside the chamber. Contours of Mach number and velocity vectors are shown in Figs.2.10 and 2.11, respectively. The flow field at upstream of the Mach disk is supersonic and becomes subsonic at downstream, due to high compression phenomena occurs across the Mach disk. There is also change in the direction of velocity vectors once they cross the Mach disk. Directions of velocity vectors are parallel to the flow field after crossing the Mach disk as shown in Fig.2.11.

2.5 Test Conditions

The boundary conditions and properties of liquid and gas for three different cases are summarized in Tables 2.2, 2.3, 2.4. To use the same boundary conditions and numerical scheme, velocity inlet condition for water is reduced till 1×10^{-5} m/s in case of planar gas-only injector. The effect of the injector geometry on the internal flow is shown by comparing the contours of static gauge pressure inside the injector for gas-only jet and aerated liquid jet as shown in Fig. 2.14. The injection pressures values were determined based on the boundary conditions detailed in Chapter 2. As the Compressible gas flows though the injector passage, the effect of wall friction becomes significant. Typical of Fanno line flow the viscous forces causes the flow properties to change along the duct. As the flow approaches to the nozzle, the pressure decreases and the velocity of the flow increase. The internal flow field of planar gas-only jet, planar aerated liquid jet, and axisymmetric aerated liquid jet are similar. However, the static gauge pressure values vary inside the nozzle among these three cases. The difference between the aerated liquid jet and the gas-only jet due can be attributed to the presence of liquid surrounding the gas.

Table 2.1 Theoretical and computational results of 2D gas-only jet configurations

Terms	Computational values	Theoretical values
P_1	13.50 (atm)	13.5 (atm)
P_2	10.90 (atm)	11 (atm)
$P_4 = P_6$	2.1 (atm)	2.1 (atm)
P_5	0.77 (atm)	0.74 (atm)
P_7	**5.15 (atm)**	**5.14 (atm)**
M_4	1.80	1.74
M_5	**2.32**	**2.41**
M_6	1.74	1.67

Table 2.2 Fluid properties and test conditions employed in the numerical investigation of 2D gas-only injector

Fluid	Compressible air
Specific heat (J/kg-k)	1006.43
Thermal conductivity (w.m-k)	0.0242
Viscosity (kg/m-s)	1.79E-05
Molecular weight (kg/kgmol)	28.966
Standard state enthalpy (J/kgmol)	0
Reference temperature	298.15
Boundary conditions	
Mass flow inlet (kg/s)	0.0018
Pressure outlet (atm)	1.17

Fluid	Water
Density (kg/m3)	998.2
Specific heat (J/kg-k)	4182
Thermal conductivity (w.m-k)	0.6
Viscosity (kg/m-s)	1.003E-03
Molecular weight (kg/kgmol)	18.0152
Standard state enthalpy	-2.858412E+08
Reference temperature	298
Boundary conditions	
Velocity inlet (m/s)	1e-5
Pressure outlet (atm)	1.17

Table 2.3 Fluid properties and test conditions employed in the numerical investigation of axisymmetric gas-only injector

Fluid	Compressible air
Specific heat (J/kg-k)	1006.43
Thermal conductivity (w.m-k)	0.0242
Viscosity (kg/m-s)	1.79E-05
Molecular weight (kg/kgmol)	28.966
Standard state enthalpy (J/kgmol)	0
Reference temperature	298.15
Boundary conditions	
Mass flow inlet (kg/s)	0.0056
Pressure outlet (atm)	1.17

Fluid	Water
Density (kg/m3)	998.2
Specific heat (J/kg-k)	4182
Thermal conductivity (w.m-k)	0.6
Viscosity (kg/m-s)	1.003E-03
Molecular weight (kg/kgmol)	18.0152
Standard state enthalpy	-2.858412E+08
Reference temperature	298
Boundary conditions	
Velocity inlet (m/s)	1e-5
Pressure outlet (atm)	1.17

Table 2.4 Fluid properties and test conditions employed in the numerical investigation of 2D aerated liquid jet injector

Fluid	Compressible air
Specific heat (J/kg-k)	1006.43
Thermal conductivity (w.m-k)	0.0242
Viscosity (kg/m-s)	1.79E-05
Molecular weight (kg/kgmol)	28.966
Standard state enthalpy (J/kgmol)	0
Reference temperature	298.15
Boundary conditions	
Mass flow inlet (kg/s)	0.0018
Pressure outlet (atm)	1.17

Fluid	Water
Density (kg/m3)	998.2
Specific heat (J/kg-k)	4182
Thermal conductivity (w.m-k)	0.6
Viscosity (kg/m-s)	1.003E-03
Molecular weight (kg/kgmol)	18.0152
Standard state enthalpy (J/kgmol)	-2.858412E+08
Reference temperature	298
Boundary conditions	
Velocity inlet (m/s)	22.5
Pressure outlet (atm)	1.17

Table 2.5 Fluid properties and test conditions employed in the numerical investigation of axi-symmetric aerated liquid jet injector

Fluid	Compressible air
Specific heat (J/kg-k)	1006.43
Thermal conductivity (w.m-k)	0.0242
Viscosity (kg/m-s)	1.79E-05
Molecular weight (kg/kgmol)	28.966
Standard state enthalpy (J/kgmol)	0
Reference temperature	298.15
Boundary conditions	
Mass flow inlet (kg/s)	0.005756
Pressure outlet (atm)	1.17

Fluid	Water
Density (kg/m3)	998.2
Specific heat (J/kg-k)	4182
Thermal conductivity (w.m-k)	0.6
Viscosity (kg/m-s)	1.003E-03
Molecular weight (kg/kgmol)	18.0152
Standard state enthalpy (J/kgmol)	-2.858412E+08
Reference temperature	298
Boundary conditions	
Velocity inlet (m/s)	22.5
Pressure outlet (atm)	1.17

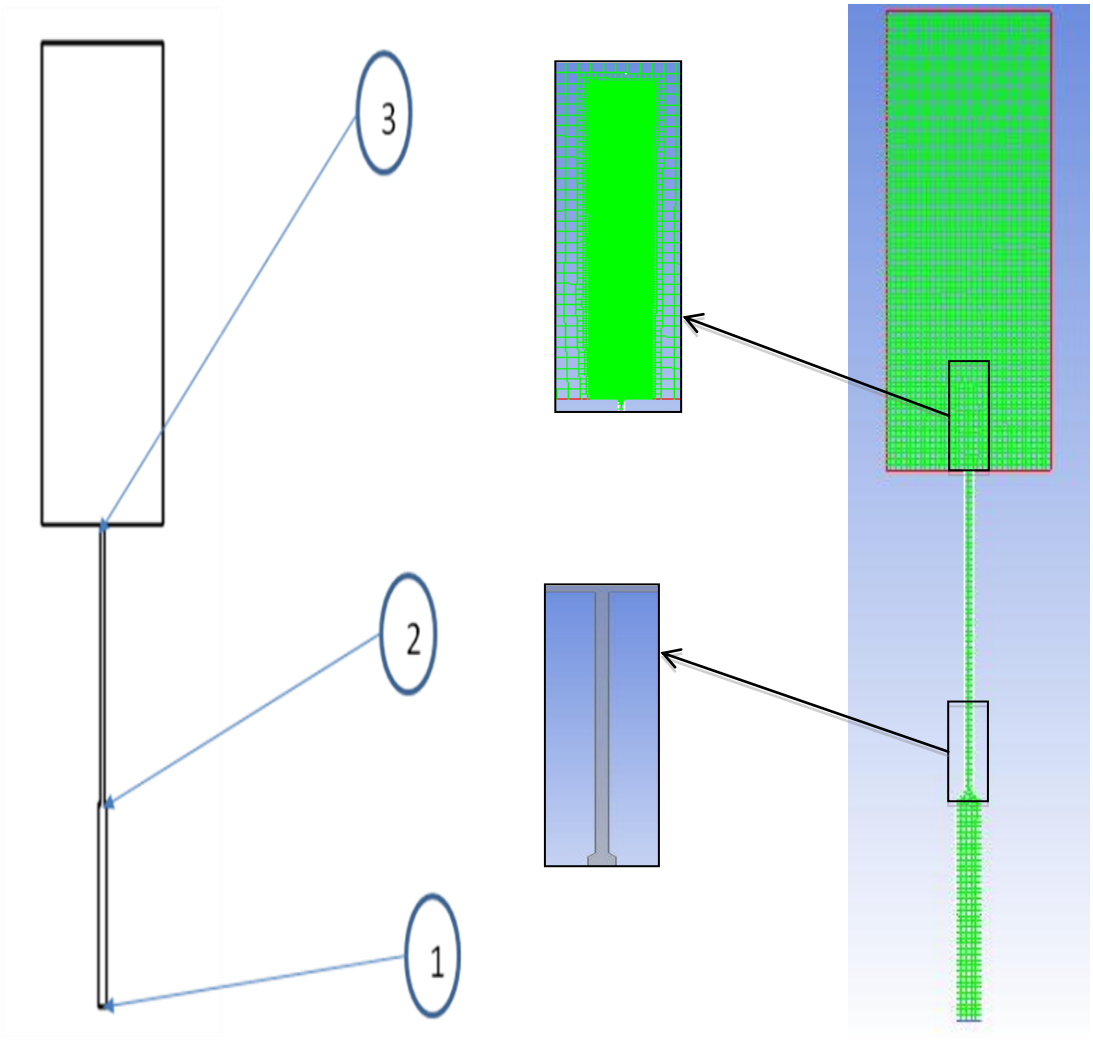

Figure 2.1 Schematic of geometry and mesh structure 1. Inlet, 2. Convergent section, 3. Exit of the fuel injector.

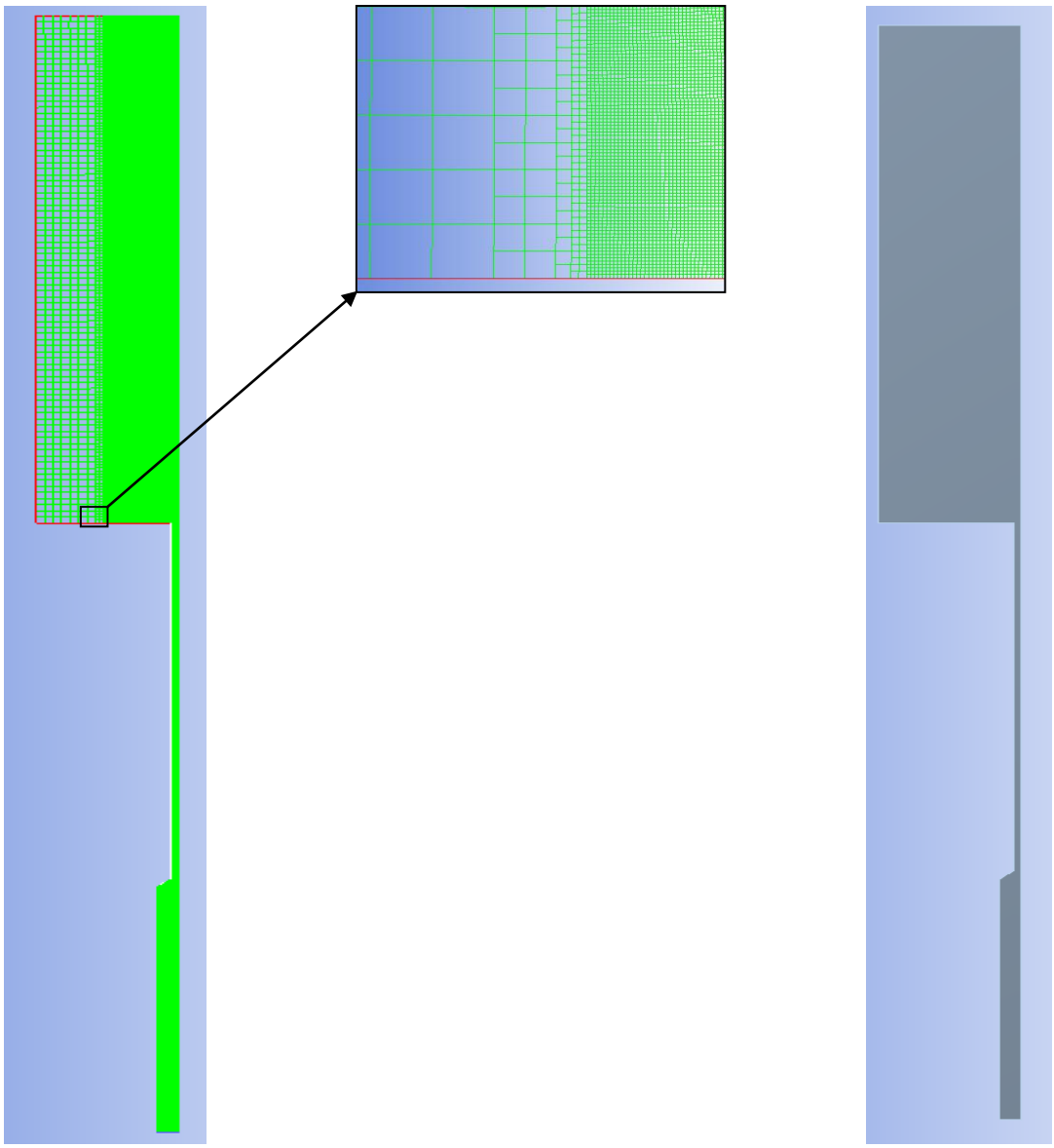

Figure 2.2 Mesh structure for axisymmetric geometry (only half the geometry is shown).

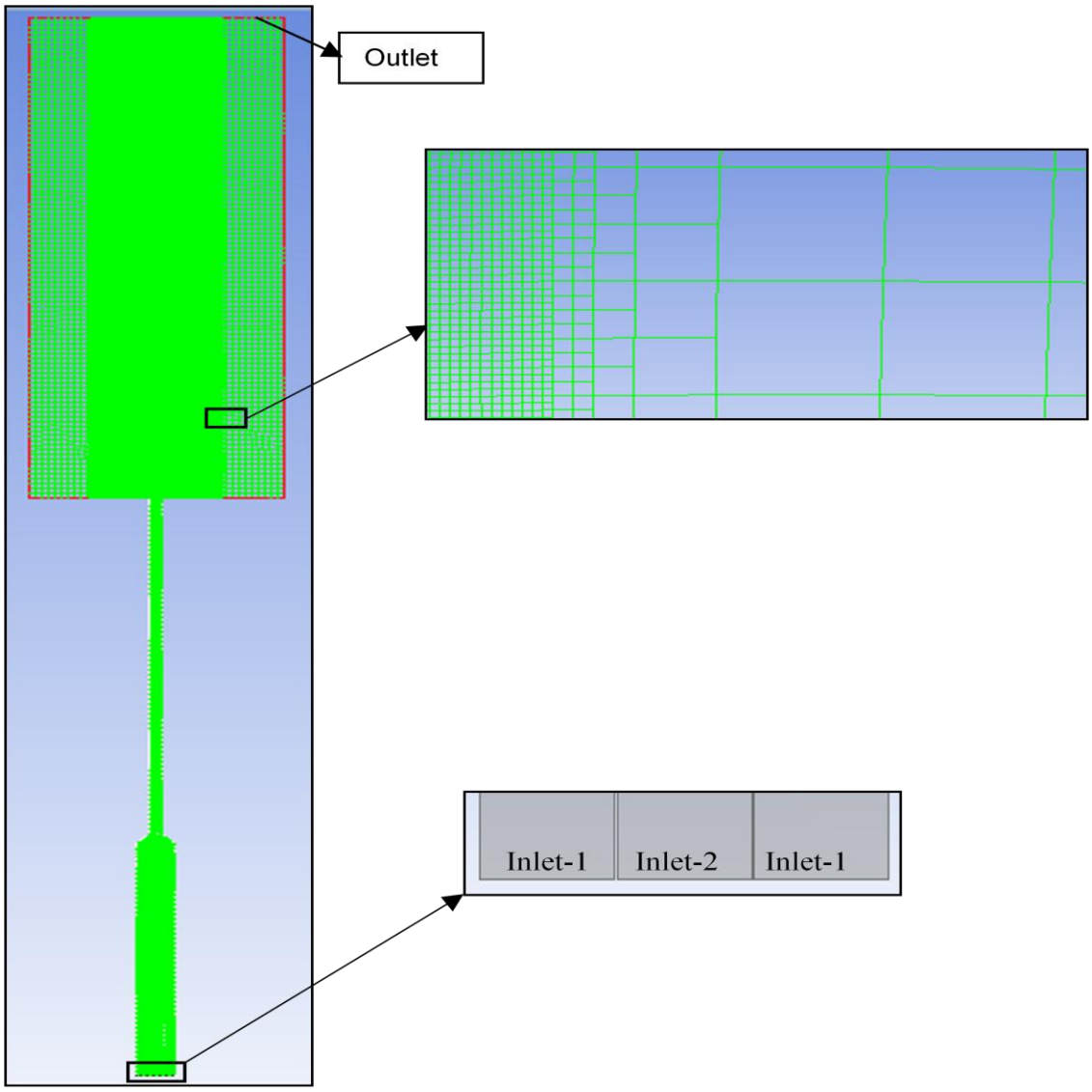

Figure 2.3 Mesh structure for aerated liquid injector (Planar geometry).

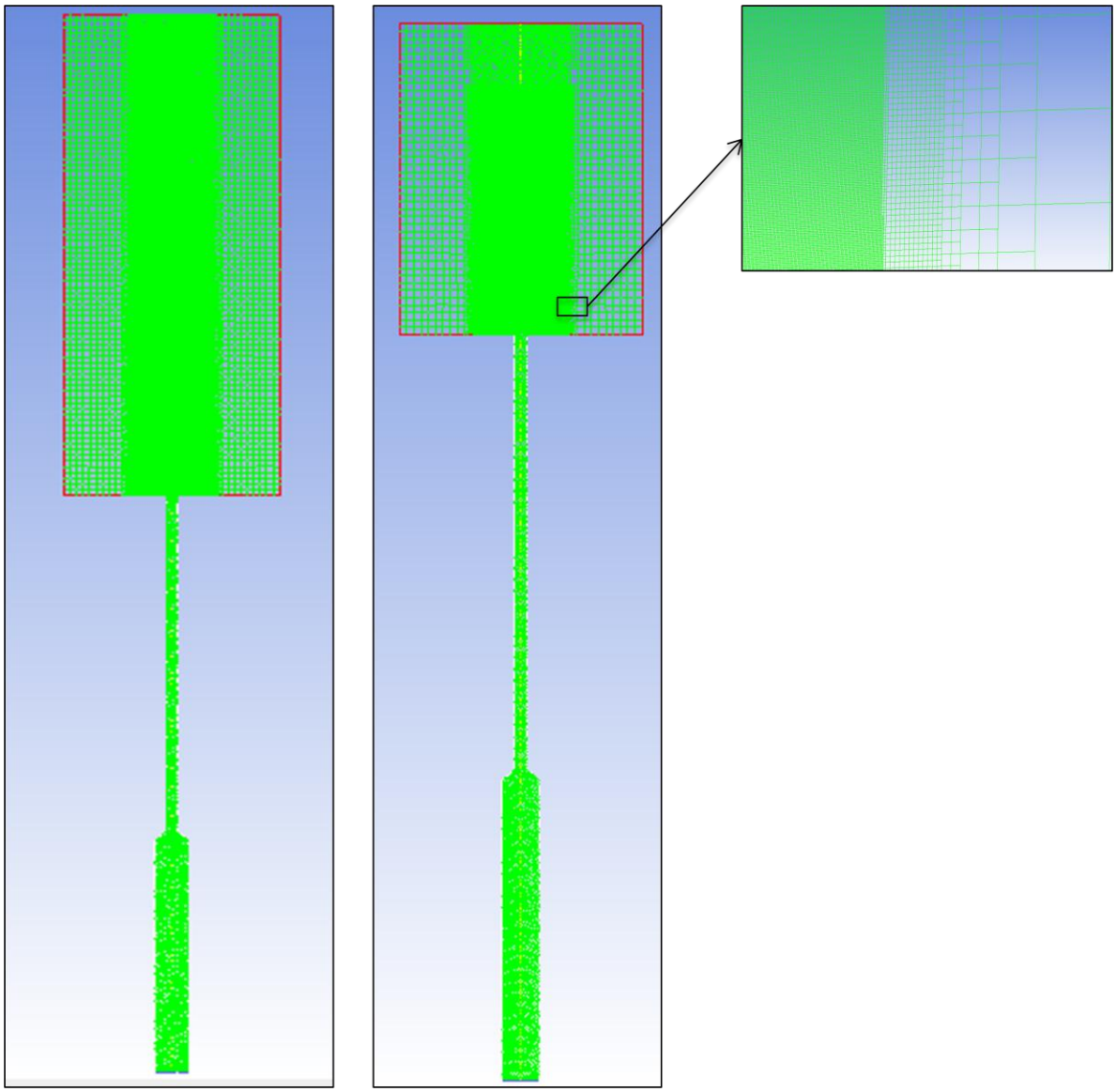

Figure 2.4 Mesh structure for aerated liquid injector (Axisymmetric geometry).

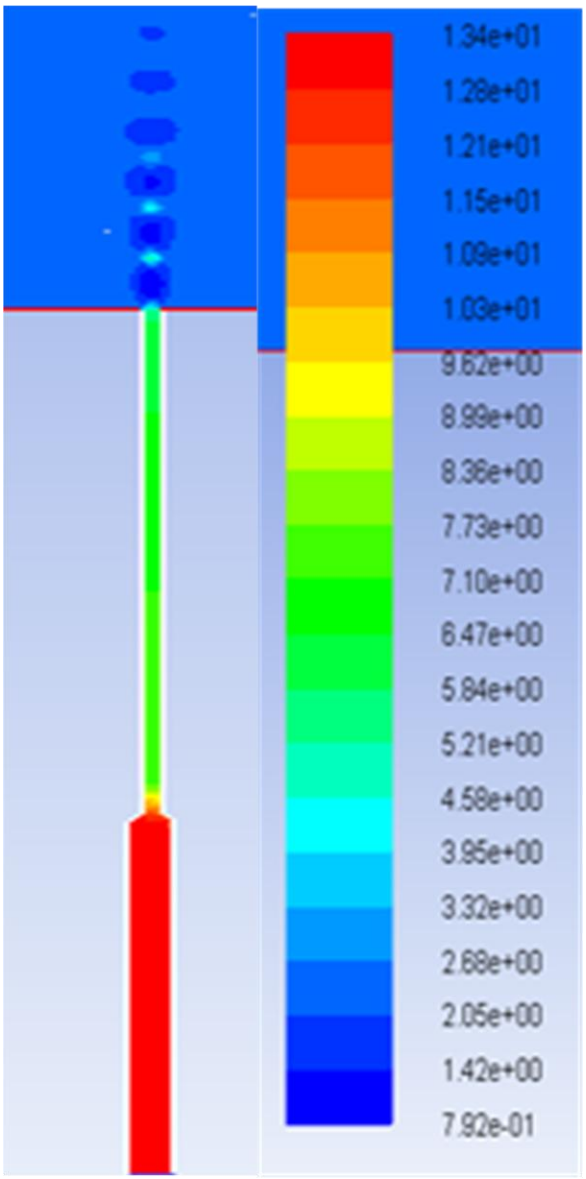

Figure 2.5 Contours of the static gauge pressure inside the injector (the legend is showing pressure values in units of atm).

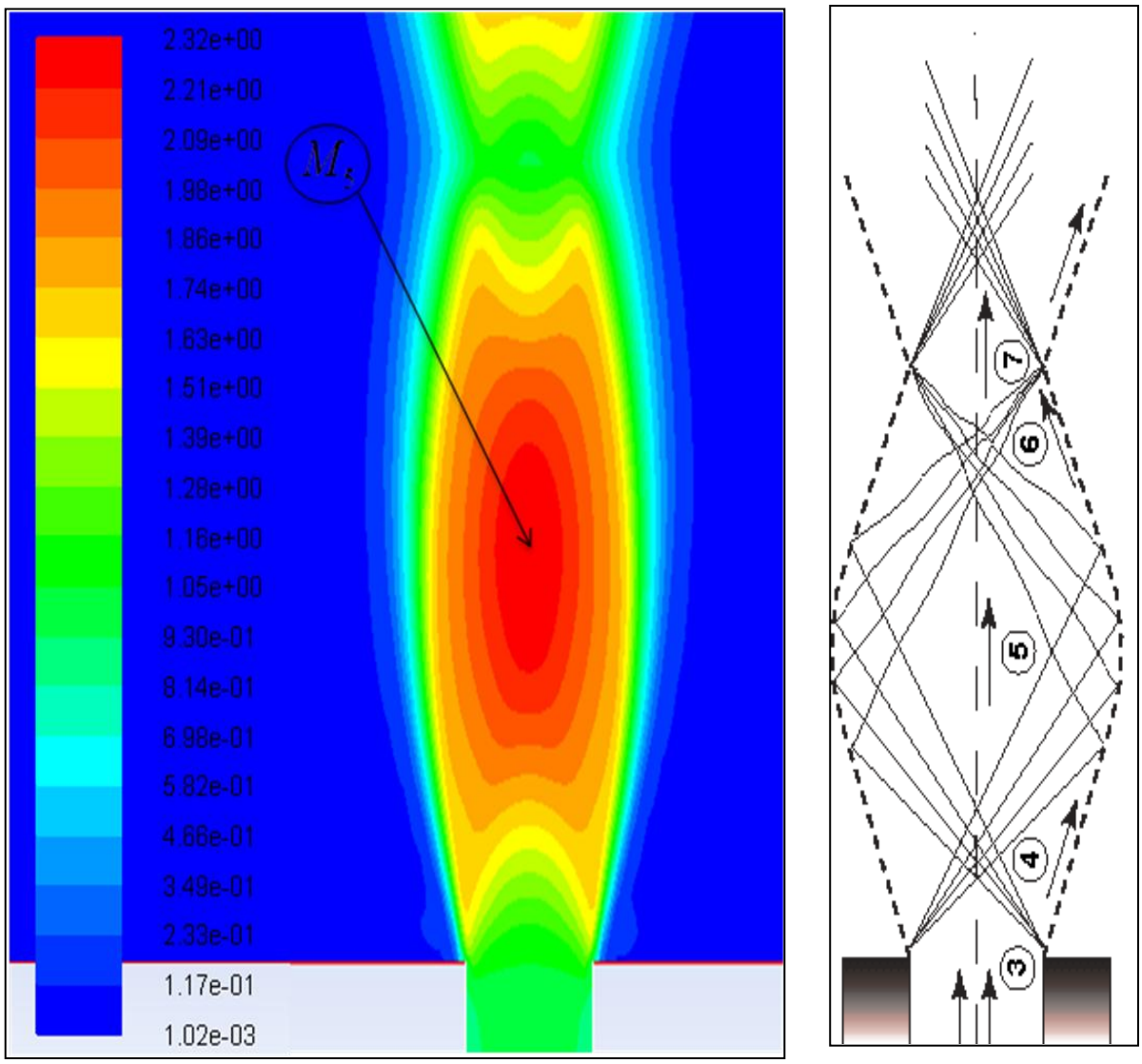

(a) **(b)**

Figure 2.6 Schematic of external flow field for underexpanded nozzle (a) simulation results of Mach number contours (b) schematic of flow structure.

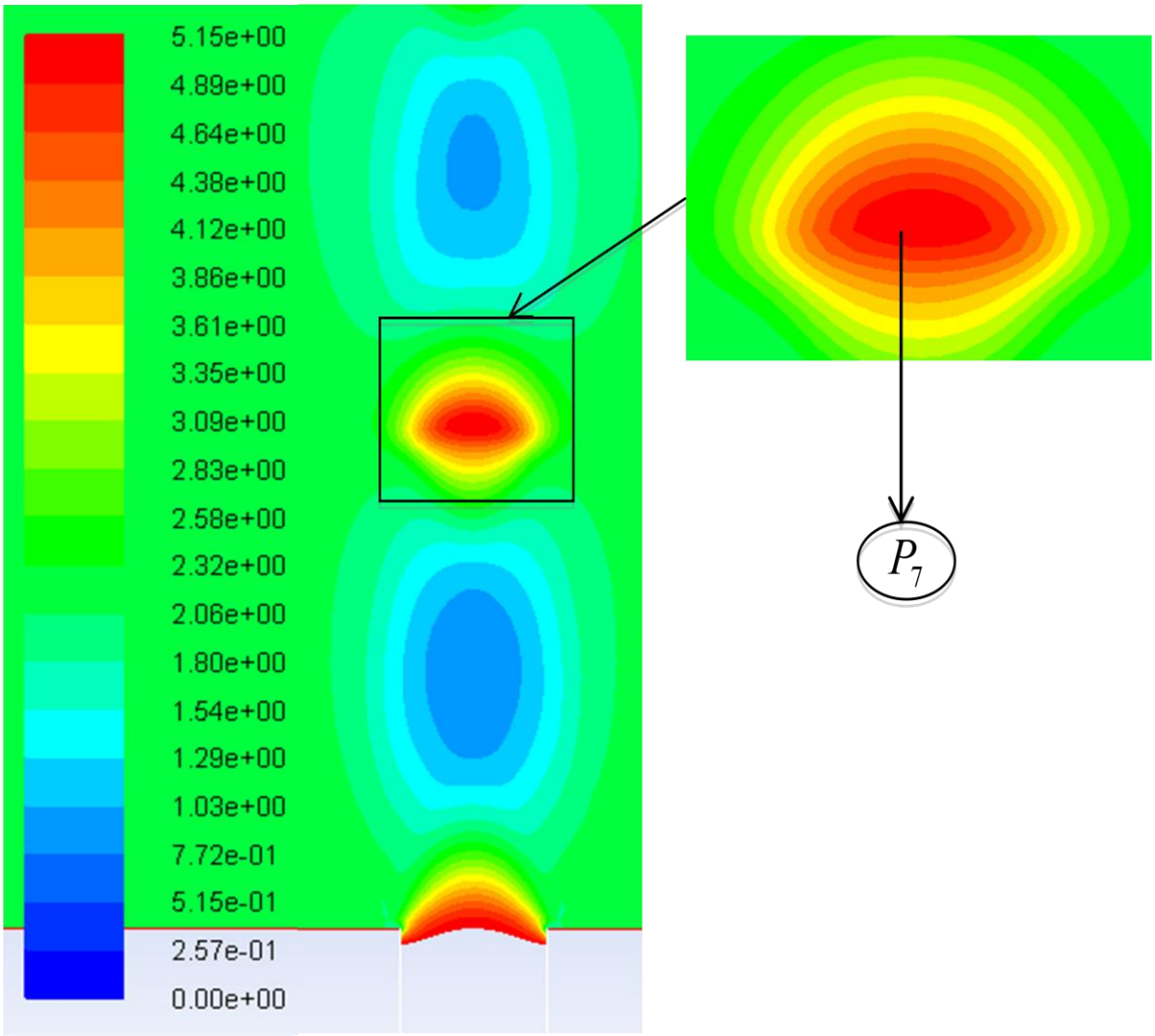

Figure 2.7 Contours of static gauge pressure inside the chamber. The inset is showing the location of maximum pressure (P_7) due to coalescence of the oblique shock waves (the legend is showing pressure values in units of atm).

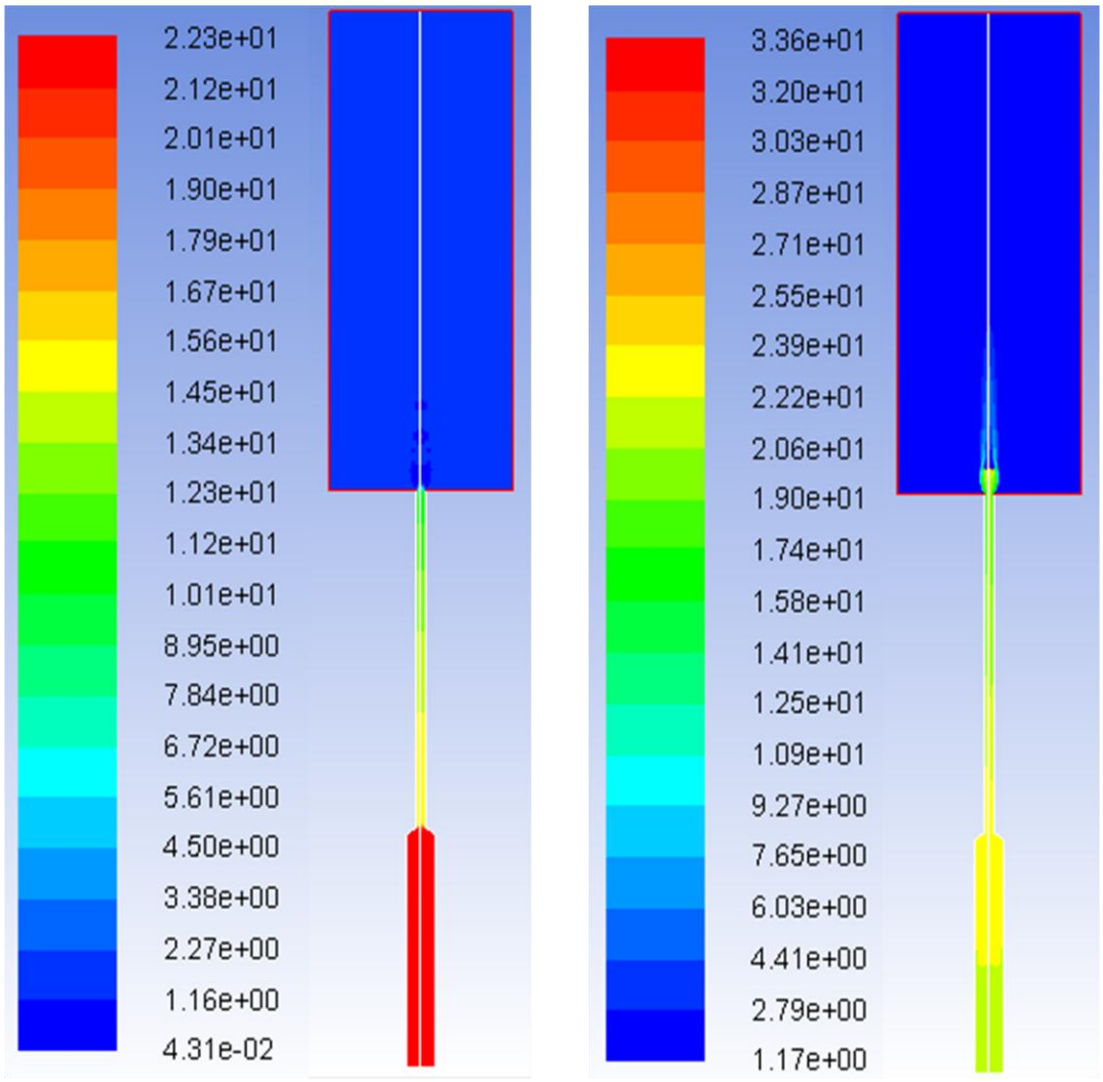

(a) (b)

Figure 2.8 Contours of gauge pressure (a) static pressure (b) stagnation pressure (the legend is showing pressure values in units of atm).

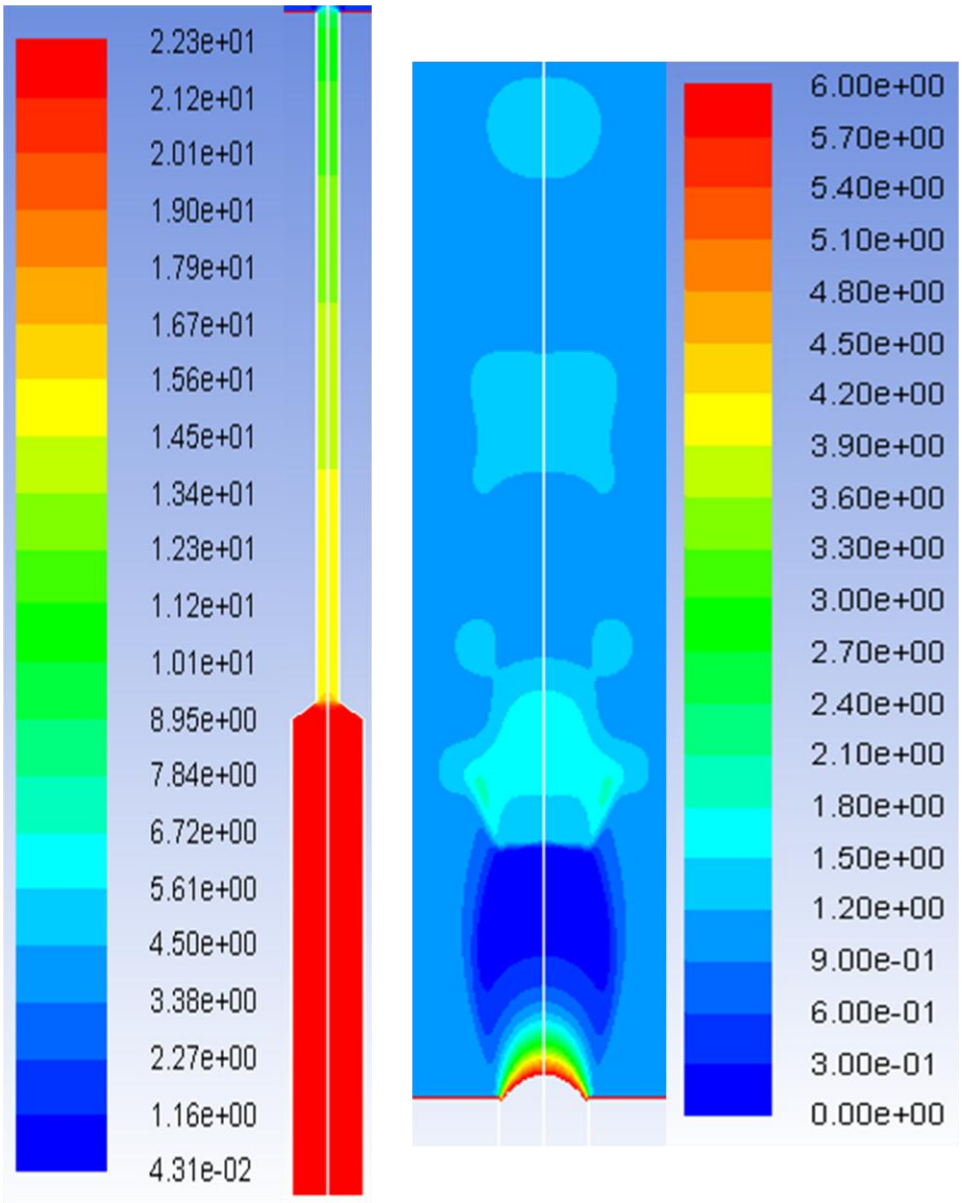

(a) (b)

Figure 2.9 Contours of static gauge pressure (a) Inside the injector (b) At exit of the injector (the legend is showing pressure values in units of atm).

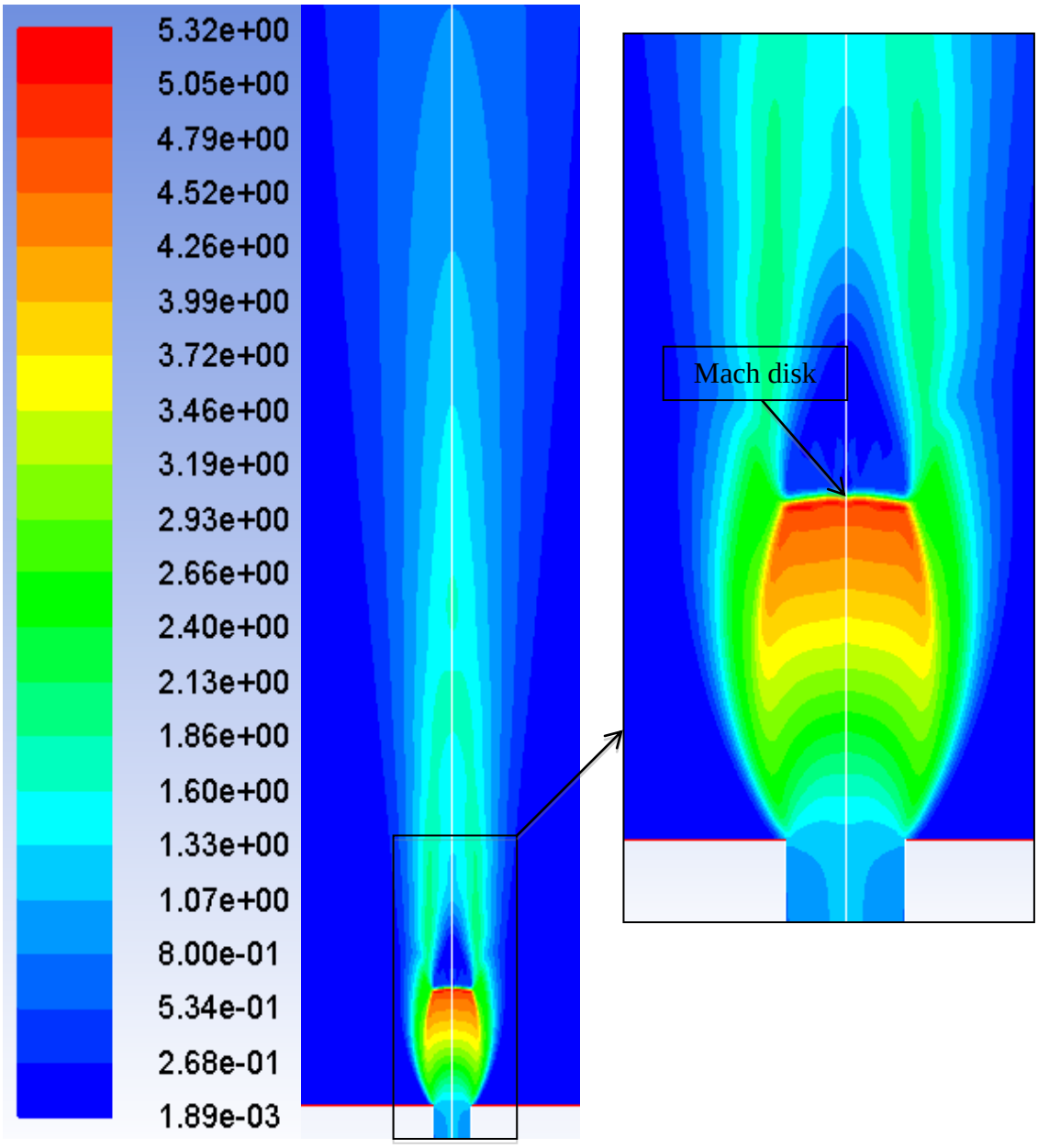

Figure 2.10 Contours of Mach number at the exit of injector. The inset is showing the location of Mach disk.

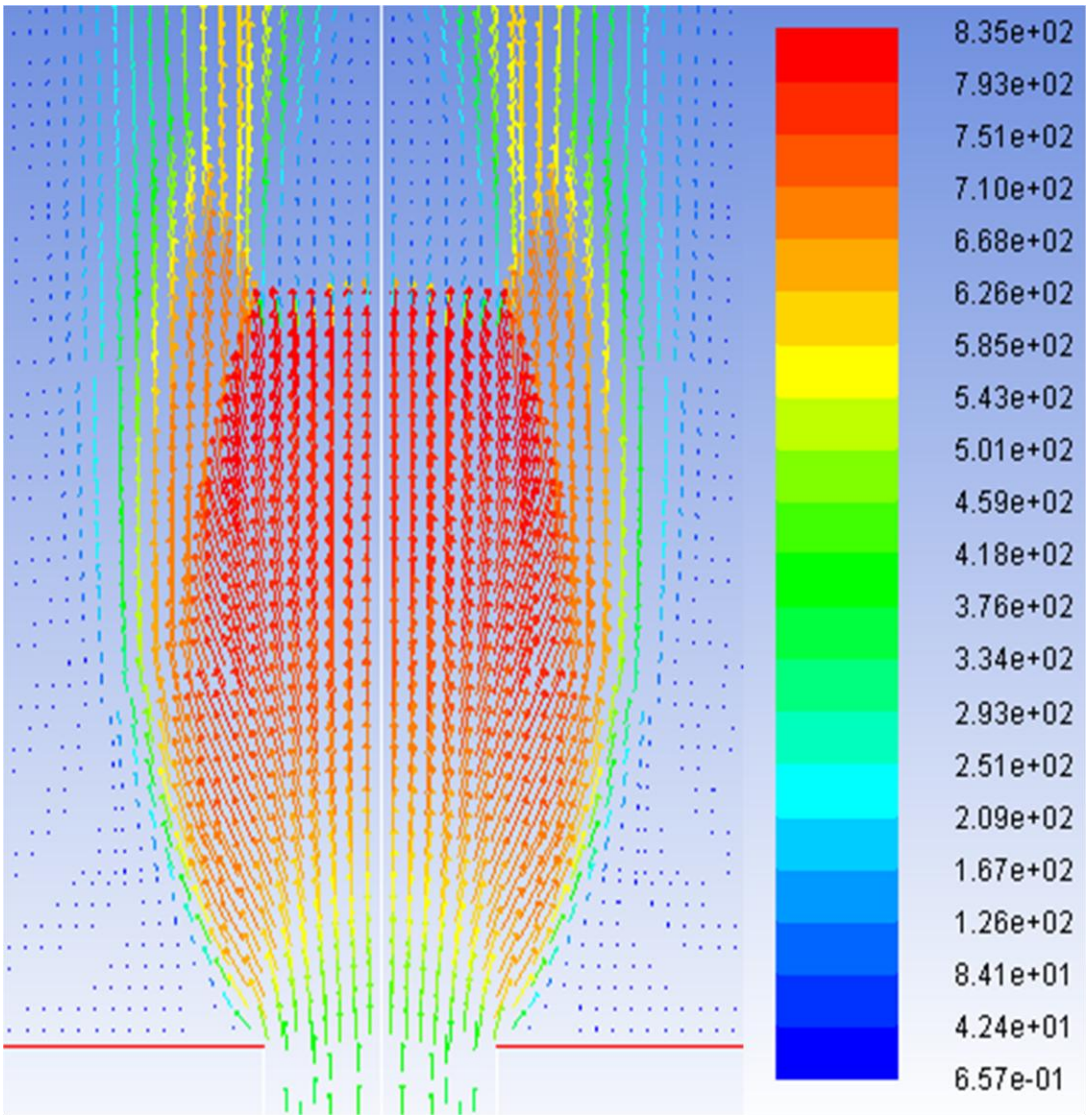

Figure 2.11 Contours of velocity vectors (the legend is showing values of velocity vectors in units of m/s).

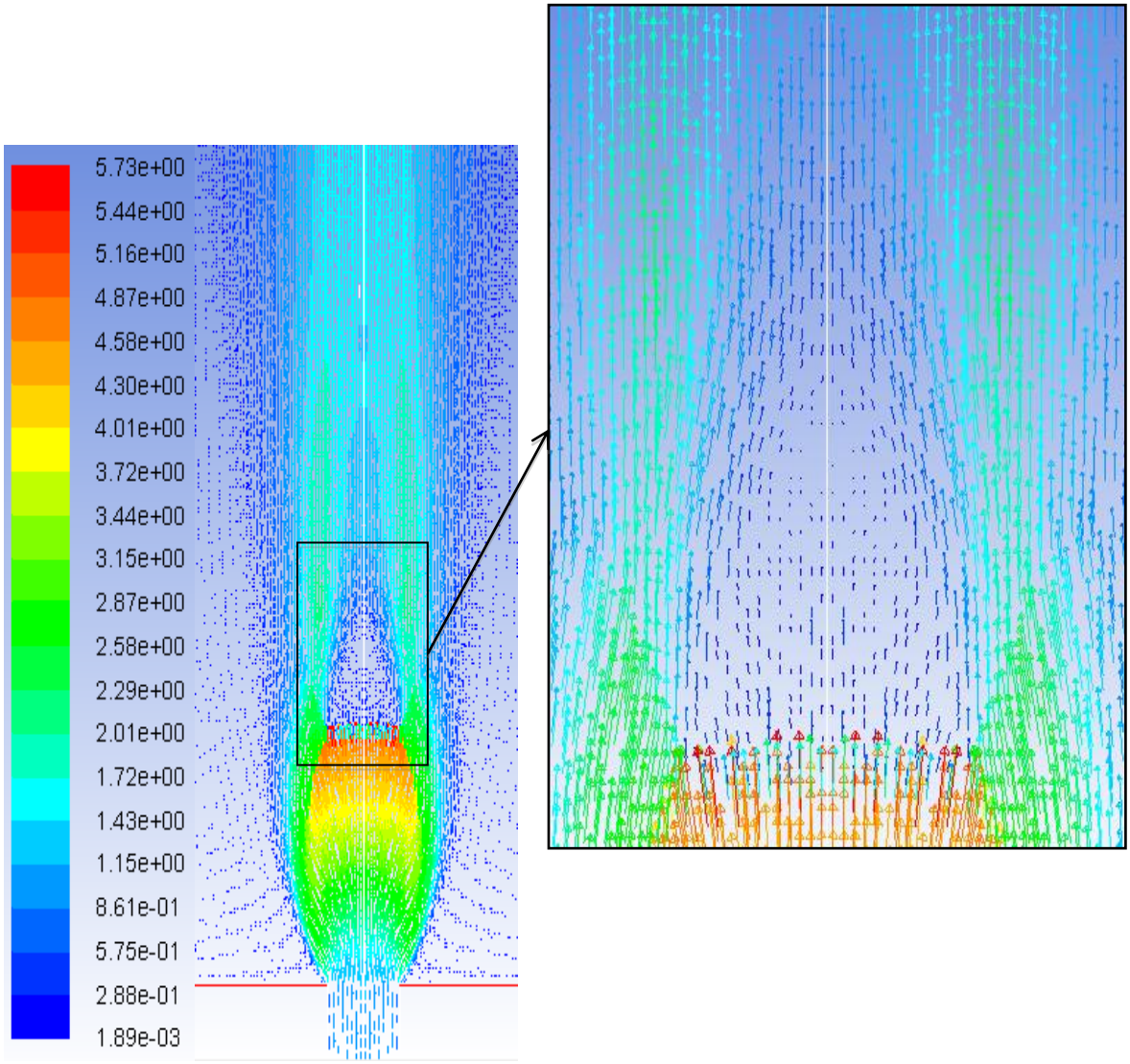

Figure 2.12 Velocity vectors colored by Mach number. The inset is showing the subsonic flow region immediately downstream of the Mach desk.

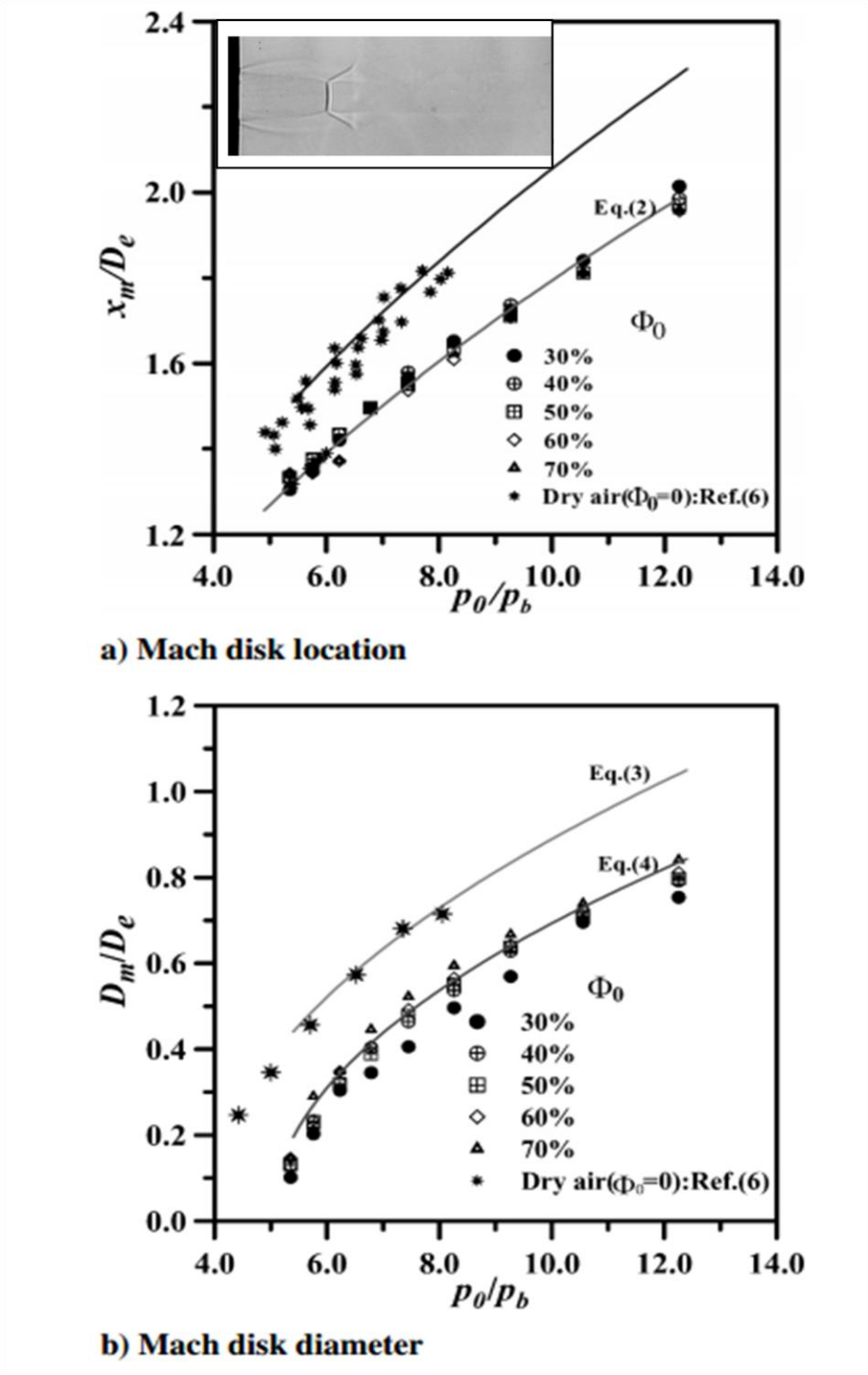

Fig.2.13 Experimental results for the location and the diameter of the Mach disk for dry and humid air. The inset is showing a shadowgraph of the Mach disk (Baek [27]).

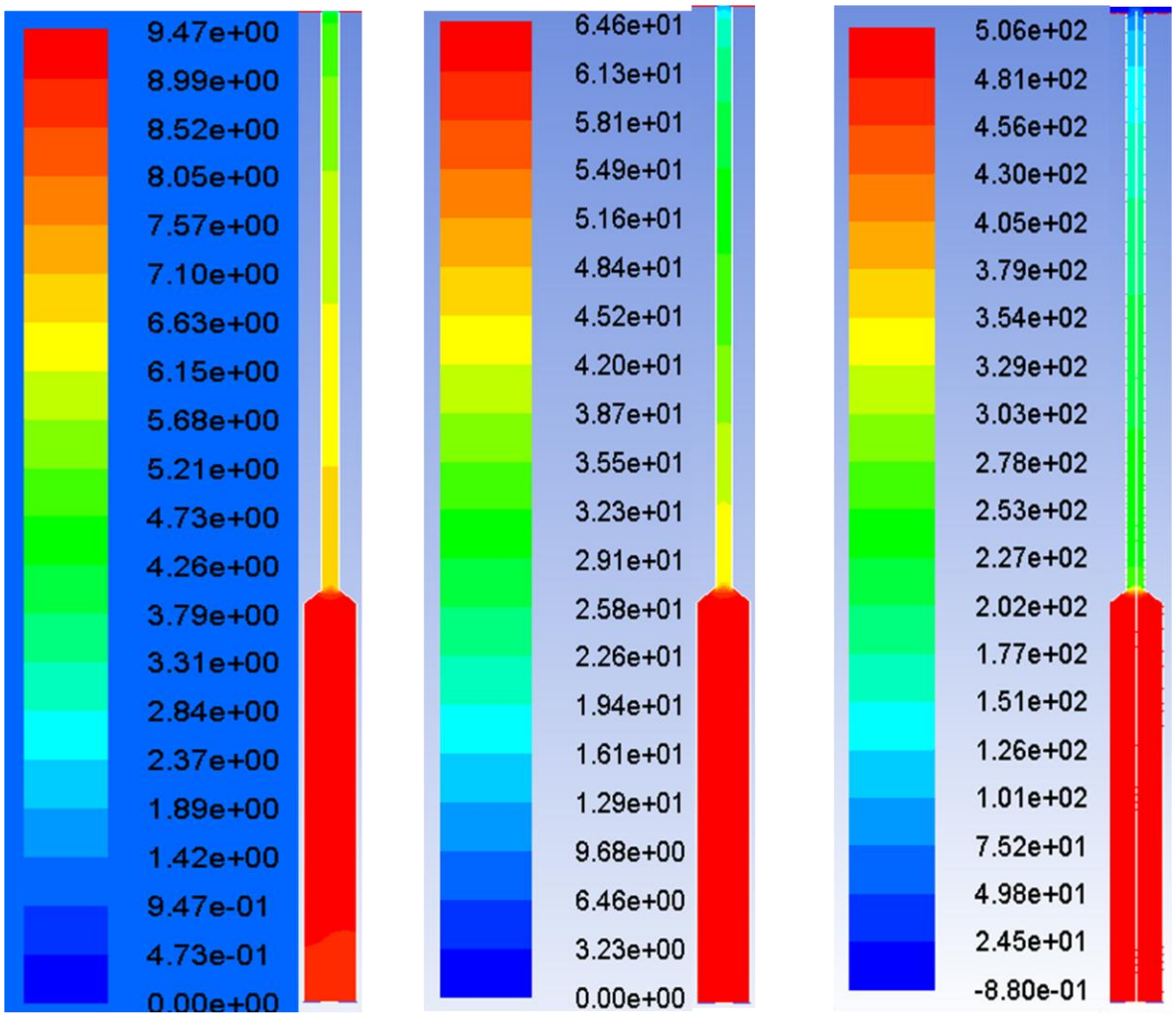

(a) **(b)** **(c)**

Fig.2.14 Contours of static gauge pressure inside the injector (a) Air injector (2D geometry) (b) Aerated liquid injector (2D geometry) (c) Aerated liquid injector (axi-symmetric geometry) (the legend is showing pressure values in units of atm).

CHAPTER III

Results and Discussion

3.1 Introduction

This chapter presents the comparison of internal and external flow fields for gas-only jet and for aerated liquid jets in both planar and axisymmetric configurations. The liquid sheet significantly affects the flow physics of the supersonic nozzle flow as will be discussed in this chapter. These effects will be evident when considering pressure, Mach and velocity contours. Gas dynamics phenomena are discussed in detail for 2D and axisymmetric aerated liquid jet cases. Experimental validation of spray cone angle is shown for 4 % GLR case for both planar and axisymmetric geometry.

3.2 Flow Visualization

The flow field for 2D gas-only and for 2D aerated liquid jets are shown in Fig. 3.1. The axisymmetric aerated liquid jet is shown in Fig. 3.2. The velocity vectors are colored by the Mach number. Schematics of expansion waves and oblique shock waves are superimposed on the flow velocity vectors in these figures. The scale of both 2D gas-only jet (Fig. 3.1.a) and axisymmetric aerated liquid jet (Fig. 3.2) are slightly enlarged compared to 2D aerated liquid jet (Fig. 3.1.b) as it is evident from the jet exit diameter which should look the same in all cases (1 mm). This was done to clarify the wave structure for slightly shorter flow field in case of 2D gas-only and axisymmetric aerated liquid jets. The flow in the three cases encounters first Prandtl-Meyer Expansion Fans due to the under-expansion test conditions, i.e. the exit flow pressure is more than the back (ambient) pressure. To match the back pressure, the flow expands to decrease its pressure and to increase its Mach number to supersonic values. The Prandtl-Meyer expansion fan consists of a number of Mach waves. These waves turn the flow gradually in the outward direction.

For clarity, only the first and the last of these Mach waves are shown in Figs. 3.1 and 3.2. Across these two waves the flow expansion starts and ends. The comparison between the height of the first set of expansion fans between 2D gas-only jet (Fig. 3.1.a) and 2D aerated liquid jet (Fig. 3.1.b) reveals that the flow field is stretched more in the case of aerated injection. This could probably be attributed to the larger nozzle pressure ratio (**NPR**) in the case of the aerated injection as well as potential effects of the inertia of the liquid film. The axisymmetric aerated liquid jet is also shorter than the 2D aerated liquid jet despite having higher NPR. The difference in height could be explained based on the geometrical configuration (round vs 2D) as will be explained further in section 3.3.

In aerated liquid jet, the momentum flux is different for gas and liquid due to different velocity and density. The density of liquid is of order of 1000 times more than the density of the gas. This can be shown by the axisymmetric aerated liquid jet velocity contours in Fig.3.14.a. Momentum flux is calculated as $\rho\ v^2$. The momentum flux of the gas at the exit of the injector is 156,025 kg/m.s^2 and the momentum flux for liquid at the same location is 76,176,000 kg/m.s^2. Further downstream at the location of maximum Mach number, the momentum flux for gas is 625,681 kg/m.s^2 and at the momentum flux for the liquid is 56,169,000 kg/m.s^2. The velocity contours for the planar aerated liquid jet are shown in Fig.3.14.b. The momentum flux of the gas and the liquid at the exit of the injector is 80,089 kg/m.s^2 and 11,303,942 kg/m.s^2, respectively. Further downstream at the location of maximum Mach number, the momentum flux for gas and the liquid is 502,681 kg/m.s^2 and 19,881,000 kg/m.s^2, respectively.

It is clear that the momentum flux values of the gas are negligible compared to the liquid for both axisymmetric and planar geometries. Also the results show that the liquid momentum decreases further downstream for the axisymmetric configuration whereas it increases for the planar case. The momentum flux affects the quality of the liquid jet atomization process. The higher momentum flux of the planar case would produce smaller droplets sizes. However, liquid film thickness plays a vital role as well. A thin liquid film associated with the axisymmetric case would produce finer spray.

3.3 Jet Expansion Angle

Expansion angle of the 2D and axisymmetric aerated liquid jet are shown in Figs. 3.3.a and 3.3.b, respectively. An experiment for measuring the jet expansion angle for aerated liquid jet injection in supersonic crossflow by Sallam et.al (2006) is shown in Fig.3.3.c for 4% GLR. Jet expansion angle affects the liquid sheet thickness and subsequently the size of the liquid droplets formed after breakup and the jet penetration capability into the chamber. Therefore, jet expansion plays vital role in the liquid jet atomization process. The comparison between computational and experimental results of aerated liquid jet injection through supersonic nozzle is shown in Fig.3.3. To compare the experimental results with computational simulation, 4% GLR is maintained in 2D and axisymmetric simulation.

Two dimensional aerated liquid jet is expected to expand more compared to axisymmetric one. This is due to the effect of geometrical configuration. Axisymmetric configuration results in a larger increase in the cross sectional area compared to 2D case. This increase leads to a decrease in the liquid surface velocity which in turn limits the jet expansion. Liquid surface velocity and thickness of the liquid film are correlated as follows (Sallam et al, 2006):

$$\frac{2b_0}{d_0} = 1 - \left(\frac{1-4\dot{Q}_L}{\pi\, v_{L,surf}\, {d_0}^2}\right)^{1/2} \qquad (3.1)$$

Therefore, the decrease in the liquid surface velocity results in a reduction in the liquid film thickness to maintain the same flow rate. This leads to a reduction in the inertia of the film with the increase in the distance form the jet exit compared to 2D case. Combined effects of all these lead to a shorter penetration height and thinner film thickness for axisymmetric aerated jet compared to 2D case.

Theory of Axisymmetric jet expansion is explained with reference to Fig.11 of NACA RM L54L31 report. Data points are plotted for half jet expansion angle (δj) Vs static injection pressure ratio (P_j / P_x) as shown in Fig.3.4. There are two best curve fits for theory of axisymmetric jet expansion.

$y = 0.1708 \times e^{0.0947x}$ equation is best fit for higher range of pressure ratios and $y = 0.8208 \times e^{0.0711x}$ is best fit for lower range of pressure ratios. Present test conditions are in the lower range of pressure

ratios and due to which $y = 0.8208 \times e^{0.0711\,x}$ equation gives the best fit for theory of axisymmetric jet expansion. x co-ordinate presents δj and y co-ordinate presents static injection pressure ratio. Rearrange the best curve fit equation in terms of y as shown below:

$$X = 2 * \left[\frac{1}{0.0711} \times \ln\left(\frac{Y}{2.30}\right)\right] \tag{3.2}$$

To plot the theory of axisymmetric jet expansion in Fig. 3.5, the theoretical jet expansion angle is determined as follow. Convert the static jet pressure ratio (P_j / P_b) into stagnation pressure ratio (P_{inj} / P_b). Following equation is used to convert the P_j / P_b to P_{inj} / P_b:

$$\frac{\text{Pinj}}{P_b} = \frac{\text{Pj}}{P_b} \times \frac{\text{Pinj}}{\text{Pj}} = \frac{\text{Pj}}{P_b} \times \left[1 + \left(\frac{\gamma-1}{2} \times M^2\right)\right]^{\frac{\gamma}{\gamma-1}} \tag{3.3}$$

jet expansion angle (θ) for axisymmetric jet is twice the half jet expansion angle (δj). From the equations 3.1 and 3.2, the jet expansion angle is calculated:

$$\theta = 2 * \left(\frac{1}{0.0711} * \ln\left[\frac{P_{inj}/P_b}{1.55}\right] \right) \tag{3.4}$$

jet expansion cone angle is a function of injection pressure ratio and this is graphically plotted for 2D and axisymmetric aerated liquid jet is shown in Fig.3.5. The graphical plot compares theoretical, computational, and experimental results of jet expansion angle with respect to injection pressure ratio.

Theory of jet expansion for 2D case and computational results for 2D jet shows in agreement with each other. The agreement of computational results of axisymmetric jet with method of characteristics of axisymmetric jet is excellent.

3.4 Liquid Volume Fraction

Liquid volume fraction for both 2D and axisymmetric aerated liquid jet is characterized by formation of liquid film inside the chamber as shown in Figs. 3.6.a and 3.7, respectively. Liquid film thickness for 2D aerated liquid jet has been resolved over seven numbers of cells, and this phenomenon is shown in

Fig.3.6.b. Structure of the liquid film inside the chamber is influenced by GLR for both cases. Inertia of the liquid film influences the compressible gas flow field inside the chamber. Present results show that the thickness of the liquid film in axisymmetric configuration decreases as jet moves away from the injector nozzle and validated with experimental formulation by Sallam et.al [22]. However, liquid film thickness remains same inside the chamber for 2D aerated liquid jet configuration. Thickness of the liquid film differs due to nozzle geometry configuration. Annular flow regime formed inside the injector for both 2D and axisymmetric injectors is shown in Fig.3.8. In annular flow regime, the gas is flowing into gas core surrounded by the liquid. Annular flow regime structure is same for 2D and axisymmetric aerated liquid jet injector.

Fraction of water content inside the liquid film is shown in Fig.3.9 for both 2D and axisymmetric aerated liquid jet configurations. Water content inside the liquid film is very small and to visualize this Log scale has been used. There is structural difference between 2D and axisymmetric volume fraction content. Fraction of water content is uniformly distributed in axisymmetric configuration and it is discontinuous for 2D geometry. The reason behind this is area inside the liquid film and the amount of water vapor generated inside the chamber. 2D configuration has huge area compared to axisymmetric one, and the generated vapor is not sufficient to fill this large area. Present results are plotted on log scale and water content goes on reducing uniformly from outside to inside. Water content is minimum at the center of shock diamond and maximum into the liquid film.

3.5 Oblique Shock Waves

Nakahira [28] investigated the effect of shock waves on fuel spray and measured the propagation speed and pressure amplitude. He confirmed that propagation speed and pressure amplitude are functions of the injection pressure and ambient pressure. The results showed that shock waves are generated only when the fuel injection speed exceeds the ambient sonic speed. Expansion fan makes the flow to move in outward direction, and later expansion waves intercept the jet boundary, and converted into compression waves. These compression waves termed as ‘Oblique Shock Waves’. The schematic of the oblique shock

waves for gas-only jet and for both 2D and axisymmetric aerated liquid jet is shown in Fig.3.1 and 3.2. Across the oblique shock wave, flow deflects in inward direction and moves towards the center. Thermodynamic properties of the flow changed across the oblique shock waves. The physics of the gas dynamics remains the same for 2D gas-only jet, 2D aerated liquid jet, and axisymmetric aerated liquid jet. The height of the oblique shock waves varies for 2D gas-only jet and aerated liquid jet and this could probably due to NPR. The flow field of planar aerated liquid je stretched more compared to axisymmetric one, this could probably due to inertia of the liquid. Shock waves travel longer distance to compress the thick liquid film of planar aerated liquid jet compared to axisymmetric aerated liquid jet having thin liquid film.

3.6 Mach Disc

Oblique shock waves compress the flow field and they united at the center to form a Mach disk. The Mach disks are shown in Figs. 3.10 and 3.11. There is sudden jump in pressure and temperature across the Mach disk and this is shown by observing the contours of static gauge pressure as shown in Fig.3.10 and 3.11. The red region is the highest pressure region inside the chamber. When the shock waves impinge on the Mach disk then it generates reflected shock. Flow turns parallel to the center line when it passes through the Mach disk and inward flow turns outward across the reflected shock. The schematic of the Mach disk and reflected shock for planar gas-only and both planar and axisymmetric aerated liquid injector are shown in Fig.3.1 and 3.2. Location and diameter of the Mach disk is influenced by NPR and inertia of the liquid jet. Liquid film surrounds the air jet and due to inertia of the liquid film Mach disk shifts farther downstream from the nozzle exit. Therefore, contours of aerated liquid jet differ from gas only jet.

3.7 Mach Diamonds Dissipation

Mach diamonds dissipation is the loss of energy inside the chamber. There is a formation of alternate expansion and compression waves inside the chamber. Compression waves coalesce to form shock diamond at the center of the flow field and they are repetitive in nature. Shock diamonds have high

pressure and high temperature region having lowest Mach number values. Mach diamonds are dissipative in nature and these diamonds are repeated inside the chamber unless all energy is not dissipated as shown in Figs. 3.12.b, 3.12.c, and 3.13. Physics of the Mach diamond dissipation is applicable for planar gas-only jet and both planar and axisymmetric aerated liquid jet. Fig.3.12 (a) shows the experimental image of Mach diamond dissipation process. There are alternate bright spots formed after the Mach disk. This region is with very high temperature and pressure and due to which these spots are shining.

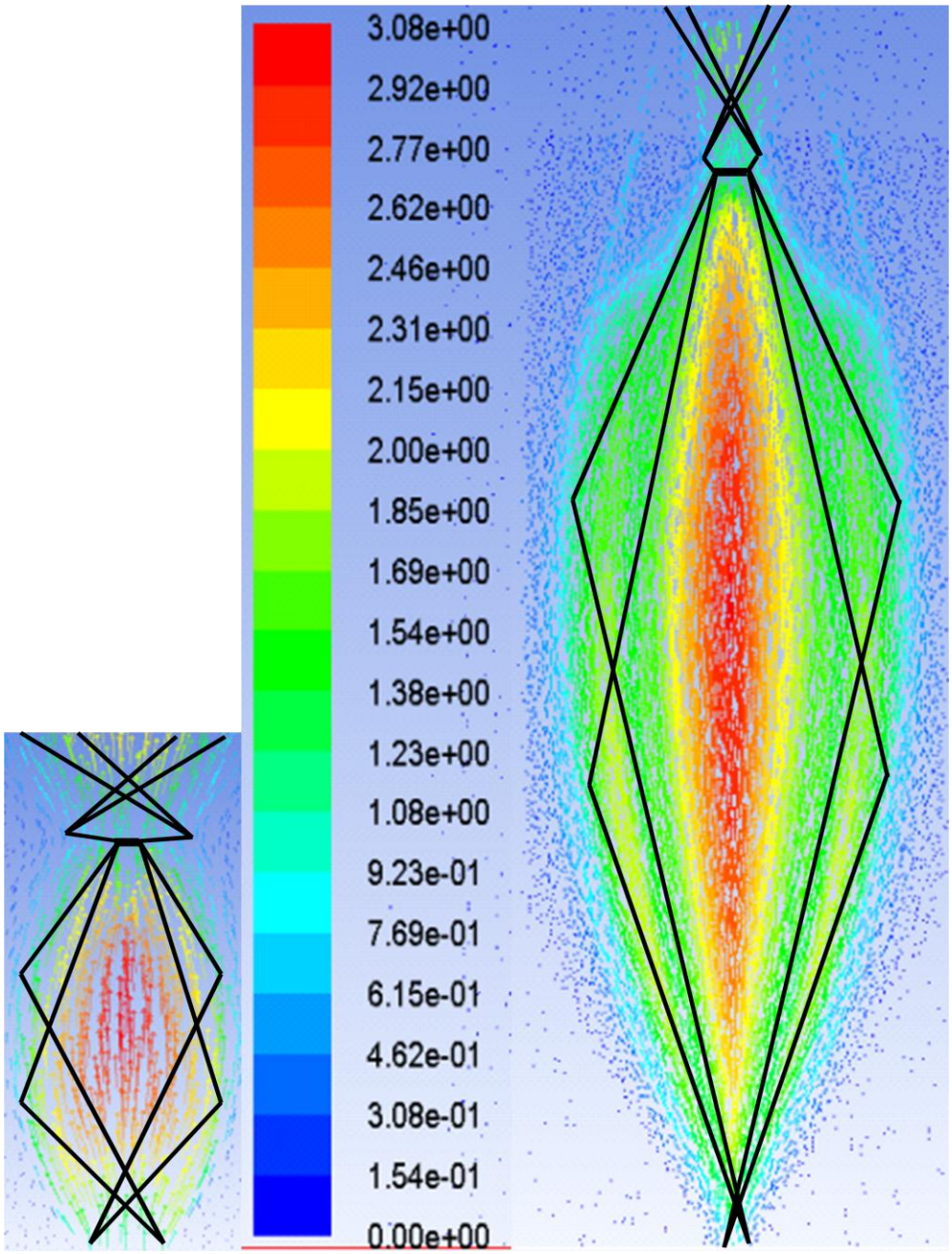

Fig. 3.1 Velocity Vectors colored by the Mach number (air) for 2D geometry (a) Gas only jet (b) Aerated liquid jet. The black lines are tracing the expansion fans and shock waves based on the velocity vectors. Only the first shock diamond is shown for both cases. The velocity vectors are plotted with a skip value of 25 for clarity.

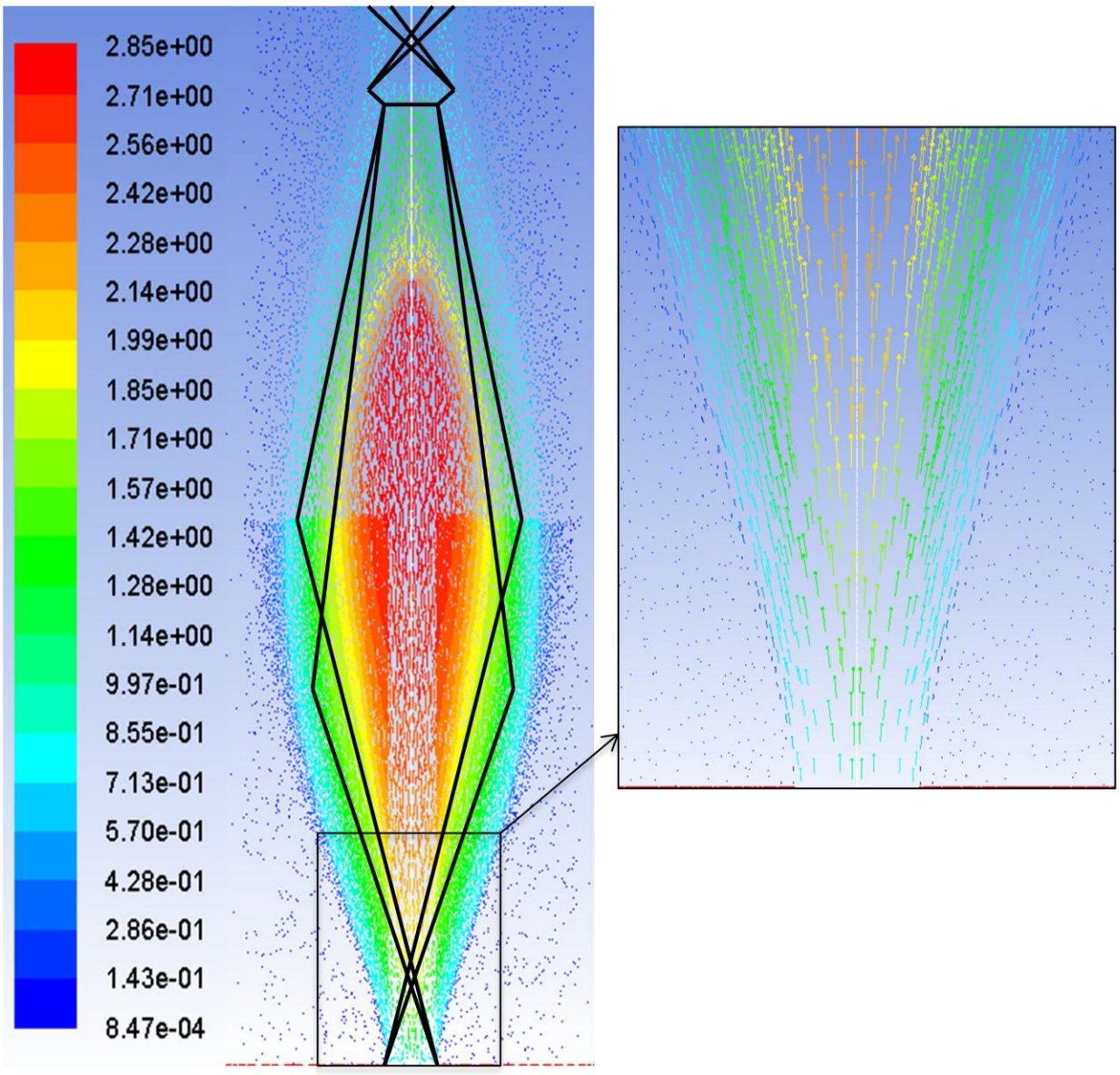

Fig. 3.2 Velocity Vectors colored by the Mach number (air) for axisymmetric geometry for aerated liquid jet. The velocity vectors are plotted with a skip value of 25 for clarity. Insight is showing the expansion fan phenomena.

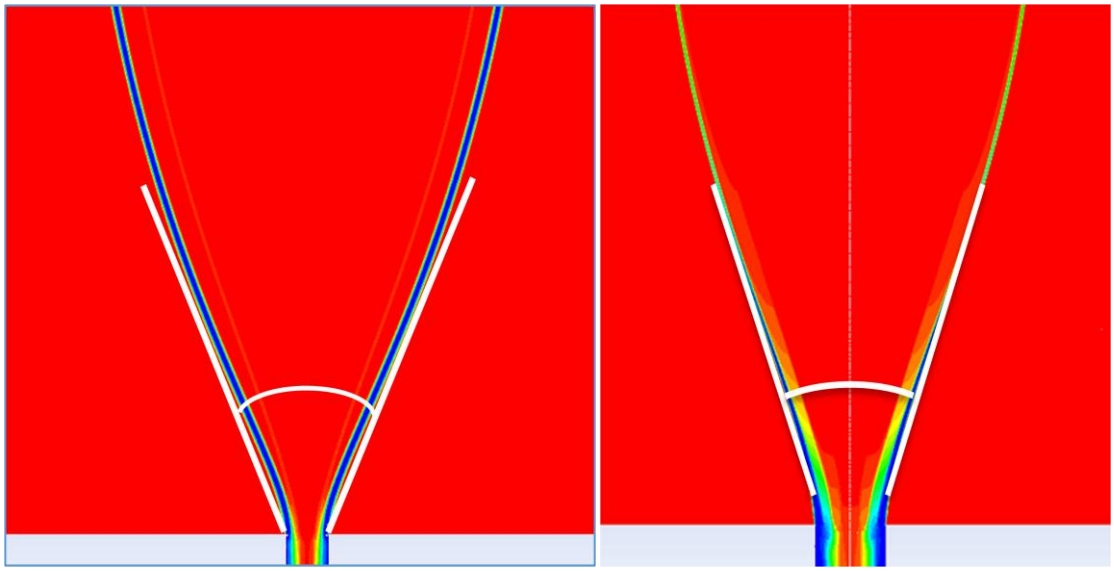

(a) (b)

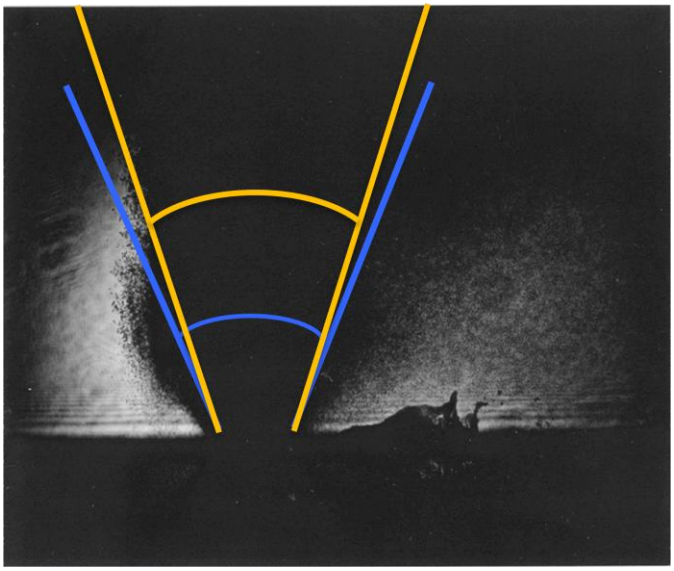

(c)

Fig. 3.3 Aerated liquid jet expansion angle:
(a) Numerically for 2D configuration (52^o)
(b) Numerically for axisymmetric configuration (45^o)
(c) Experimentally by Sallam et.al, 2006 (60^o) Test conditions for the experiments include, GLR = 4%, Q_L = 1.04 L/min, D_j = 1 mm in supersonic crossflow M =1.97.

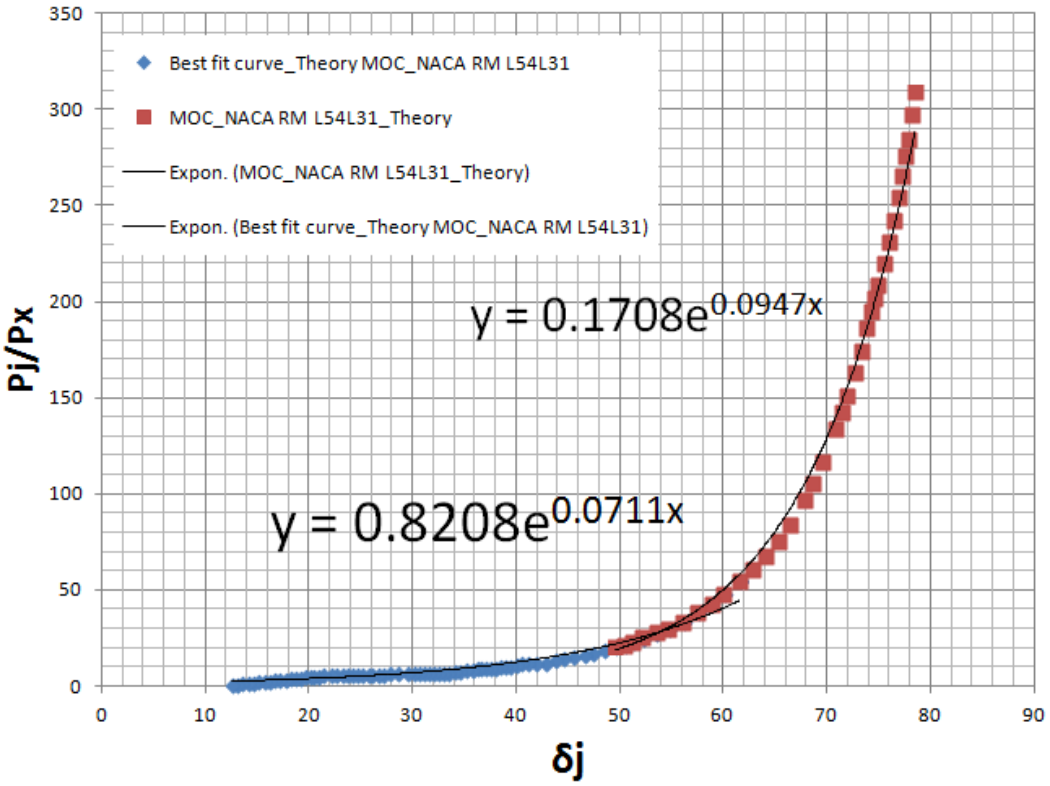

Fig.3.4 Best fit curve of MOC for Axisymmetric jet.

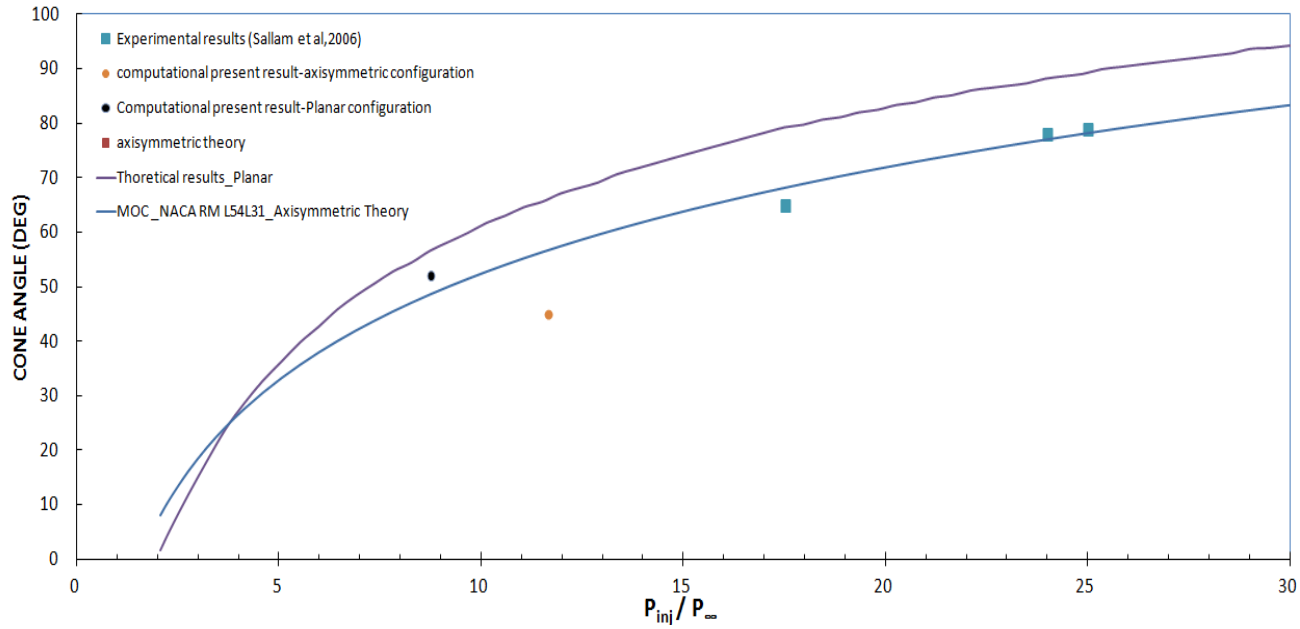

Fig.3.5 Spread Cone Angle as a function of Nozzle Pressure Ratio. Experimental results are from Sallam et.al [22].

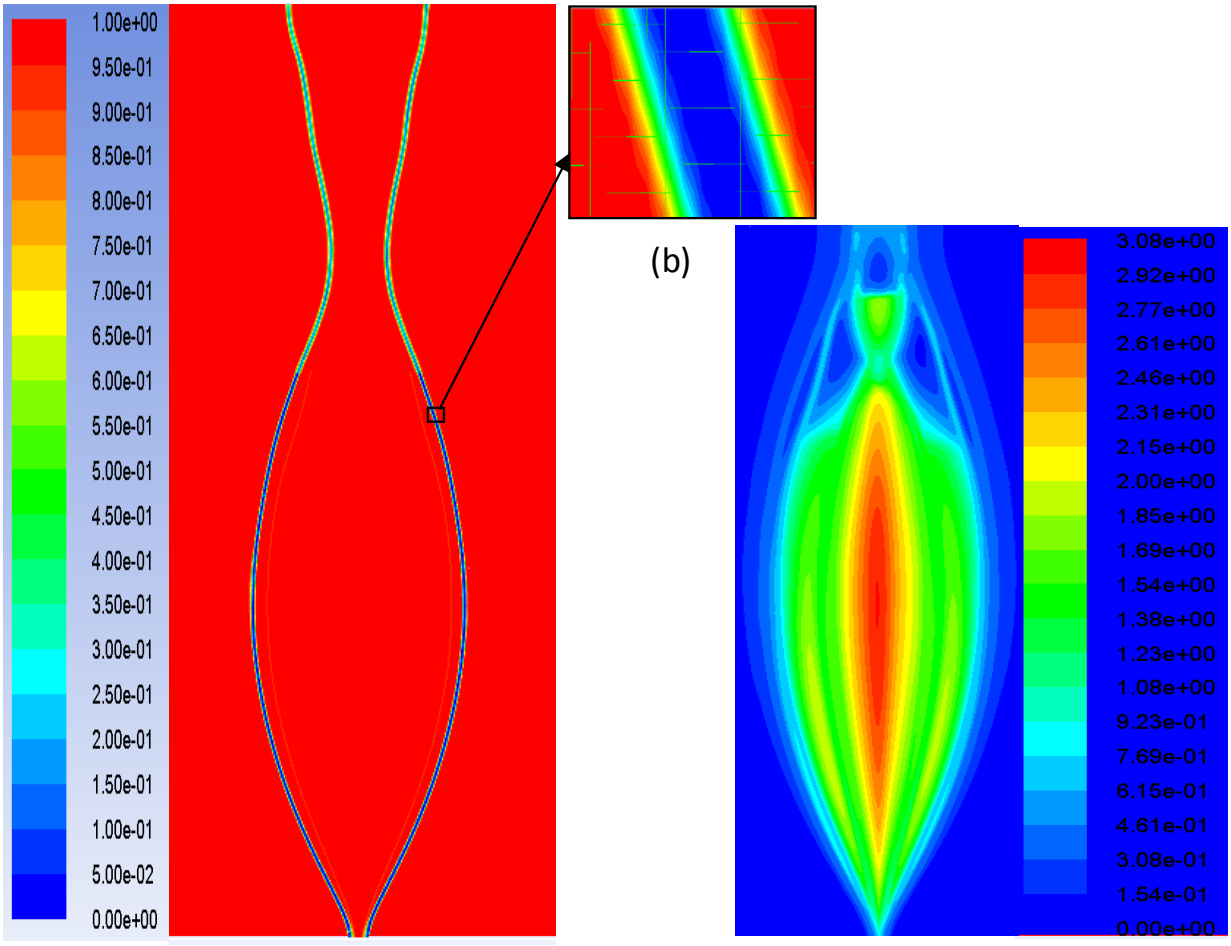

Fig.3.6 Contours of Volume fraction (air) for 2D geometry (a) outside the injector (b) film thickness resolved using current mesh (c) contours of Mach number (air).

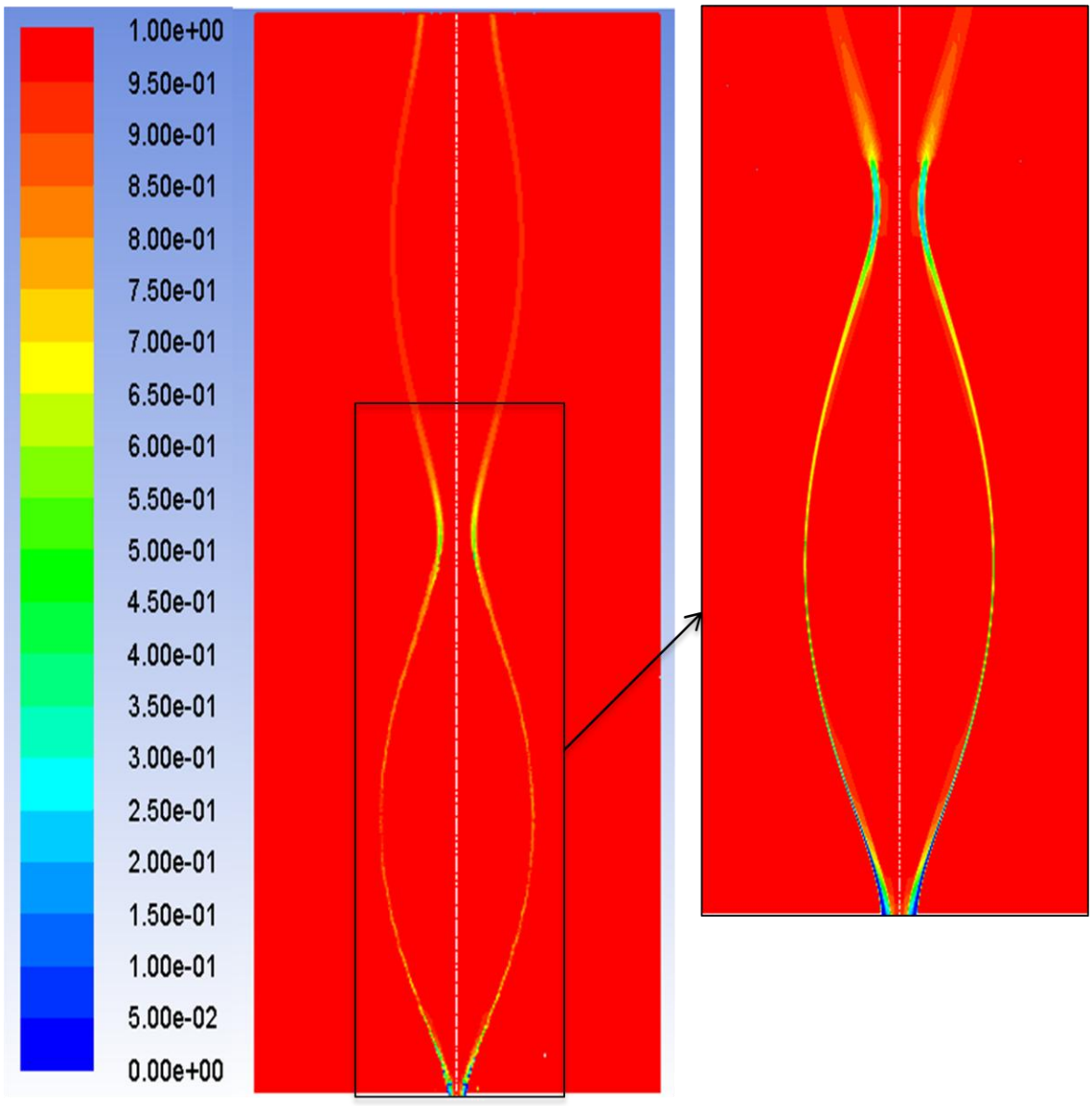

Fig.3.7 Contours of Volume fraction (air) outside the injector for axi-symmetric geometry. The inset is showing zoomed view of liquid film at the exit of injector.

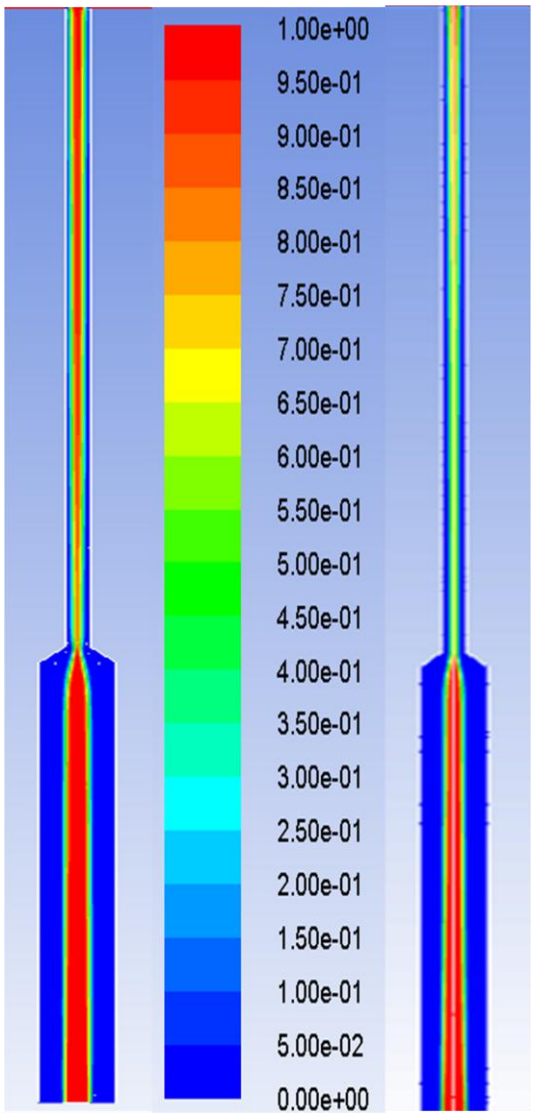

(a) **(b)**

Fig.3.8 Liquid volume fraction inside the injector (a) 2D configuration (b) Axisymmetric configuration.

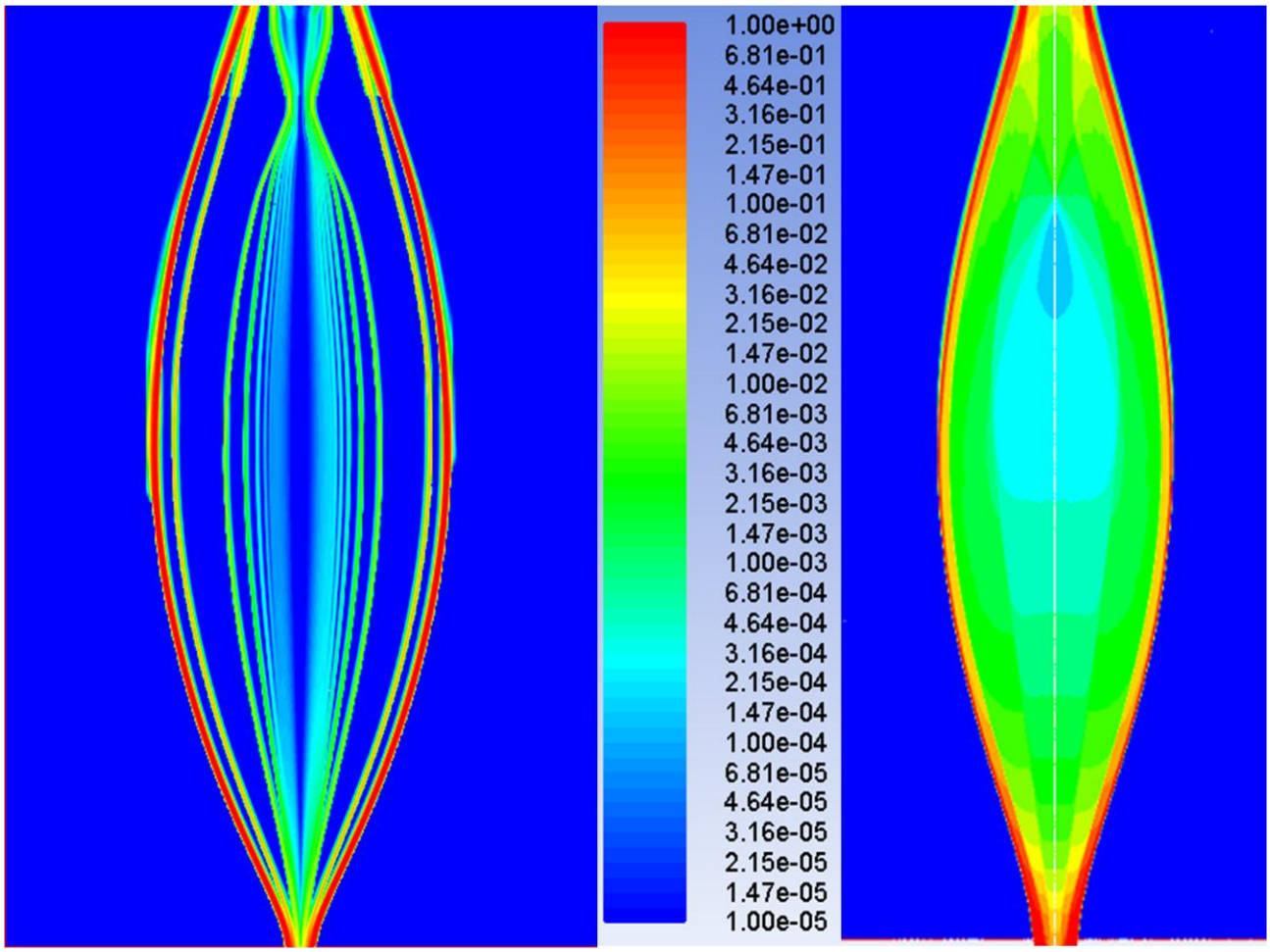

(a) **(b)**

Fig.3.9 Contours of volume fraction (water) on Log scale (a) planar geometry (b) axisymmetric geometry.

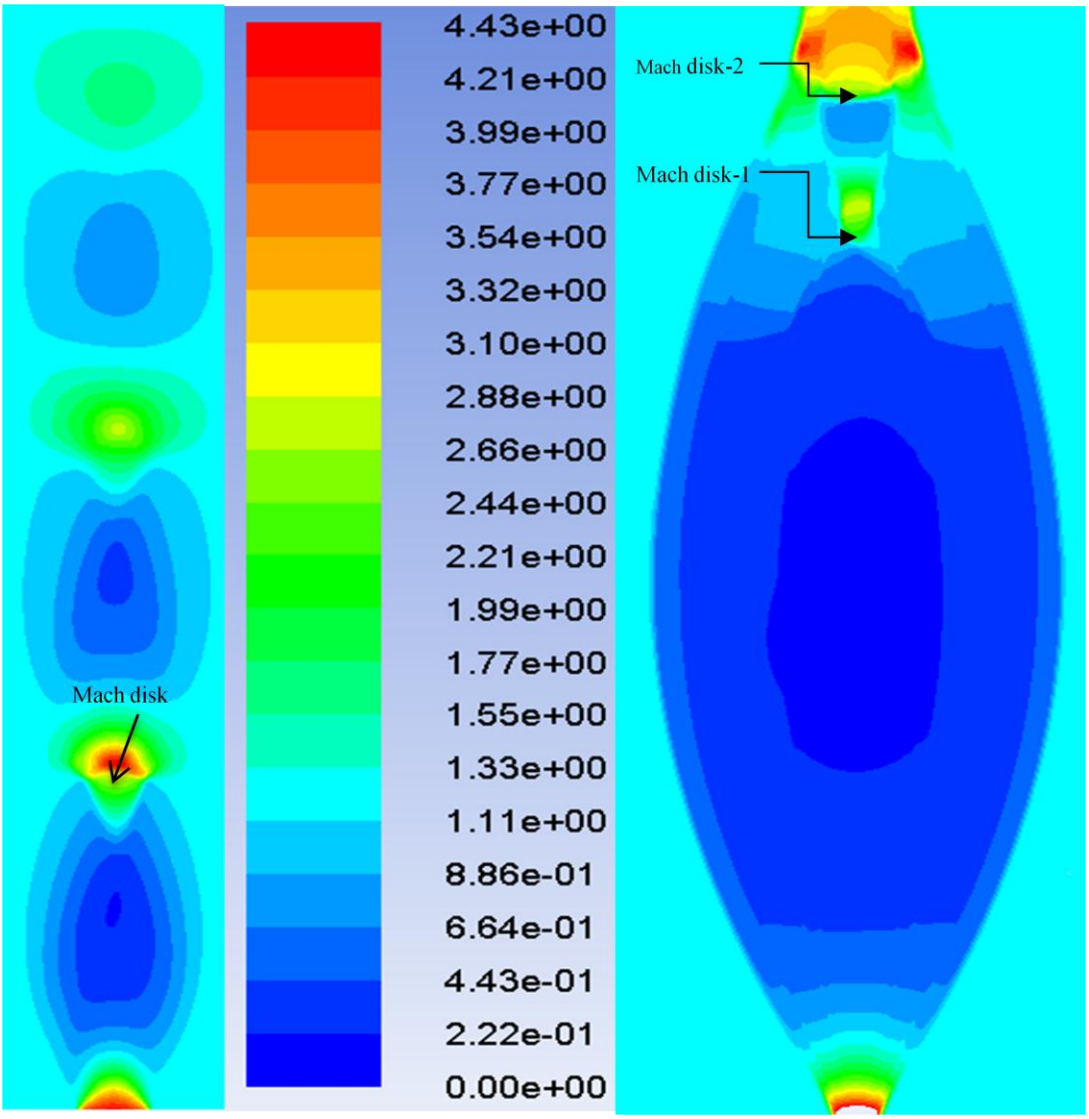

(a) **(b)**

Fig. 3.10. Contours of static gauge pressure inside the chamber for 2D geometry (a) Gas only jet (b) Aerated liquid jet (the legend is showing pressure values in units of atm).

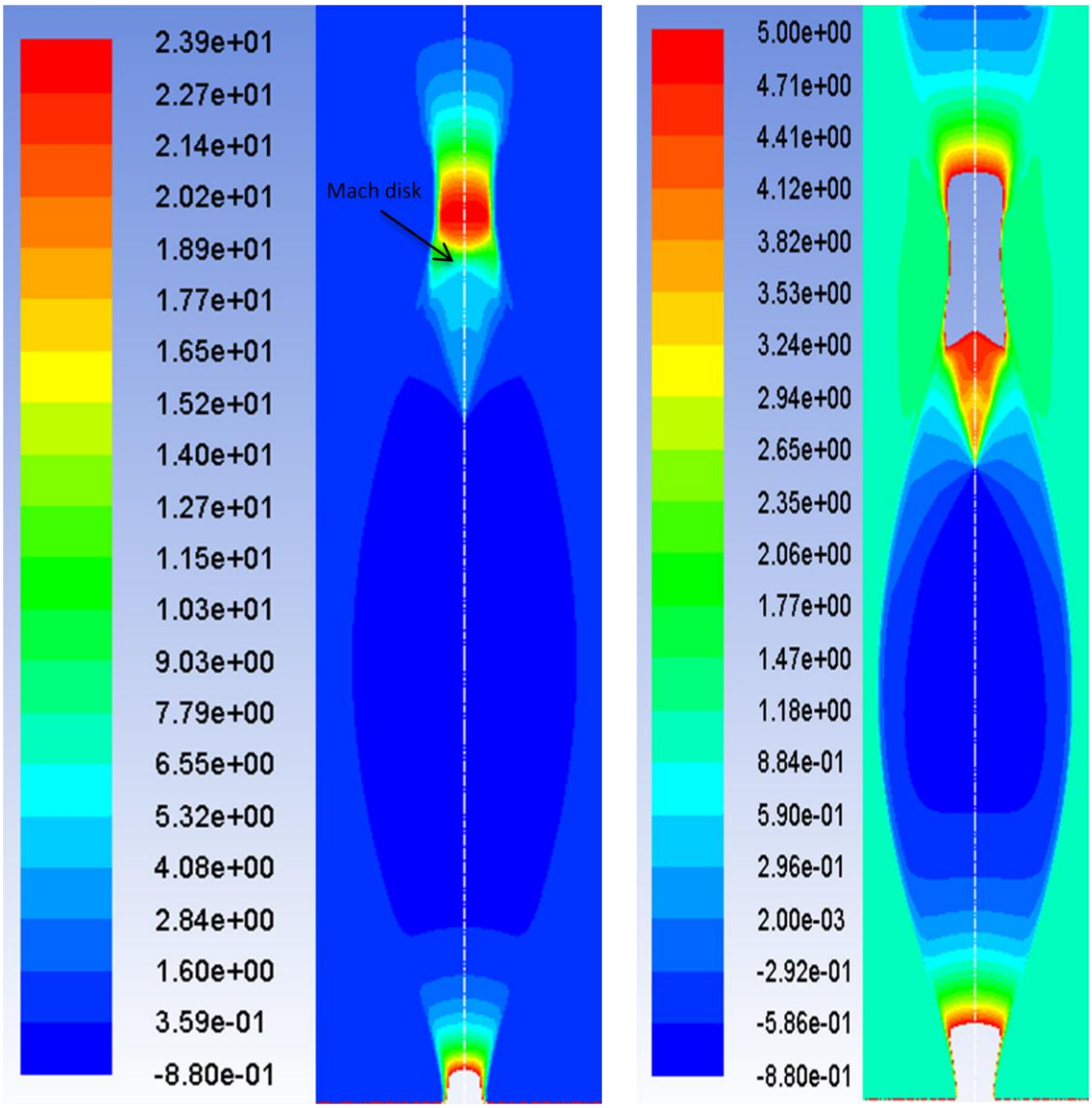

Fig.3.11 Contours of static gauge pressure inside the chamber for axisymmetric geometry (the legend is showing pressure values in units of atm).

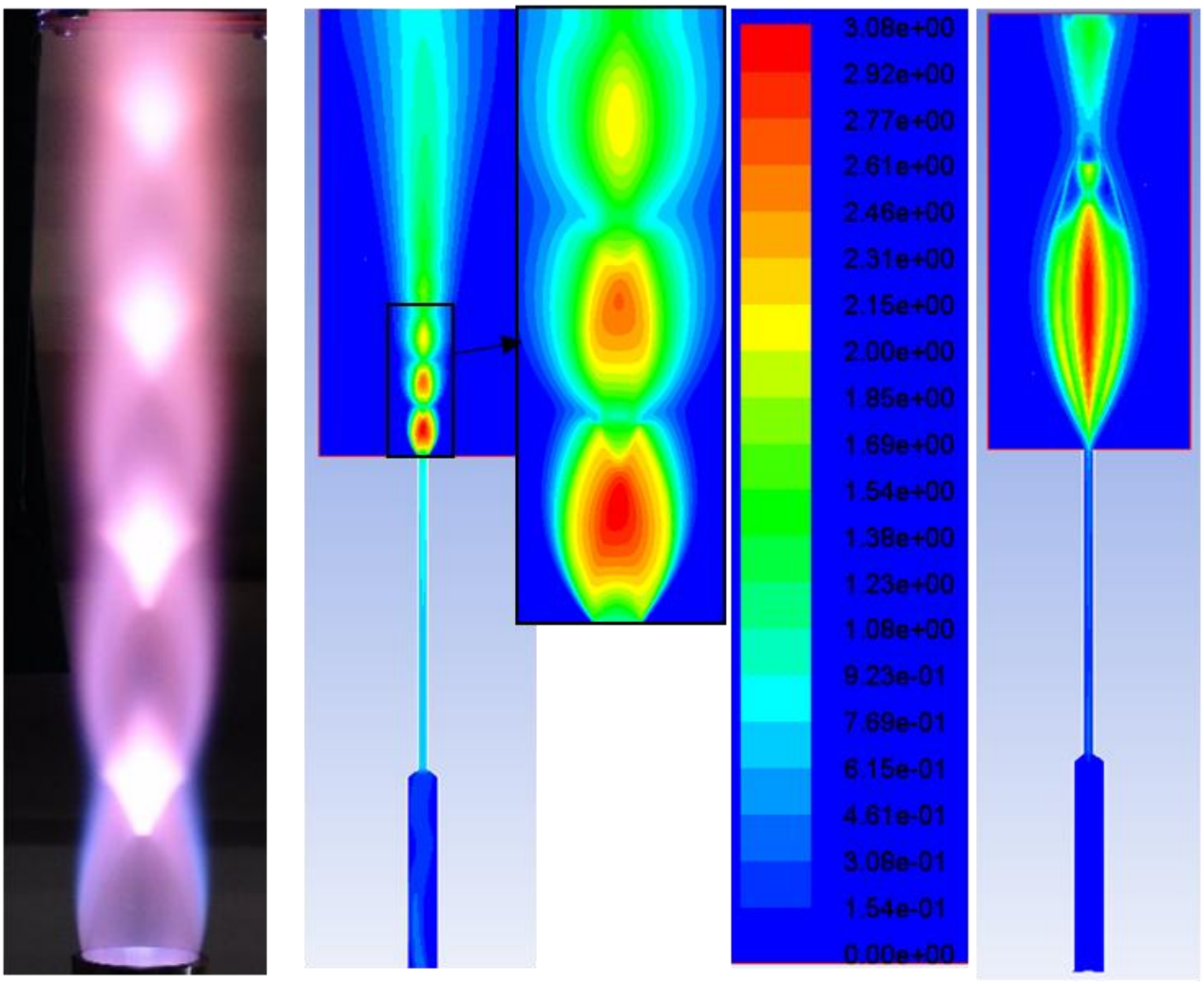

(a) **(b)** **(c)**

Fig.3.12. (a) Mach diamonds Swiss propulsion laboratory [31], Contours of Mach number (air) for 2D geometry (b) Air injector (c) Aerated liquid injector.

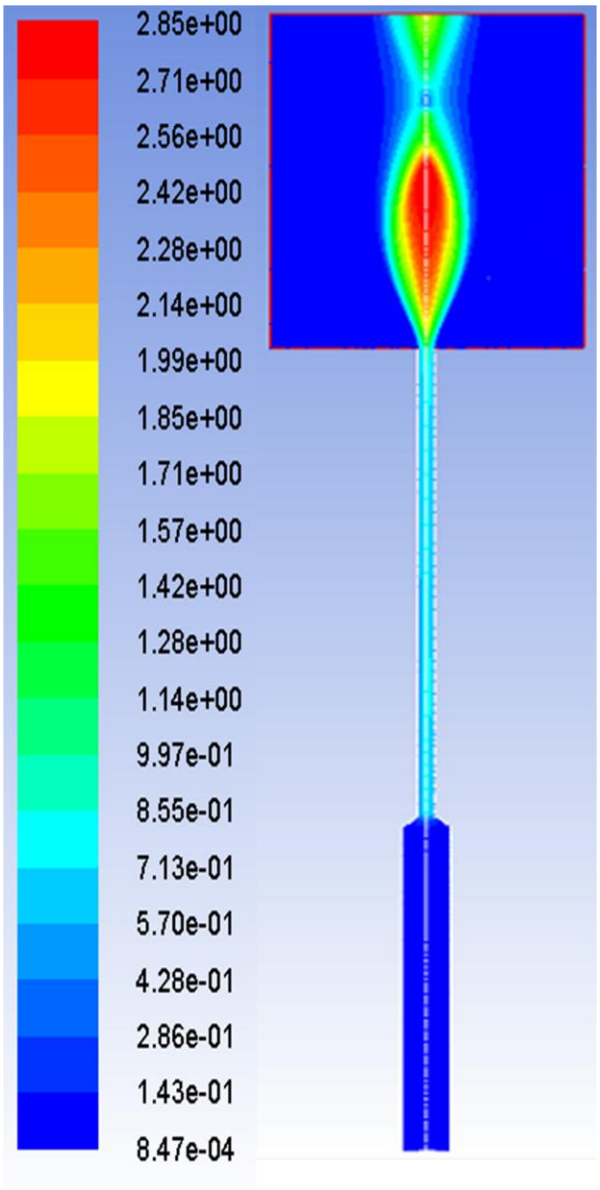

Fig.3.13. Contours of Mach number for axisymmetric aerated liquid jet injector.

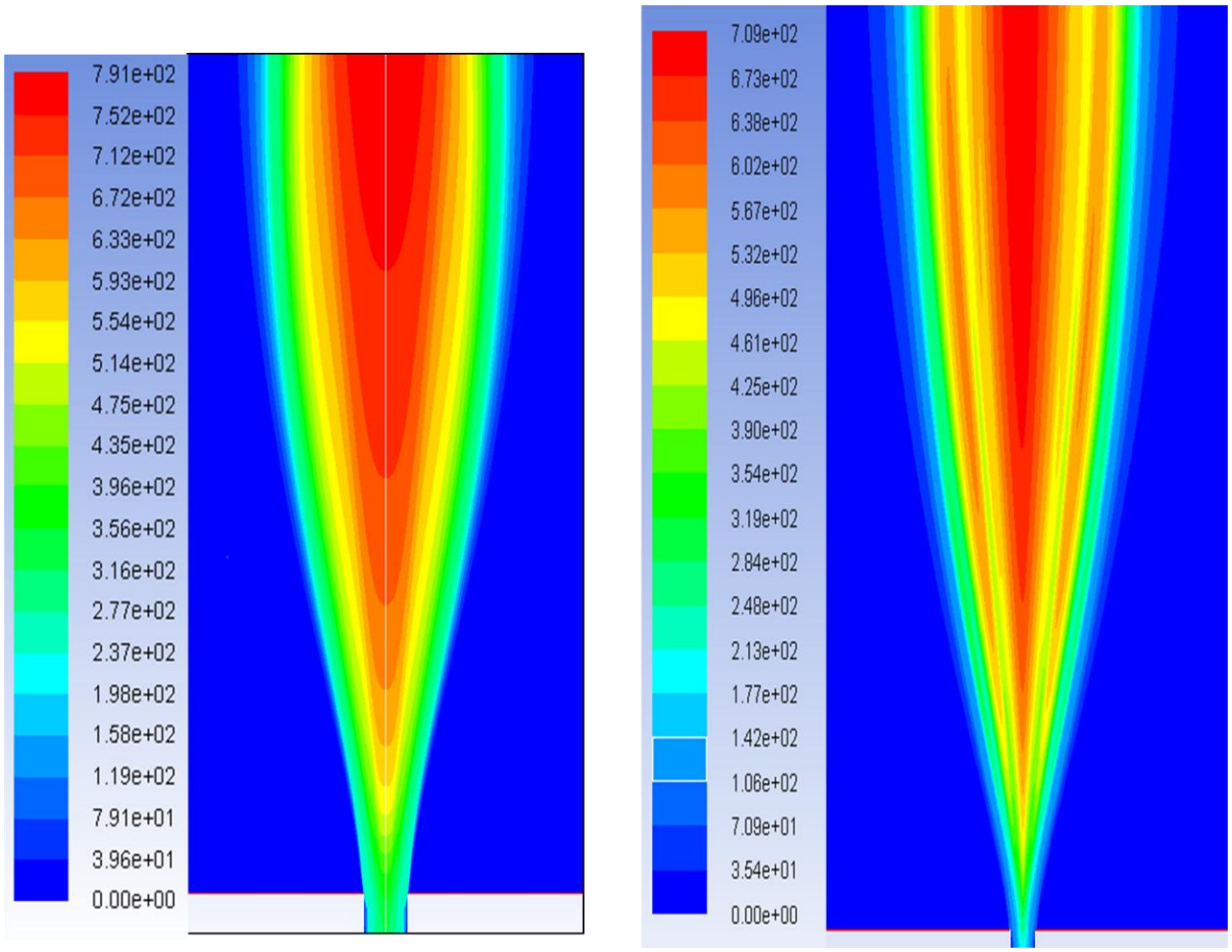

(a) (b)

Fig.3.14. Contours of Velocity magnitude (mixture) of aerated liquid jet
(a) Axisymmetric geometry (b) Planar geometry

CHAPTER IV

SUMMARY AND CONCLUSIONS

4.1 Summary

Computational simulation of gas-only jet is carried out for 2D nozzle configuration and validates the results with theory of gas dynamics. To validate the numerical schemes used in the present simulation injector nozzle diameter of 1 mm and injector inlet static gauge pressure of 13.50 atm and chamber back pressure is considered as 1.17 atm. The present results of 2D gas-only jet of underexpanded nozzle are compared with the theory of gas dynamics. The present computational results show very good agreement with theory of gas dynamics.

Present numerical schemes are validated with experimental results using Baek [27] equation. For the present results 1 mm injector nozzle diameter with 22.50 atm as injector inlet static gauge pressure with 1.17 atm as back pressure is considered. The location and diameter of the Mach disk are calculated using the present numerical scheme and compared with the experimental values.

The present results also discussed the flow physics of aerated liquid jet for both 2D and axisymmetric configuration. The contours of Mach number and pressure values are compared between 2D gas-only jet and 2D aerated liquid jet along with axisymmetric aerated liquid jet. The injector nozzle diameter is 1 mm for all cases. In both 2D and axisymmetric configuration 4 % GLR is maintained with liquid inlet velocity as 22.5 m/s and chamber back pressure as 1.17 atm.

The effect of liquid on the flow field of gas jet is discussed for both 2D and axisymmetric nozzle configuration. The liquid jet expansion is plotted for 2D and axisymmetric aerated liquid jet, and compared it with theory as well as experimental results. The present results are presented at 8.75 injector nozzle pressure ratio for 2D geometry and 11.66 injector nozzle pressure ratio for axisymmetric nozzle configuration.

4.2 Conclusions

The present computational results for gas-only and aerated liquid jet of 2D as well as axisymmetric nozzle configuration yielded the following conclusions:

1. The flow field of supersonic gas-only jet of underexpanded nozzle can be explained using the theory of gas dynamics. The values of max static pressure and max Mach number are within 0.1 % and 4% of theoretical results.
2. The present computational result of the gas-only jet underexpanded nozzle is experimentally validated using axisymmetric nozzle configuration. The location and diameter of the Mach disk are in agreement with experimental values.
3. The flow field of aerated liquid jet for 2D configuration differs significantly from the gas-only jet. The location of the Mach disk is shifted farther downstream in the case of aerated liquid jet. This is not surprising, however, due to the inertia of the liquid jet.
4. The liquid jet expansion for axisymmetric configuration is less compared to 2D configuration. This is a result of the confinement effect of the increasing cross sectional area of the axisymmetric geometry.
5. The flow field of axisymmetric aerated liquid jet and 2D aerated liquid jet were compared for the same inlet liquid velocity and the same GLR%. The axisymmetric aerated jet is shorter than the 2D aerated liquid jet. This could probably be explained based on the large inertia of the liquid sheet for 2D aerated jet compared to the relatively thinner sheet for the axisymmetric one.
6. Present computational results for the expansion angle of aerated liquid sheet generally agree with the theoretical results for gas-only jet expansion based on the Prandtl-Meyer analysis for 2D

configuration and method of characteristics for axisymmetric configuration. The computed cone angle is always smaller than theoretical results. This is plausible because of the inertia of the liquid sheet.

7. The present study shows that the measurements of the cone angle for aerated round liquid jet can be explained using the theoretical analysis of the method of characteristics for axisymmetric gas jet rather than using the 2-dimensional Prandtl-Meyer analysis as has been done previously in the literature.

4.3 Recommendations for future work

Based on the present results of injection of aerated liquid jet the following recommendations are made concerning future study of the process:

1. The present results are limited for particular nozzle injection pressure ratio. There is scope for investigation at different pressure conditions.
2. The present study is limited for quiescent flow condition, but there is future scope on investigation for injection of aerated liquid jet in supersonic crossflow.
3. In practical fuel injectors, injector walls are hotter than the liquid fuel to be injected. The effects of heat transfer from the wall should be part of future investigations.
4. The present study investigated the injection from a straight injector. Geometries of practical injectors should be investigated as well.

REFERENCES

[1] Lefebvre, A.H., Wang, X.F., Martin, C.A., "Spray Characteristics of Aerated-Liquid Pressure Atomizers," J. Prop. Power, vol. 4, pp. 293–298, 1988.

[2] Sabel'nikov, V.A., Korontsvit, Y.P., Schadow, K., "Investigation of Supersonic Combustion Enhancement Using Barbotage and Injectors with Noncircular Nozzles," AIAA, Reston, VA, Paper No. 98-1516, 1998.

[3] Tian, M., Edwards, J.R., Lin, K.C., Jackson, T.A., "Numerical simulation of transient two-phase flow within aerated-liquid injectors," 33rd AIAA Fluid Dynamics Conference and Exhibit., (2003).

[4] Tian, M., A Numerical Simulation of Internal Two-Phase Flow for Aerated Liquid injectors, MS. Thesis, North Carolina State University (2002).

[5] Senesh, K., Babu, V., "Numerical simulation of subsonic and supersonic jets," Proceedings of the 11th AIAA/CEAS Aeroacoustics conference, pp. 3699-3711, (2005).

[6] Murugan, T., De, S., Thiagarajan, V., "Validation of three-Dimensional Simulation of Flow through Hypersonic Air-Breathing Engine," Defense Science Journal, 65(4):272-8, (2015).

[7] Karimi, M., Fartaj, A., Rankin, G., Vanderzwet, D., Birtch, W., Villfurete J., "Numerical Simulation of the Cold Gas Dyanamic Spray Process," Journal of Thermal Spray Technology., 15(4), pp.518-23,(2006).

[8] Park, J.J., Lee, M.W., Yoon, S.S., Kim, H.Y., James, S.C., Heister, S.D., "Supersonic Nozzle Flow Simulations for Particle Coating Applications: Effects of Shockwaves, Nozzle Geometry, Ambient Pressure, and Substrate location upon Flow Characteristics," Journal of thermal spray technology. 2011; 20(3):514-22.

[9] Zhang, L., Ruan, W.J., Wang, H., Wang, P.X., "Numerical Simulation of Supersonic Gas Jet Flows and Acoustic Fields," World Academy of Science, Engineering and Technology, International Journal of Mechanical, Aerospace, Industrial, Mechatronic and Manufacturing Engineering.;10(2):232-6 (2016).

[10] Lagumbay, R.S., Vasilyev, O.V., Haselbacher, A., Wang, J.," Numerical simulation of a high pressure supersonic multiphase jet flow through a gaseous medium," ASME 2004 International Mechanical Engineering Congress and Exposition, pp. 97-106 (2004).

[11] Pianthong, K., Zakrzewski, S., Behnia, M., Milton, B.E., "Characteristics of impact driven supersonic liquid jets," Experimental thermal and fluid science., 27(5), pp. 589-98, (2003).

[12] Zakrzewski, S., Milton, B.E., Pianthong, K., Behnia, M., "Supersonic liquid fuel jets injected into quiescent air," International Journal of Heat and Fluid Flow., 25(5), pp. 833-40, (2004).

[13] Wang, G.L., Lu, X.Y., "Effects of the jet-to-crossflow momentum ratio on a sonic jet into a supersonic crossflow," Theoretical and Applied Mechanics Letters., 1(1), pp.012005, (2011).

[14] Vuorinen, V., Yu, J., Tirunagari, S., Kaario, O., Larmi, M., Duwig, C., Boersma, B.J., " Large-eddy simulation of highly underexpanded transient gas jets," Physics of Fluids (1994-present). Jan 1; 25(1):016101, (2013).

[15] Fu, D., Yu, Y., Niu, Q., "Simulation of underexpanded supersonic jet flows with chemical reactions," Chinese Journal of Aeronautics, 27(3), pp. 505-13, (2014).

[16] Thanigaiarasu, S., Karthick, R., Arunprasad, R., SyedMusthafa, H., Elangovan, S., Rathakrishnan, E., "Study of Underexpanded Sonic Jets by Numerical Simulation," Int. J. Turbo Jet-Engines., 30(1), pp.101-9, (2013).

[17] Bensler, H., Buhren, F., Lozet, A., "An Experimental and Numerical Study of Diesel Injection Spray Phenomena," SAE Technical Paper Series 2010-01-010.

[18] Liu, H., Guo, Y., Lin, W., " Numerical simulations of transverse liquid jet to a supersonic crossflow using a pure two-fluid model," Advances in Mechanical Engineering., 8(1), pp.1687814016629341, (2016).

[19] Du, H., Liu, J., Tang, J., "CFD Investigation on the Nozzle of Orifices Distributing in Different Space layers," SAE Technical Paper Series 2008-01-0948.

[20] Cassidy, D.A., Choi, J.I., Tian, M., Edwards, J.R., Lin, K.C., Jackson, T.J., "Numerical Simulation of Two-Phase Flow Within an Aerated Liquid Injector," AIAA Paper 98, (2010).

[21] Lin, K.C., Kennedy, P.J., Jackson, T., "Structures of internal flow and the corresponding spray for aerated-liquid injectors," 37th AIAA/ASME/SAE/ASEE Joint Propulsion Conference and Exhibit, (2001).

[22] Sallam, K.A., Aalburg, C., Faeth, G.M., Lin, K.C., Carter, C.D., Jackson, T.A., "Primary breakup of round aerated-liquid jets in supersonic crossflows," Atomization and Sprays.,16(6), (2006).

[23] Balabel, A., Hegab, A.M., Nasr, M., El-Behrey, S.M., "Assesment of Turbulence Modeling for Gas Flow in Two- Dimensional Convergent-Divergent Rocket Nozzle," Applied Mathematical Modelling, 35 (3048-3422), (2011).

[24] Ansys-Fluent Theory Guide 15, Ansys Inc, Canonsburg, PA, 2013.

[25] Ansys-Fluent User's Guide 15, Ansys Inc, Canonsburg, PA, 2013.

[26] John, J., Keith, T., A handbook to Gas Dynamics. New Jersey: Pearson Education (2006).

[27] Baek, C., Kwon, S., Kim, H., "Study of Moderately Underexpanded Supersonic Moist Air Jets," AIAA Journal.,44(7), (2006).

[28] Nakahira, T., Komori, M., Nishida, M., Tsujimura, K., "The shock wave generation around the diesel fuel spray with high pressure injection," SAE Technical Paper, (1992).

[29] Linfield, K.W., A Study of the Discharge Coefficients of Jets from Angled Slots and Conical Orifices, PhD Thesis, University of Toronto, (2000).

[30] http://www.nasa.gov/centers/langley/news/factsheets/X43A_2006_5.html

[31] http://3.bp.blogspot.com/_ZL2xfh2o35k/TNY2UwLxX8I/AAAAAAAAAHA/2f3CiA-WUQ/s1600/Untitled.jpg

[32] http://spl.ch/products/img/diamonds2.5kN.jpg

[33] Love, E., Grigsby, C., NACA Research Memorandum RM L54L31, 1957.

APPENDIX A

Simulation of pure air jet for axisymmetric geometry

1. Open the Ansys-Fluent and select *Fluid Flow (Fluent)* option from analysis systems

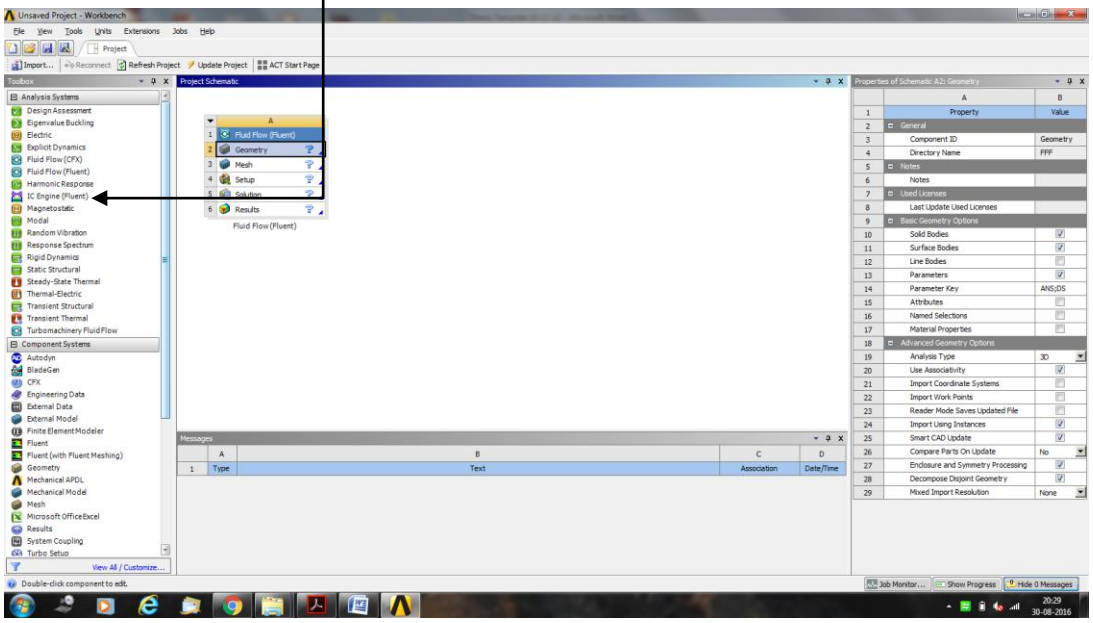

2. Select *Geometry* option and change the *analysis type to 2D* from Advanced Geometry Options.

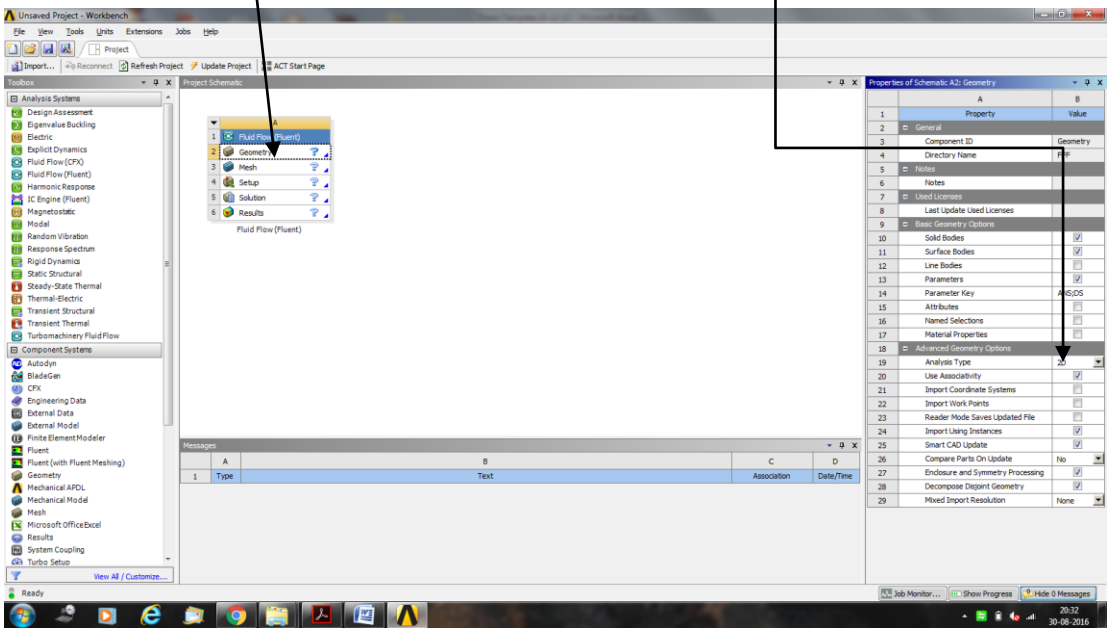

3. Make sketch in XY plane as shown in fig. Consider X-axis as *axis* of the sketch and make half portion of the sketch in *+Y region*.

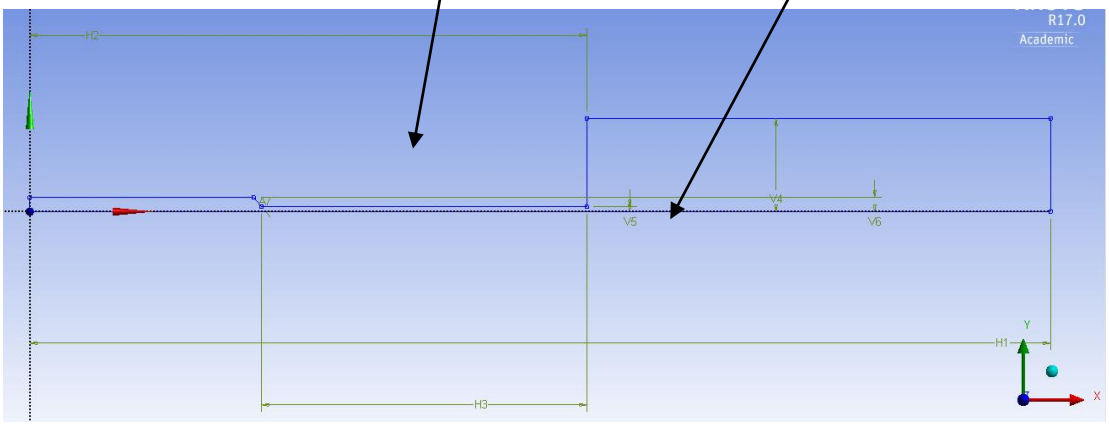

Figure 1: Axisymmetric sketch

4. Create the surfaces from the sketch by selecting *surfaces from sketches* as shown in fig. and the sketch.

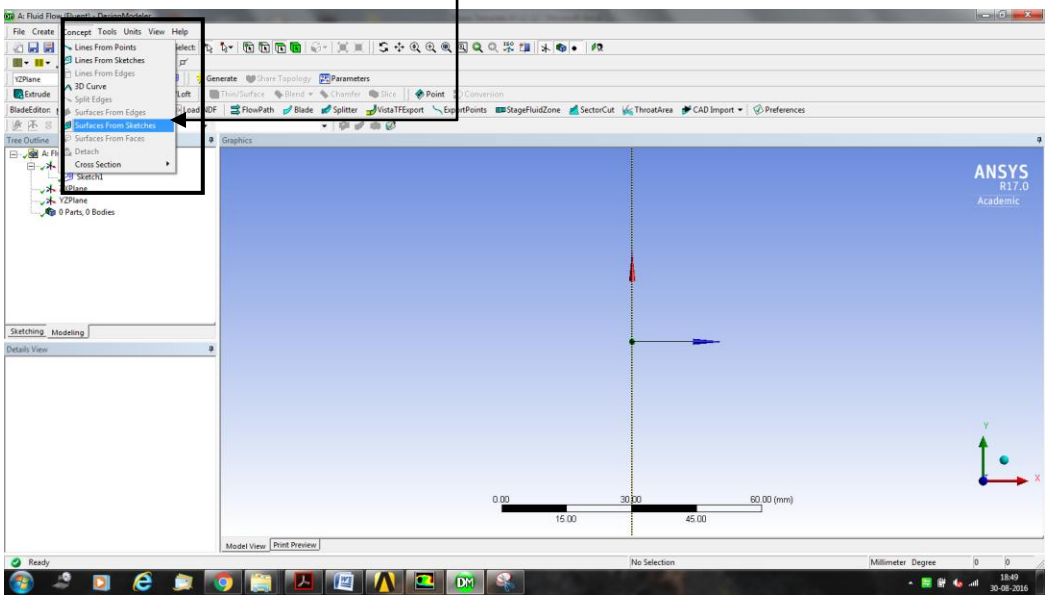

5. Surface of from the sketch is formed as shown in fig.

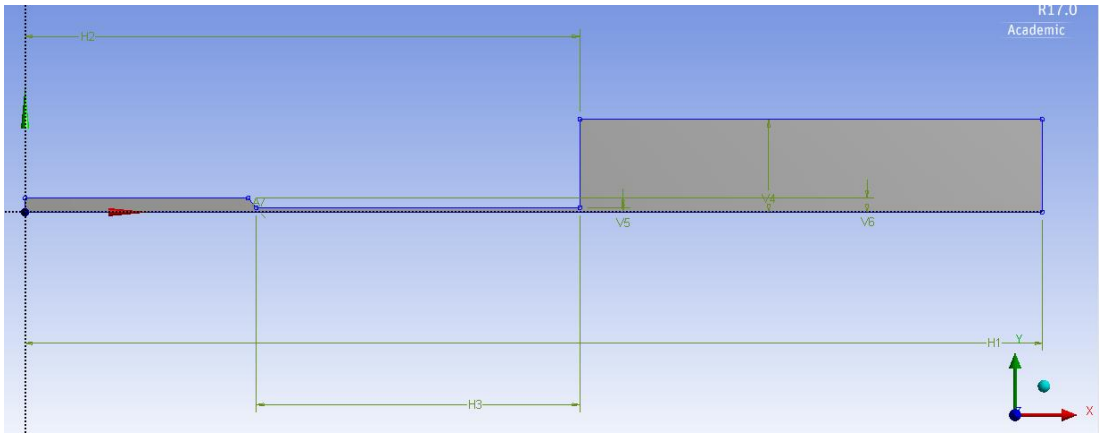

6. Close the geometry option from the fluent and open the mesh option. It will automatically import the geometry in mesh option as shown in fig.

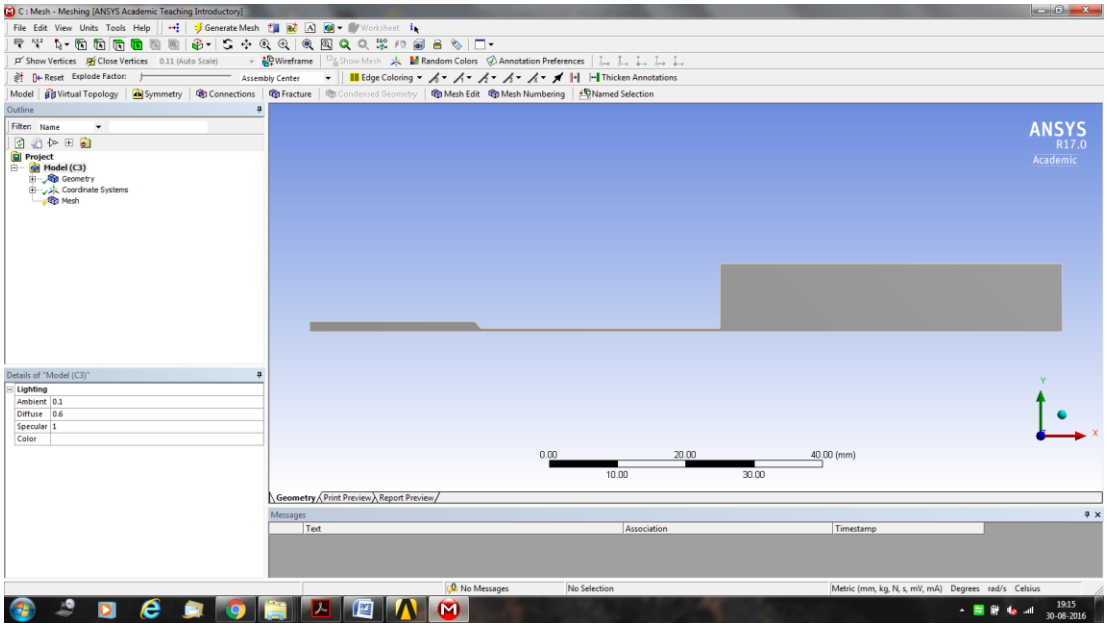

7. Select mesh option from the option and click *Generate Mesh* option and then select *Sizing* option to form suitable mesh structure as shown in fig.

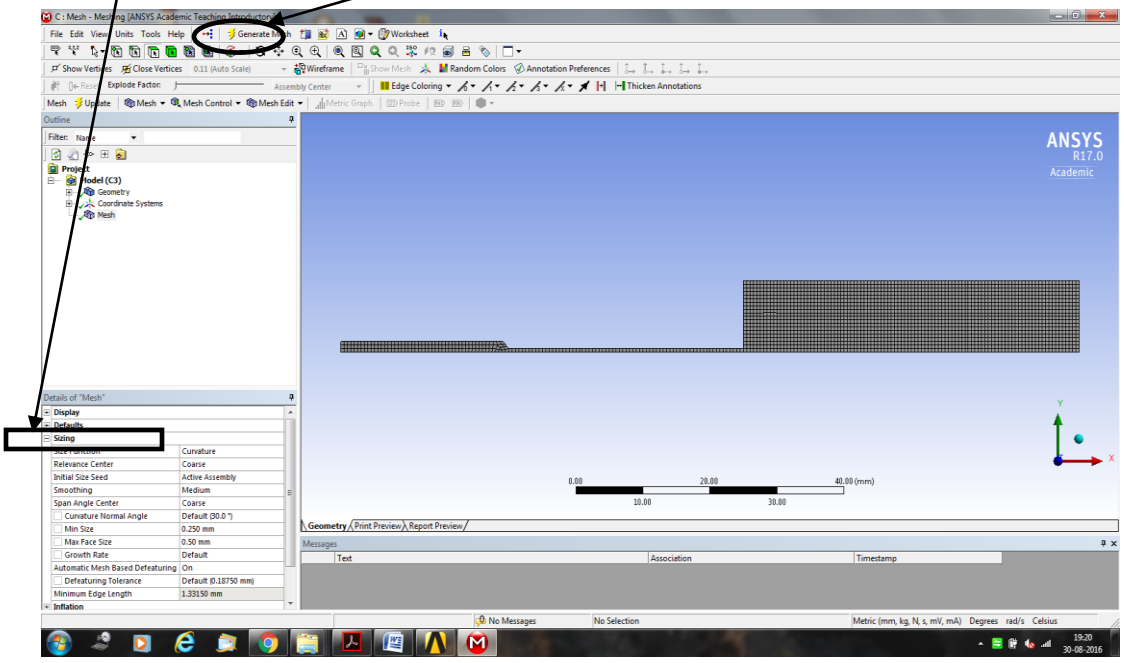

8. After generating the suitable mesh, select the *Edge* option and then name that edge by selecting the *Naming tool* as indicated in fig.

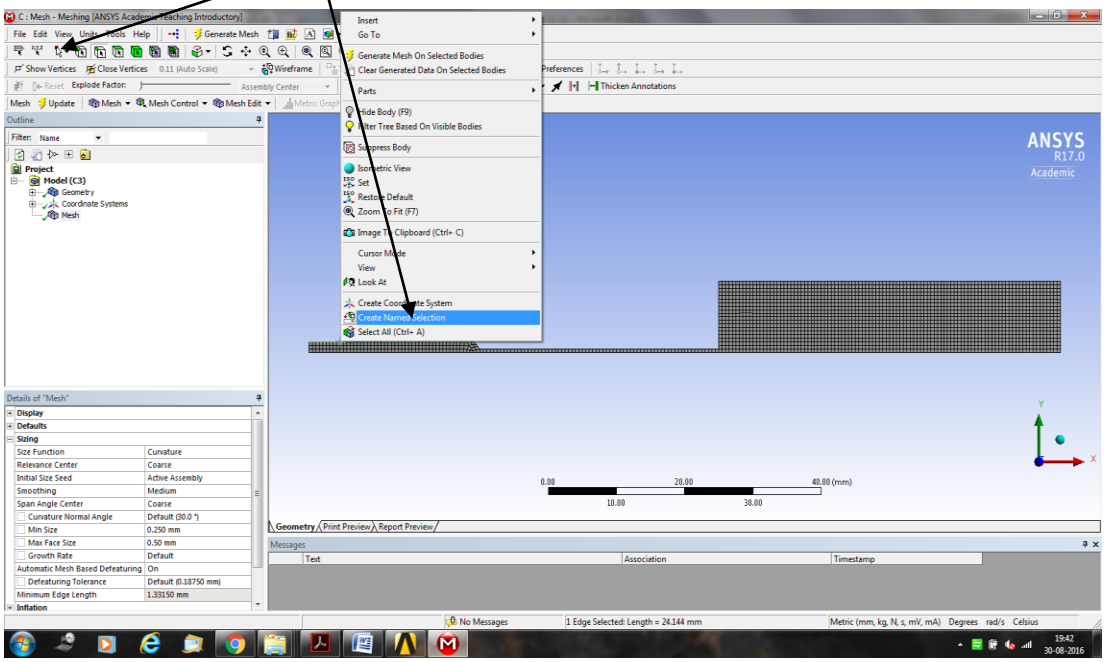

9. Name the edges as inlet, outlet, surfaces, walls and *axis* as shown in fig.

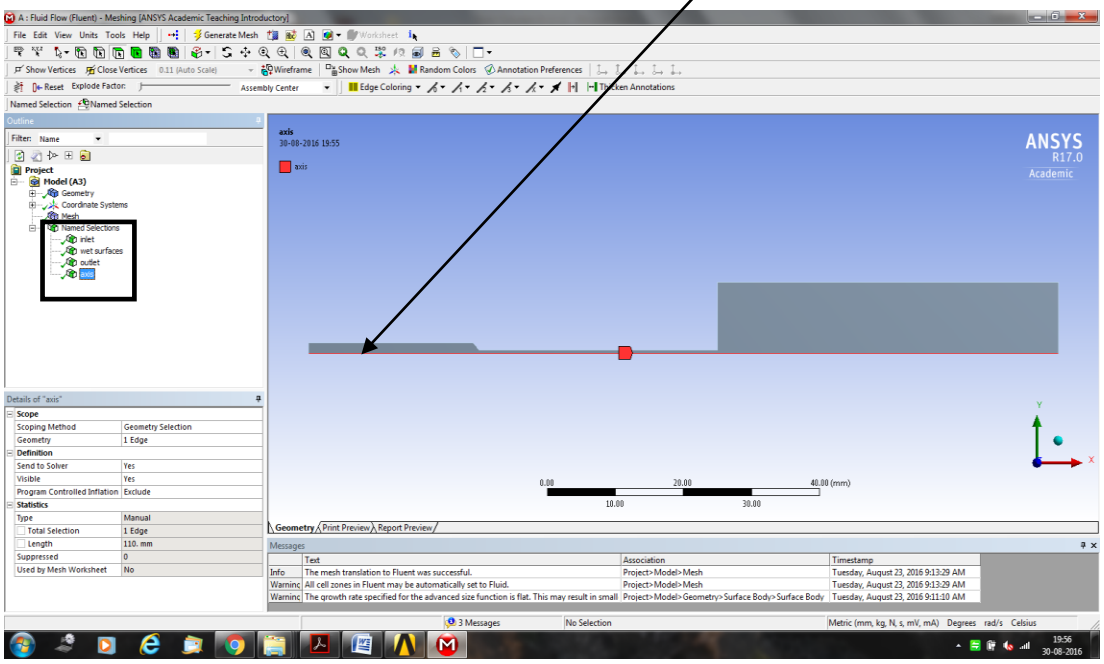

10. Close the mesh option and select settings option and select *axisymmetric* option from 2D space option in *General Setup* the suitable numerical schemes to get the converged solution.

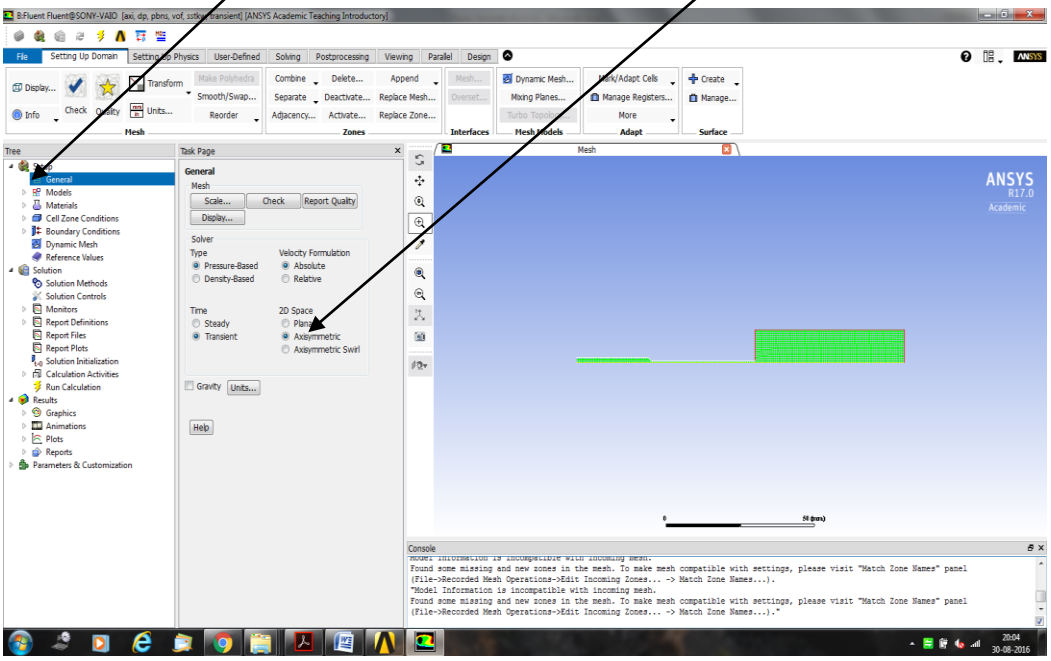

11. To view the whole geometry select *viewing* option and press *views* icon. Press *axis* option from the mirror planes

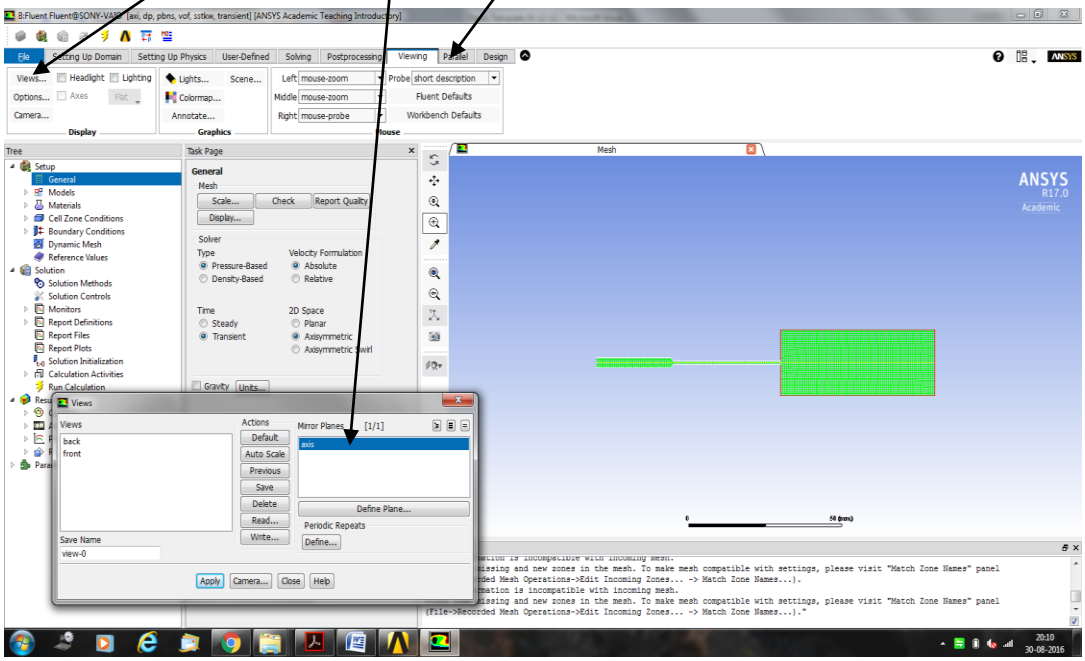

12. Select *pressure based* solver and *axisymmetric* 2D space from the General setup section

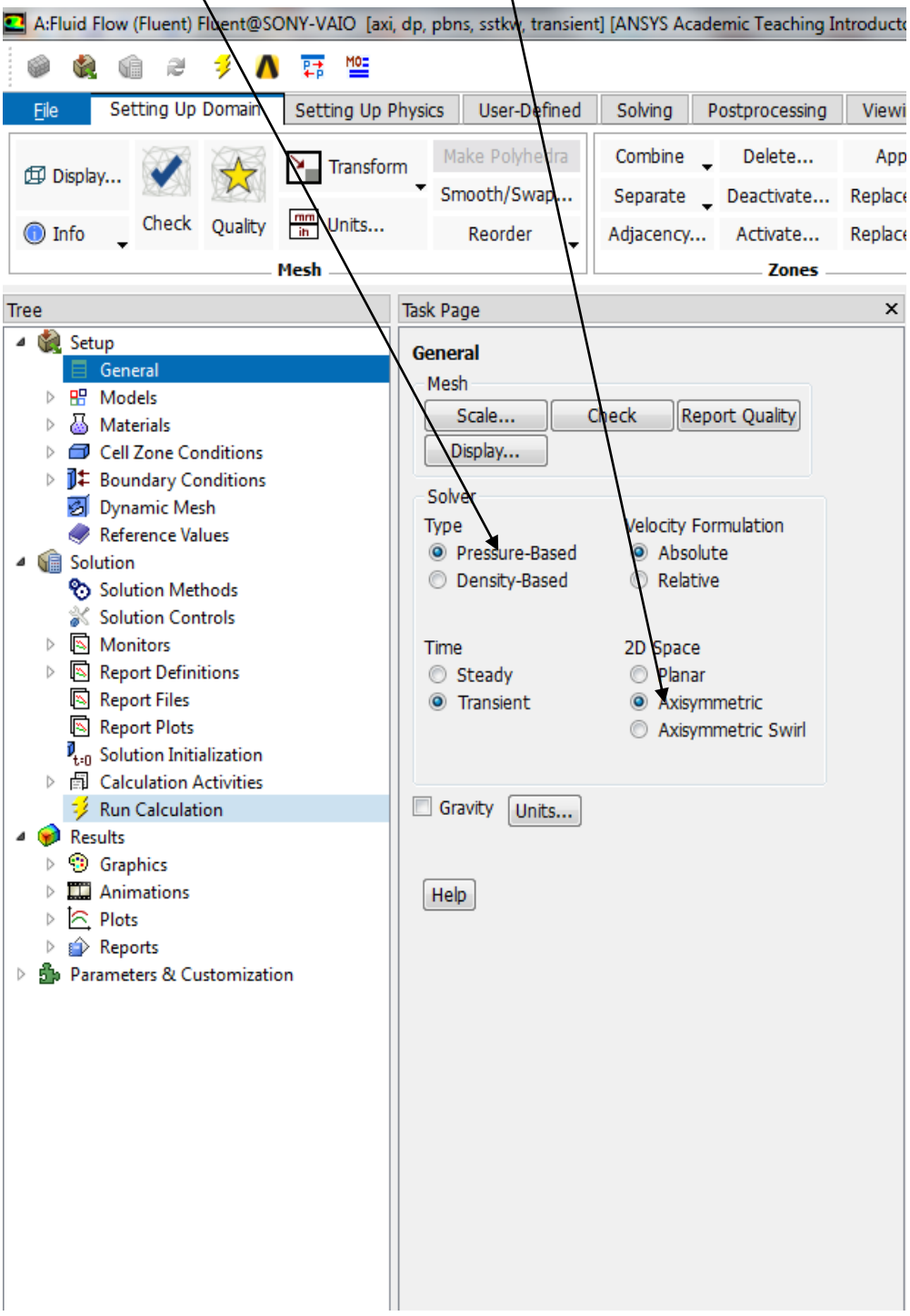

13. Select the viscous model *SST k-ω* for the numerical simulation

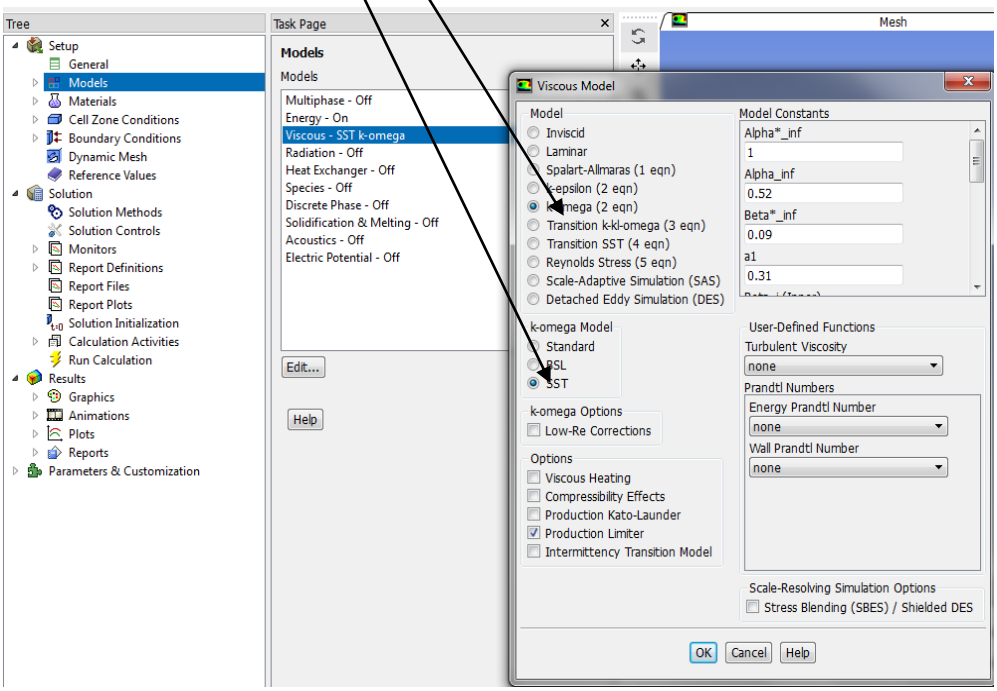

14. Material section shows air as default material, and make it compressible gas by changing the density to *ideal gas* from the properties

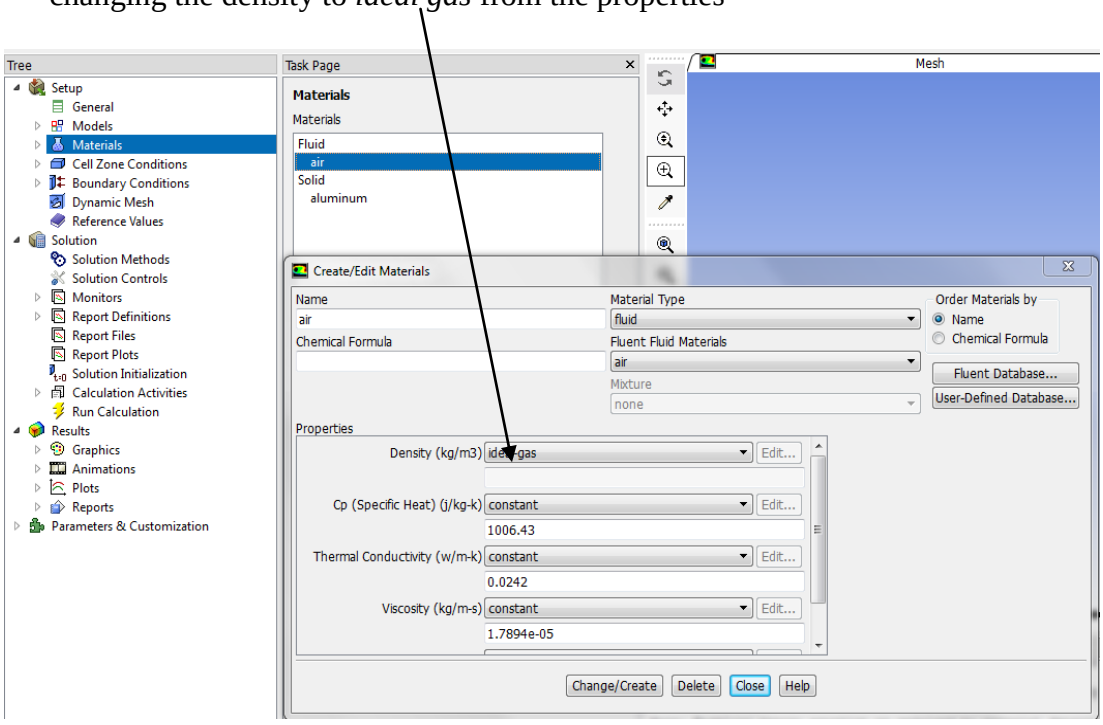

15. Select boundary conditions for *inlet* and *outlet* zones as *mass flow inlet* and *pressure outlet* respectively

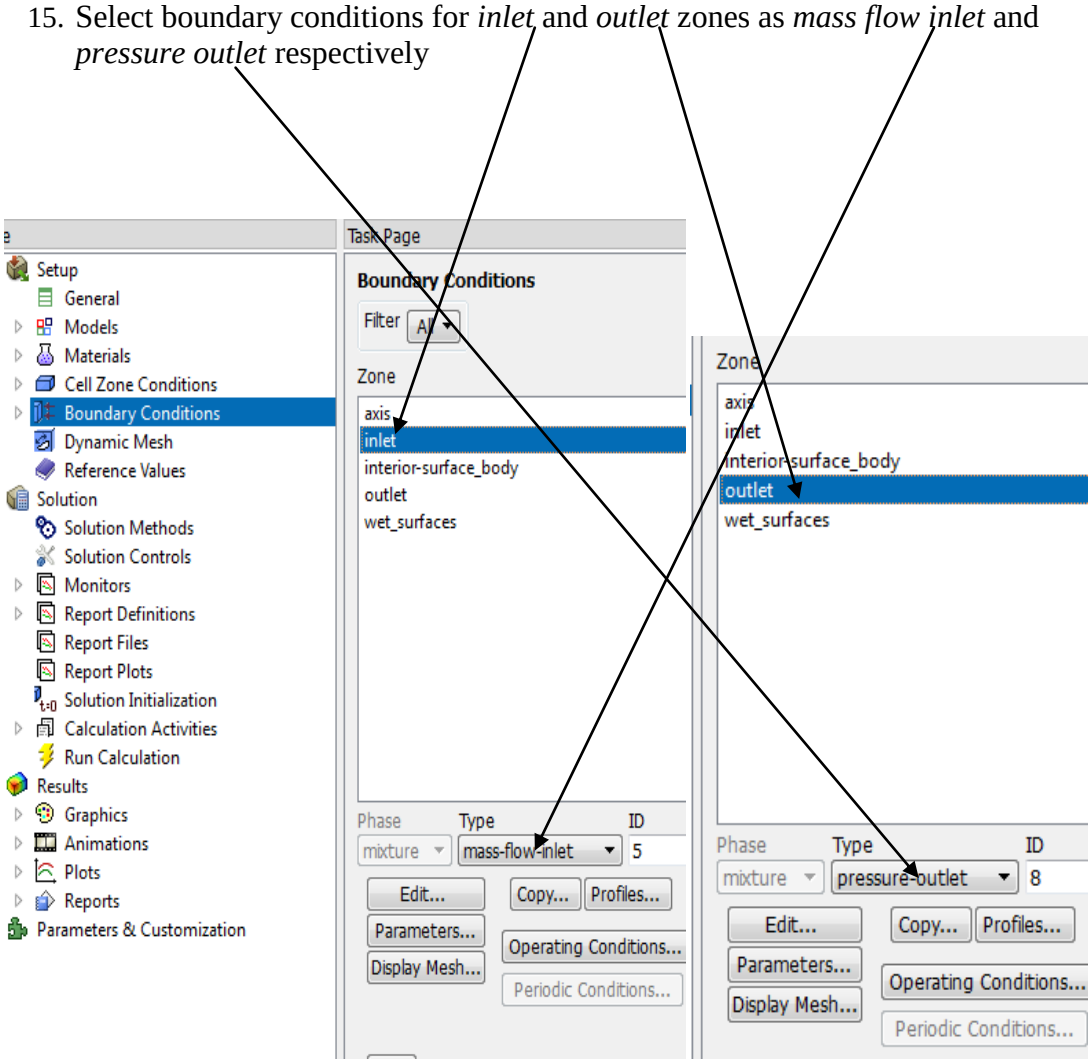

16. Select *solution methods* as indicated in the snapshot

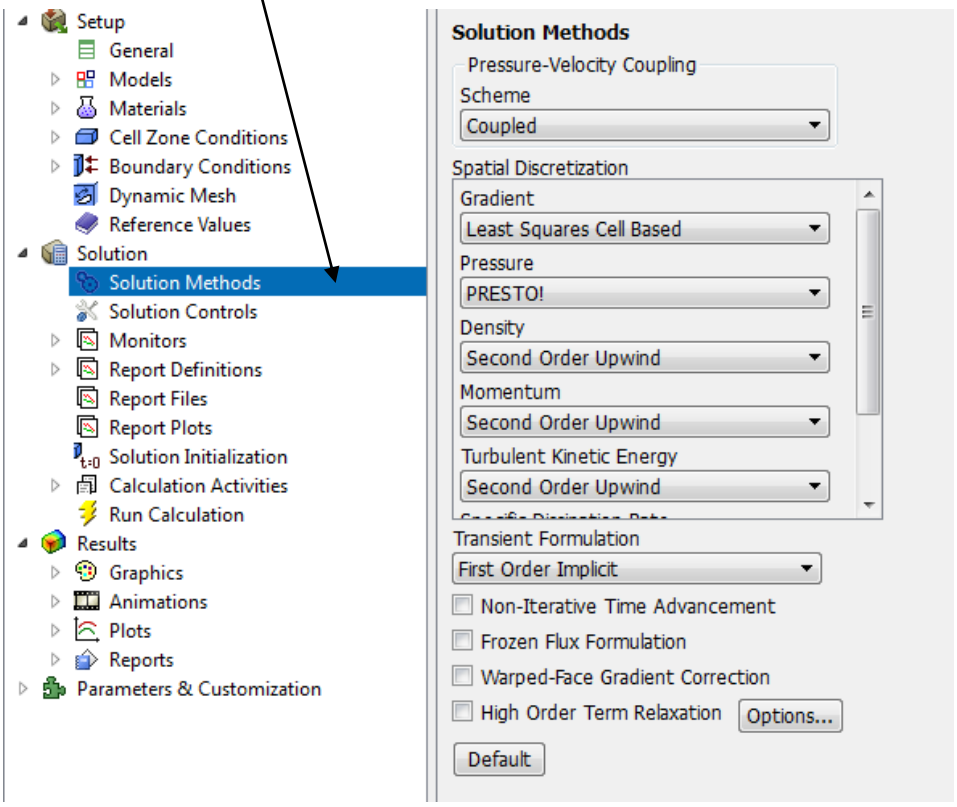

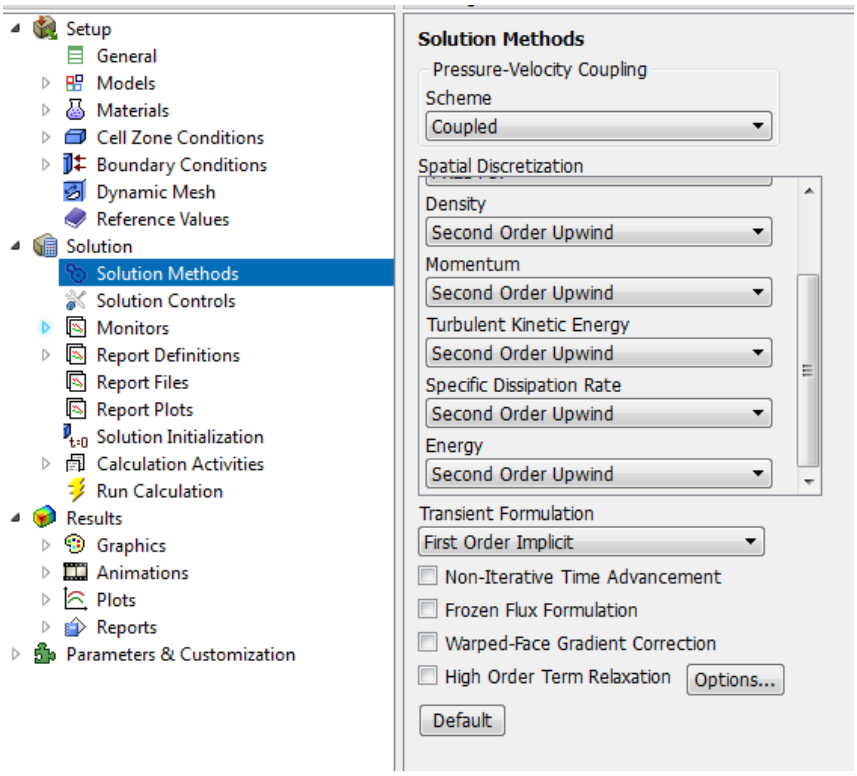

17. Initialize the solution as *hybrid*

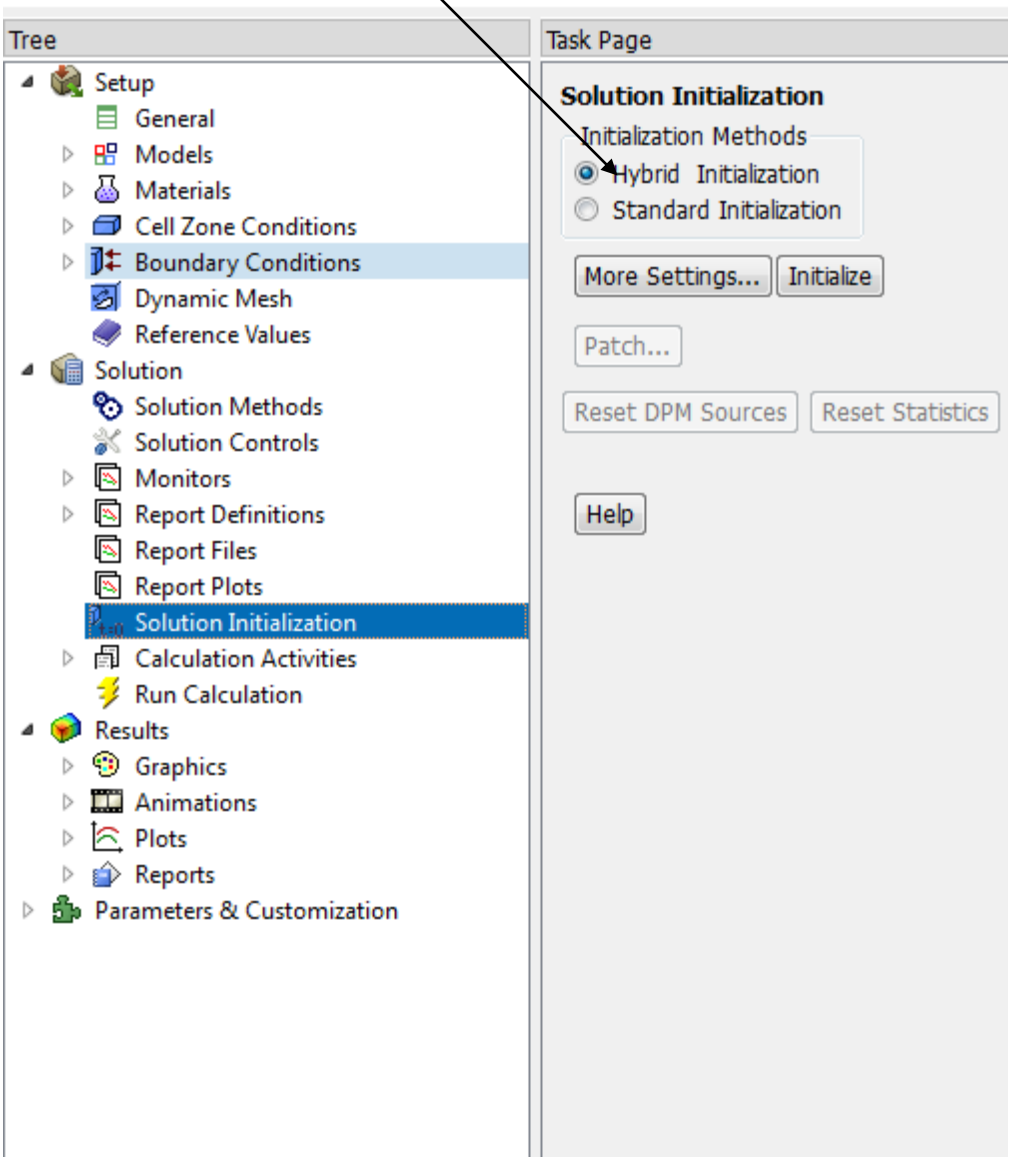

18. Run the calculation for number of time steps to converge the solution

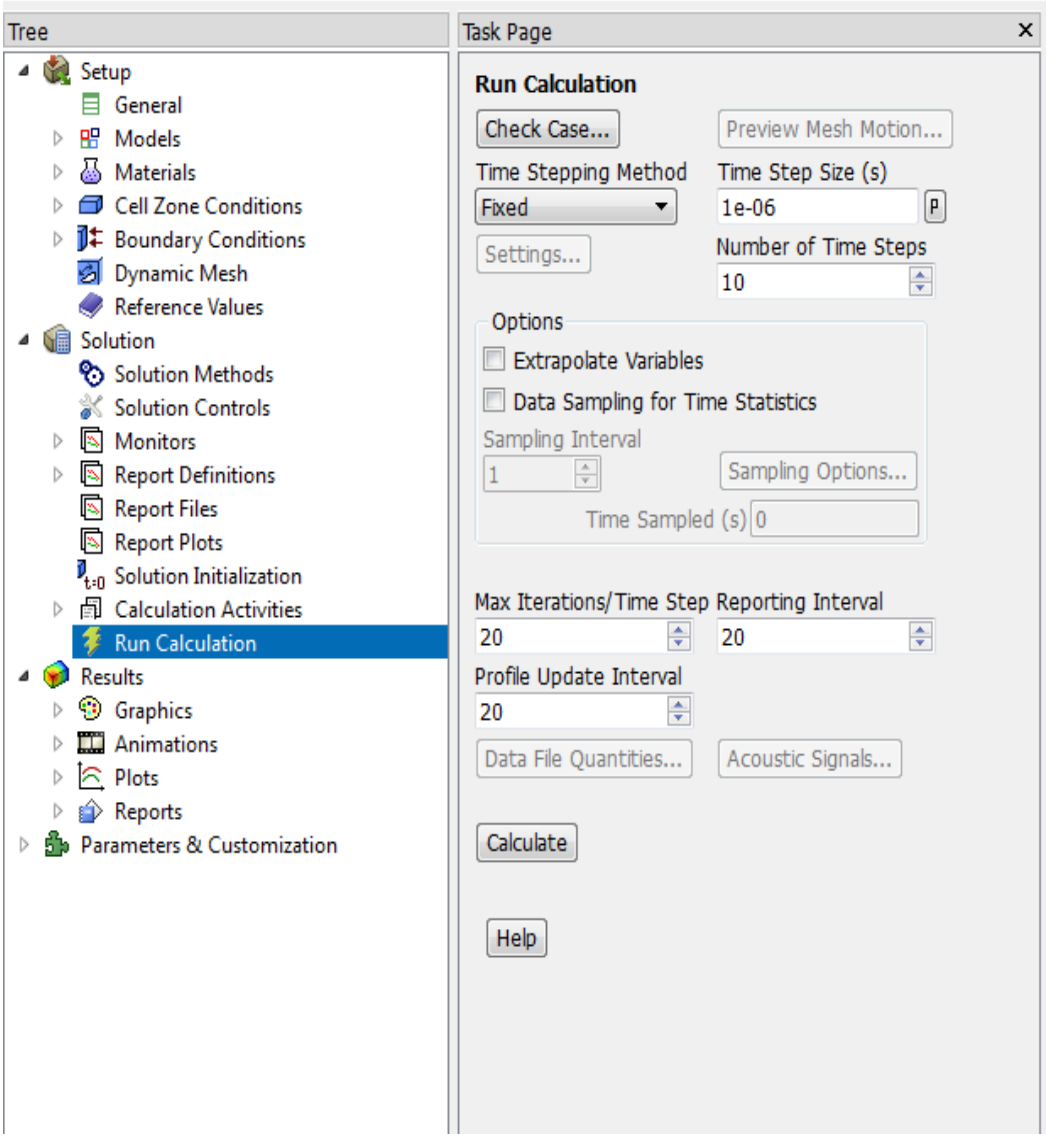

VITA

Abhijit Subhash Choudhari

Candidate for the Degree of

Master of Science

Thesis: SIMULATION OF SUPERSONIC INJECTION OF UNDEREXPANDED AERATED LIQUID JET

Major Field: Mechanical & Aerospace Engineering

Biographical:

Personal Data: Born in Sangli on 20th February, 1988. Son of Mr.Subhash Choudhari and Mrs.Sunita Choudhari

Education: Completed the requirements for the Master of Science in Mechanical Engineering at Oklahoma State University, Stillwater, Oklahoma in December, 2016. Completed the requirements for the Bachelor of Engineering in Mechanical Engineering at Shivaji University, Kolhapur, India in 2010.

Experience: Worked as a senior mechanical engineer at Larsen & Toubro Ltd. Employed by MAE, OSU as teaching assistant for Compressible Fluid Flow, Experimental Fluid Dynamics, Energy Conversion, Mechanical Measurements & Control.

Name: Abhijit Subhash Choudhari Date of Degree: December 2016

Institution: Oklahoma State University Location: Stillwater, Oklahoma

Title of Study: SIMULATION OF SUPERSONIC INJECTION OF UNDEREXPANDED AERATED LIQUID JET

Pages in Study: 74 Candidate for the Degree of Master of Science

Major Field: Mechanical Engineering

Scope and Method of Study:

The present study computationally investigates the flow physics of the injection of aerated liquid jet into a quiescent chamber and to observe the properties of the conical liquid sheet emitted from the injector exit. Properties of conical liquid sheet include spray cone angle, liquid film thickness, and velocities of the liquid sheet. The simulation is carried out for gas-only jet and for aerated liquid jet for both 2D and axisymmetric nozzle configurations.

Findings and Conclusions:

Flow field of gas-only jet for 2D nozzle is explained using 2D Prandtl-Meyer and oblique shock waves analysis. The computational results of axisymmetric gas-only jet were validated using previous experimental results. The flow field of axisymmetric aerated liquid jet is shorter than 2D aerated liquid jet, due to the reduction in the inertia of the liquid film for axisymmetric aerated liquid jet. The experimental results of aerated liquid jet expansion can be explained by the method of characteristics for axisymmetric gas-only jets rather than 2D Prandtl Meyer expansion analysis.

ADVISOR'S APPROVAL: Khaled A. Sallam .